ANALYTICAL AND EXPERIMENTAL EVALUATION OF THE

LEAKAGE AND STIFFNESS CHARACTERISTICS OF HIGH

PRESSURE POCKET DAMPER SEALS

A Thesis

by

AHMED MOHAMED GAMAL ELDIN

Submitted to the Office of Graduate Studies of
Texas A&M University
in partial fulfillment of the requirements for the degree of

MASTER OF SCIENCE

December 2003

Major Subject: Mechanical Engineering

ANALYTICAL AND EXPERIMENTAL EVALUATION OF THE

LEAKAGE AND STIFFNESS CHARACTERISTICS OF HIGH

PRESSURE POCKET DAMPER SEALS

A Thesis

by

AHMED MOHAMED GAMAL ELDIN

Submitted to Texas A&M University
in partial fulfillment of the requirements
for the degree of

MASTER OF SCIENCE

Approved as to style and content by:

John M. Vance (Chair of Committee)	Dara W. Childs (Member)
Robert E. Randall (Member)	Dennis L. O'Neal (Head of Department)

December 2003

Major Subject: Mechanical Engineering

ABSTRACT

Analytical and Experimental Evaluation of the Leakage and Stiffness
Characteristics of High Pressure Pocket Damper Seals. (December 2003)
Ahmed Mohamed Gamal Eldin, B.Sc., The American University in Cairo, Egypt
Chair of Advisory Committee: Dr. John M. Vance

This thesis presents numerical predictions for the leakage and direct stiffness coefficients of pocket damper seals. Modifications made to earlier flow-prediction models are discussed. Leakage and static pressure measurements on straight-through and diverging configurations of eight-bladed and twelve-bladed seals were used for code validation and for calculation of seal discharge coefficients. Higher than expected leakage rates were measured in the case of the twelve-bladed seal, while the leakage rates for the eight-bladed seals were predicted reasonably accurately.

Results are presented for shake tests conducted on the seals at pressures of up to 1000 Psi (6.90 MPa). Test variables included pressure drop across the seals and rotor speed. The experimentally obtained stiffness coefficients are compared to results of a rotordynamic damper seal code, which uses the corrected mass flow-rate calculation method. Results show that the code under-predicts the magnitude of the seal's stiffness for most test cases. However, general trends in the frequency dependency of the direct stiffness are more accurately predicted. The expectation of high values of negative stiffness in diverging seals is confirmed by the results, but the frequency at which the sign of the stiffness becomes positive is considerably lower than is predicted.

In addition to presenting high-pressure test data, this thesis also attempts to provide some insight into how seal parameters can be modified to obtain desired changes in seal stiffness.

DEDICATION

In memory of Dr. Sherif T. Noah

"Unlike the doctor, his is not a life among the weak. Unlike the soldier, destruction is not his purpose. Unlike the lawyer, quarrels are not his daily bread. To the engineer falls the job of clothing the bare bones of science with life, comfort, and hope."

- Herbert Hoover

ACKNOWLEDGMENTS

I would like to express my heartfelt appreciation and gratitude to Dr. John M. Vance for his guidance and support. His exhaustive knowledge of turbomachinery and engineering in general proved to be of invaluable assistance over the course of my research. Dr. Vance's understanding and kind advice have served as additional sources of inspiration that aided me in completing this thesis.

Sincere thanks are also due to Dr. Dara W. Childs for his recommendations and his input regarding seal rotordynamics, as well as for allowing the use of his test facility. I would also like to thank Dr. Robert E. Randall for his help in serving on my committee.

Bugra Ertas, my project partner, has been a guide as well as a colleague. He deserves special thanks for his help every step of the way, from component design to data analysis.

I am grateful to Arthur Picardo and Jonathan Wade for their help in test-rig assembly and testing. I would also like to acknowledge the friendship and support of my coworkers at the Turbomachinery Laboratory, without whom the past three years would have been nowhere near as much fun.

I must also thank my friends in College Station for every day that was spent studying, as well as for every day that was spent not studying. Finally, I will always be indebted and grateful to my family, who have never wavered in their support and love.

TABLE OF CONTENTS

LIST OF FIGURES

LIST OF TABLES

NOMENCLATURE

A_i	Area of flow for the ith construction [L^2]
A_{pi}	Area on which the pressure in the ith cavity acts [L^2]
C_i	Direct damping generated in the ith cavity [Ft/L]
C_{ij}	Damping coefficient [Ft/L]
Cd_{in}, Cd_{exit}	Inlet and exit blade discharge coefficients [-]
Cl_{in}, Cl_{exit}	Inlet and exit blade clearances [L]
CR	Ratio of exit to inlet blade clearances [-]
d	Diameter of shaft [L]
d_{si}	Inner diameter of seal [L]
D_{ij}	Relative displacement [L]
δ	Weight per unit volume of shaft material [F/L^3]
E	Modulus of Elasticity for shaft material [F/L^2]
f_x, f_y	Forces applied in the x and y directions [F]
f_{Sx}, f_{Sy}	Seal forces in the x and y directions [F]
F	Force developed in seal pocket [F]
F_x, F_y	Forces in the frequency domain [F]
ϕ	Phase angle [Angle]
g	Acceleration due to gravity [L/t^2]
γ	Gas constant [-]
H_{ij}	Impedance [F/L]
k	Cross-coupled stiffness coefficient [F/L]
K_i	Direct stiffness generated in the ith cavity [F/L]
K_{ij}	Stiffness coefficient [F/L]
$\dot{m}_i$	Mass flow-rate through the ith constriction [M/t]
m_S	Mass of stator [M]
M_{ij}	Direct mass coefficient [M]

n	Number of seal blades [-]
N	Number of pockets [-]
ν	Poisson's Ratio for shaft material [-]
PD	Pressure drop across the seal [F/L^2]
P_{in}	Pressure upstream of the seal [F/L^2]
P_{exit}	Pressure downstream of the seal [F/L^2]
P_i	Pressure in the ith cavity [F/L^2]
PR	Ratio of inlet to exit pressures [-]
ΔP	Difference between inlet and exit pressures [F/L^2]
R	Gas constant [FL/(MT)]
R_S	Shaft radius [L]
ΔR	Increase in shaft radius [L]
RPM	Revolutions per minute [1/t]
ρ	Density of gas
T_i	Temperature in the ith cavity [T]
t	Time [t]
V_i	Volume of the ith pocket [L^3]
W_i	Width of ith cavity [L]
ω	Frequency of vibration [1/t]
x	Journal displacement [L]
x, y	Displacement directions [-]
$\ddot{x}, \ddot{y}$	Acceleration of stator in the x and y directions [L/t^2]
$\Delta\dot{x}, \Delta\dot{y}$	Relative velocities in the x and y directions [L/t]
$\Delta x, \Delta y$	Relative displacements in the x and y directions [L]
X	Amplitude of journal displacement [L]
Z	Ratio of exit to inlet pressures [-]

CHAPTER I

INTRODUCTION

The use of high-speed turbomachines has become essential in several industries today. Numerous modern applications in the oilfield, aviation, defense, and power generation industries would be infeasible without the rotating equipment that is regularly employed. With a constant demand for higher rates of productivity, turbomachines are being designed to run faster, operate more efficiently, and last longer. The result is a need to reach an optimum balance between a turbomachine's leakage characteristics and its rotordynamic performance while dealing with ever-tightening clearances between rotor and stator.

The operating speeds that can be reached today would not have been possible without significant research in the area of rotordynamics. Annular gas seals are essential to the successful operation of a turbomachine in that they limit the leakage across regions of unequal pressure. Labyrinth seals have been invaluable in this respect due to their desirable leakage prevention characteristics and their non-contacting nature, which allows rotor speed to be increased significantly. These seals do, however, have certain undesirable rotordynamic characteristics, mainly related to instability. In addition, they offer only limited damping of rotor vibrations, leaving the bearing locations as the only feasible location to add significant damping.

POCKET DAMPER SEAL BACKGROUND

In 1991 a seal was developed at Texas A&M University that did not exhibit the labyrinth seal's instability problems, and at the same time allowed the application of a considerable amount of damping at the seal location. Since that time, this Pocket

_____

This thesis follows the style and format of the ASME Journal of Engineering for Gas Turbines and Power.

Damper Seal (PDS), known as the TAMSEAL®, has shown in both tests and field applications that it can lower rotor vibration amplitudes significantly. These seals can be used in place of the labyrinth seals currently employed in compressors. As was indicated above, the requirements of low leakage and high damping are at times contradictory and must be optimized for each specific application. For the maximum possible damping, the PDS would have only two blades (and therefore one cavity), but this configuration is unlikely to meet a given application's leakage requirements. Thus far, the PDS's leakage characteristics have been less well understood than its rotordynamic properties, especially the direct damping.
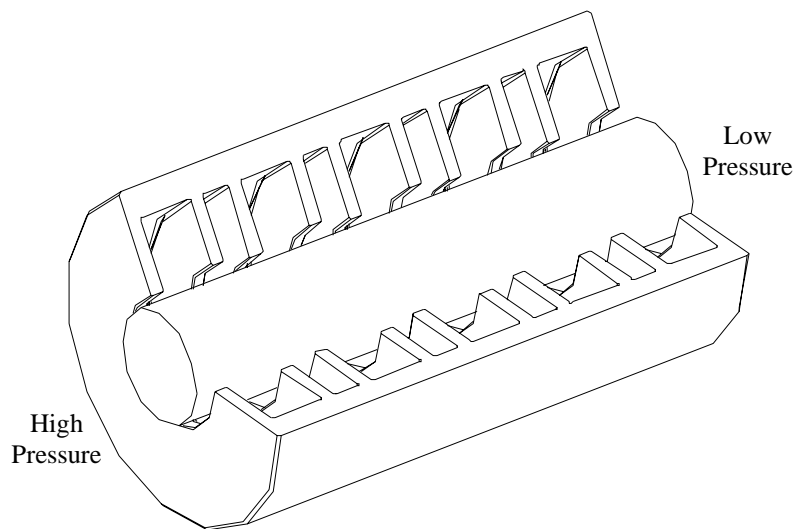
Figure 1 Diverging Ten-Bladed PDS

The PDS's superior stability arises mainly from the fact that the annular cavities formed by the seal's blades are divided by partition walls. These walls greatly reduce circumferential fluid flow around the seal, which in turn reduces the destabilizing cross-coupled stiffness of the seal. The PDS's damping characteristics result from the pressure that develops in the pockets (the sections of the cavity closed in by the partition walls).

If the seal's tooth-to-rotor clearances diverge along the direction of fluid flow, the resulting dynamic pressure will ideally be about 90° out of phase with the displacement, in a direction opposing the velocity (this, by definition, is positive damping).

In order to avoid a series of progressively increasing clearances (which would be detrimental to the seal's leakage characteristics), the PDS features an *inactive* cavity that serves to equalize the pressure before the fluid passes into the next *active* cavity. Figure 1 shows a schematic of a ten-bladed PDS (five active and four inactive cavities) with diverging clearances.

Recently, the diverging clearances have been replaced with notches in the exit blades, and the seals are currently being tested under considerably higher pressures than before.

RESEARCH OBJECTIVE

An important characteristic of the PDS is that it has negative stiffness. While this would, in most cases, be too small to offset an actual system's stiffness and make it negative, it does have an effect on the system's rotordynamics.
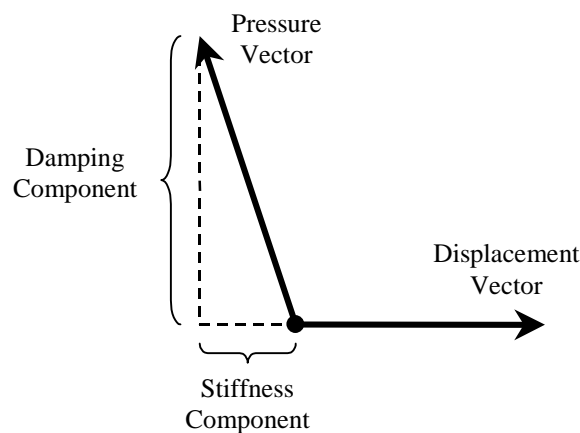
Figure 2 Pocket Pressure Vector Plot

Figure 2 represents a vector diagram of the pressure in a pocket of a diverging PDS and the relative displacement between the rotor and the stator. In this case, the pressure components that are responsible for the damping and stiffness forces are positive and negative respectively.

The first objective of this thesis is to determine, both analytically and experimentally, the effects of several design factors on the sign and magnitude of the direct stiffness of pocket damper seals. The three major parameters that a designer usually has control over while designing a seal for a given application are the depth of the pockets, the clearances (and clearance ratio), and the number of blades.

The effects of these parameters will be analyzed using a code developed at the Turbomachinery Laboratory to determine seal rotordynamic characteristics. Due to errors in predicting the mass flow-rate, a second objective is to modify the code to correct the mass flow-rate calculation and to verify this modified calculation experimentally.

The third objective of this thesis is to present the results of high pressure tests carried out to find the direct stiffness coefficients of eight-bladed and twelve bladed pocket damper seals.

In summary, this research aims at providing methods of predicting the direct stiffness of the seals and testing the predictions experimentally. The objectives are:

- To modify the current code to correctly calculate the leakage as well as to calculate the phase angle in each cavity.

- To study the effects of changing the number of blades, the clearances, and the pocket depth on the direct stiffness

- To experimentally determine the direct stiffness coefficients of the seals through high pressure testing (pressure drops of several hundred pounds per square inch across the test seals)

- To analyze the empirical stiffness and leakage results and compare them with theoretical predictions

NEED STATEMENT

In the past, engineers working with turbomachines have had a general aversion to the idea of employing a seal with negative stiffness, mainly due to mistaken intuition. Depending on the system into which it is to be installed, a seal with negative stiffness could have either a desirable or a detrimental effect. If the system has a very low overall stiffness, or if its operating speed is slightly lower than the critical speed, installing a PDS with negative stiffness could have serious undesirable effects. On the other hand, an engineer would not readily select a seal with positive stiffness for use in a turbomachine operating at a speed slightly higher than its critical speed.

Since the damping characteristics of a pocket damper seal are its most attractive feature, the stiffness of the seal is at times only a secondary concern. While, the damping values may be more important to a PDS user, the considerations mentioned above demonstrate that examining the stiffness characteristics of the seal is also worthwhile.

OVERVIEW

This thesis reviews the theoretical models used to predict the leakage and stiffness characteristics of pocket damper seals at high pressures. These predictions are compared with experimentally obtained results. Discrepancies between model predictions and measured data are explained where possible through re-examination of either the test conditions or model assumptions. In addition to presenting high-pressure test data, this thesis attempts to provide an insight into how seal parameters can be modified to obtain desired changes in seal stiffness.

CHAPTER II

LITERATURE REVIEW

An analysis of annular seals was published by Alford [1] in 1965 in which he presented a method of predicting the direct damping (*C*) coefficients of labyrinth seals. This analysis was limited to two-bladed seals with choked flow. Alford postulated that the time-varying pressure distribution around a seal would oppose vibratory velocity in the case of a diverging clearance along the direction of fluid flow and drive the vibratory velocity in the case of a converging clearance. In other words, a diverging clearance would result in positive damping while a converging clearance would result in negative damping. A fundamental flaw in Alford's analysis was the assumption that the gas pressure could vary around the continuous annular groove in a labyrinth seal without circumferential flow of the gas.

Two other rotordynamic coefficients of interest in seals, the direct (*K*) and the cross-coupled (*k*) stiffnesses were measured by Benckert and Wachter [2] for various labyrinth geometries. They displaced the rotor and examined the resulting reaction forces both inline with and tangential to the displacement. They concluded that while the direct stiffness was negligible, the cross-coupled stiffness was not, and that it was caused by the circumferential flow of the fluid around the annular seal. They also employed swirl-brakes to reduce this flow and eliminate the destabilizing tangential force.

Murphy and Vance [3] further developed Alford's theory to account for unchoked flow and for seals with multiple blades. Their analysis contained the same conceptual error as Alford's. It misleadingly showed that a diverging-clearance ten-bladed labyrinth seal with a 10:1 pressure ratio would have about 500 lb-s/in (87.6 KN-s/m) damping, far more than has ever been obtained by a labyrinth seal. According to Childs and Vance [4], the cross-coupled stiffness, which was not considered in Alford's theory, becomes the dominant factor in labyrinth seals, and decreases the effective damping. Were a pressure differential to be created around the seal, a pressure wave travelling at the speed

of sound would equalize the pressures around the seal annulus. Also, the friction between the fluid and the rotor creates circumferential fluid flow that in turn creates a follower force that is normal to the rotor deflection. This is not the case, however, with the PDS, which incorporates walls that prevent circumferential flow. Sundararajan and Vance [5] developed an analysis based on unconnected circumferential control volumes for a bearing damper. This analysis also produces relatively accurate predictions for PDSs. It is based on the pressure differentials across the seal due to changes in the fluid density. In the case of a PDS, the effective damping is approximately equal to the direct damping, at least at low pressures.

Armstrong and Perricone [6] showed that honeycomb seals could be used in place of labyrinth seals to eliminate instabilities in steam turbines. Childs and Vance [4] state that while the honeycomb seal has superior leakage characteristics, the pocket damper seal provides higher damping. In addition, for small seal lengths, the two seals have similar leakage characteristics, and the PDS becomes the clear choice.

Childs and Vance [4] present empirical data showing that decreasing the blade-clearances in a PDS increases the damping and reduces the leakage. Reducing the number of blades will increase the damping, but it will also increase the leakage.

In 1974, Lund [7] published a paper in which he cited the desirability of being able to install a damping mechanism (which he modeled with a bearing damper) at the center of a rotor. Vance and Shultz [8] developed the TAMSEAL$^{®}$, which could perform this exact role. The seal's partition walls allow for radial pressure differentials around the seal and at the same time greatly reduce any circumferential flow. Shultz [9] demonstrated through static tests that a two-bladed PDS has higher damping than a comparable labyrinth seal. Dynamic tests were conducted by Li and Vance [10] to study the effect of clearance ratio on seal performance. Vance and Li [11] published results showing how a PDS could be used to virtually eliminate a system's response to imbalance. Richards et al. [12] cited the use of PDSs in industrial compressors to suppress sub-synchronous vibration. The stiffness and damping coefficients of a short PDS were determined experimentally by Ransom et al. [13]. Laos [14] compared two

configurations of a four-bladed PDSs (with four and eight pockets) with a six-bladed labyrinth seal. The damping of the labyrinth seal was found to be lower than that of either PDS and the labyrinth seal became violently unstable at pressures above 3 bar (44 Psi). The eight-pocket PDS was found to have higher damping than the four-pocket PDS. Li et al. [15] presented results for rotating tests on a "slotted" gas damper seal at pressures up to 14.5 bar, or about 210 Psi. This seal features partition walls in all cavities.

CHAPTER III

THEORY AND MATHEMATICAL MODELS

Two main mathematical models form the core of the theory on which both the analytical and experimental portions of this thesis are based. These are the basic theory of operation of pocket damper seals and the modeling of the forces generated within a seal. The former leads to the expressions for the seal's rotordynamic coefficients while the latter makes possible the evaluation of these coefficients through the analysis of experimental data.

POCKET DAMPER SEALS

The expressions for the stiffness and damping of a two-bladed pocket damper seal were derived by Shultz [9]. The first stage of the derivation assumes no journal vibration. This static model is used to calculate the mass flow-rate across the blades of the seal and the steady-state pressures in the pockets. The second stage of the derivation; the perturbation analysis; uses the calculated flow-rate as an input and obtains expressions for the seal's direct rotordynamic coefficients.

Static Model

For the purpose of calculating the mass flow-rate through the seal, a static model is assumed in which the journal does not vibrate. Shultz's [9] two-bladed seal model is shown in Figure 3 (the nomenclature has been modified to match the subscript convention used in this thesis).
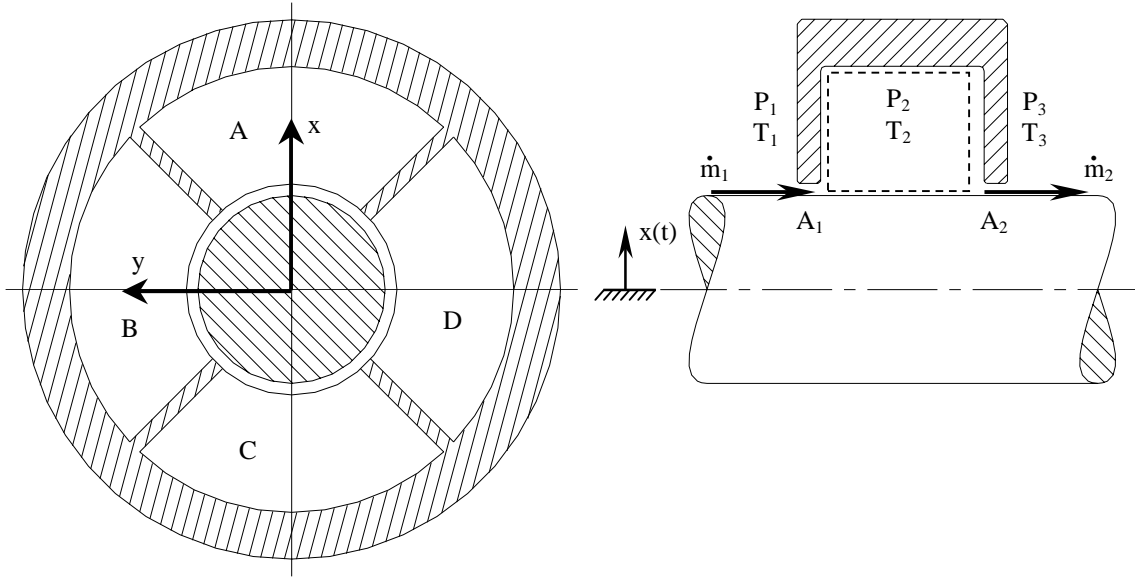
Figure 3 Two-Bladed Seal Model

For the static case *x(t) = 0*, the following steady-state condition for the flow-rates across each seal blade applies:

$$\dot{m}_1 = \dot{m}_2 = \dot{m}_3 = ... = \dot{m}_n = \dot{m}$$ (1)

Where *n* is the number of blades in the seal, $\dot{m}_1$ is the flow-rate through area A_1, and $\dot{m}_n$ is the flow-rate through area A_n. Assuming that the fluid passing through the seal is a perfect gas and that the process is isentropic, the mass flow-rate for the unchoked flow condition is given by the St. Venant Equation (Shultz [9]) as:

$$\dot{m}_i = \frac{P_i \cdot A_i}{\sqrt{\gamma \cdot R \cdot T_i}} \cdot \sqrt{\frac{2 \cdot \gamma^2}{\gamma - 1} \cdot \left[\left(\frac{P_{i+1}}{P_i} \right)^{2/\gamma} - \left(\frac{P_{i+1}}{P_i} \right)^{\gamma+1/\gamma} \right]}$$ (2)

For choked flow, the flow-rate becomes independent of the downstream pressure and is given by the expression:

$$\dot{m}_i = \beta \cdot P_i \cdot A_i / \sqrt{T_i} \tag{3}$$

Where $\beta = 0.5283$ for air.

With assumed cavity pressures, the mass flow-rates ($\dot{m}_1$, $\dot{m}_2$, ..., $\dot{m}_n$) can be calculated, and the solution can be iterated until Equation (1) is satisfied.

Dynamic Model

For a journal oscillating with a frequency of vibration ω, the journal motion is assumed to be sinusoidal and given by:

$$x(t) = X \cdot \sin(\omega \cdot t)$$

In this case, there will be a variation with time in the pressures within the cavities. Writing the conservation of mass equation:

$$\begin{array}{ccc} \textit{Rate of flow of} & = & \textit{Rate of flow of} \\ \textit{mass into cavity} & & \textit{mass out of cavity} \end{array} + \begin{array}{c} \textit{Rate of change of} \\ \textit{mass in cavity} \end{array}$$

Which can be stated symbolically as:

$$\dot{m}_i = \dot{m}_{i+1} + \frac{\partial}{\partial t}\left(\rho_{i+1} \cdot V_{i+1}\right) \tag{4}$$

The latter part of the right side of this equation is an expression for the rate of

change of mass in the pocket due to time variations of the density and volume, which can be expanded as follows:

$$\frac{\partial}{\partial t}\left(\rho_i \cdot V_i\right) = V_i \cdot \frac{\partial \rho_i}{\partial t} + \rho_i \cdot \frac{\partial V_i}{\partial t}$$

$$\therefore \frac{\partial}{\partial t}\left(\rho_i \cdot V_i\right) = V_i \cdot \frac{\partial \rho_i}{\partial P_i} \cdot \frac{\partial P_i}{\partial t} + \rho_i \cdot \frac{\partial V_i}{\partial t} \tag{5}$$

For an ideal gas, $P = c\rho^\gamma$ where c is a constant. Taking the natural logarithm of this expression and differentiating yields:

$$\frac{1}{P} - \frac{\gamma}{\rho} \cdot \frac{\partial \rho}{\partial P} = 0 \qquad \therefore \frac{\partial \rho}{\partial P} = \frac{\rho}{P \cdot \gamma}$$

For a perfect gas, $P = \rho R T$, therefore:

$$\frac{\partial \rho}{\partial P} = \frac{1}{\gamma \cdot R \cdot T}$$

Hence, from Equation (5):

$$\frac{\partial}{\partial t}\left(\rho_i \cdot V_i\right) = \frac{V_i}{\gamma \cdot R \cdot T_i} \cdot \frac{\partial P_i}{\partial t} + \frac{P_i}{R \cdot T_i} \cdot \frac{\partial V_i}{\partial t}$$

Substituting this expression in Equation (4):

$$\dot{m}_i - \dot{m}_{i+1} = \left(\frac{V_{i+1}}{\gamma \cdot R \cdot T_{i+1}}\right) \cdot \frac{\partial P_{i+1}}{\partial t} + \left(\frac{P_{i+1}}{R \cdot T_{i+1}}\right) \cdot \frac{\partial V_{i+1}}{\partial t} \tag{6}$$

In this form, the difference in the mass flow-rates across two consecutive blades is a function of two time-dependent parameters; the pressure $P_{i+1}(t)$ in the ith cavity and the pocket volume $V(t)$ (which is a function of the journal displacement $x(t)$).

$$\dot{m}_i - \dot{m}_{i+1} = f\left(P_{i+1}(t), x(t)\right) \tag{7}$$

Equation (7) can be expanded in the form of a Taylor Series up to first order derivatives as follows:

$$\dot{m}_i - \dot{m}_{i+1} = \left.\frac{\partial \dot{m}_i}{\partial P_{i+1}}\right|_{P_{i+1}} \cdot P_{i+1}(t) + \left.\frac{\partial \dot{m}_i}{\partial x}\right|_{x} \cdot x(t) - \left.\frac{\partial \dot{m}_{i+1}}{\partial P_{i+1}}\right|_{P_{i+1}} \cdot P_{i+1}(t) + \left.\frac{\partial \dot{m}_{i+1}}{\partial x}\right|_{x} \cdot x(t) \tag{8}$$

Substituting Equation (8) into Equation (6) yields:

$$\left.\frac{\partial \dot{m}_i}{\partial P_{i+1}}\right|_{P_{i+1}} \cdot P_{i+1}(t) + \left.\frac{\partial \dot{m}_i}{\partial x}\right|_{x} \cdot x(t) - \left.\frac{\partial \dot{m}_{i+1}}{\partial P_{i+1}}\right|_{P_{i+1}} \cdot P_{i+1}(t) - \left.\frac{\partial \dot{m}_{i+1}}{\partial x}\right|_{x} \cdot x(t)$$

$$= \left(\frac{V_{i+1}}{\gamma \cdot R \cdot T_{i+1}}\right) \cdot \frac{\partial P_{i+1}}{\partial t} + \left(\frac{P_{i+1}}{R \cdot T_{i+1}}\right) \cdot \frac{\partial V_{i+1}}{\partial t}$$

$$\therefore \left(\frac{\partial \dot{m}_i}{\partial P_{i+1}} - \frac{\partial \dot{m}_{i+1}}{\partial P_{i+1}}\right) \cdot P_{i+1} + \left(\frac{\partial \dot{m}_i}{\partial x} - \frac{\partial \dot{m}_{i+1}}{\partial x}\right) \cdot x$$

$$= \left(\frac{V_{i+1}}{\gamma \cdot R \cdot T_{i+1}}\right) \cdot \frac{\partial P_{i+1}}{\partial t} + \left(\frac{P_{i+1}}{R \cdot T_{i+1}}\right) \cdot \frac{\partial V_{i+1}}{\partial t} \tag{9}$$

The partial derivatives with respect to pressure of Equation (9) can be expanded as:

$$\frac{\partial \dot{m}_i}{\partial P_{i+1}} = \frac{1}{2} \cdot \frac{P_i \cdot A_i}{\sqrt{\gamma \cdot R \cdot T_i}} \cdot \left[\frac{\dfrac{4 \cdot \gamma}{(\gamma - 1) \cdot P_i} \cdot \left(\dfrac{P_{i+1}}{P_i} \right)^{(2-\gamma)/\gamma} + \dfrac{2 \cdot \gamma \cdot (\gamma + 1)}{(k - 1)} \cdot \left(\dfrac{P_{i+1}}{P_i} \right)^{1/\gamma}}{\sqrt{\dfrac{2 \cdot \gamma^2}{\gamma - 1} \cdot \left[\left(\dfrac{P_{i+1}}{P_i} \right)^{2/\gamma} + \left(\dfrac{P_{i+1}}{P_i} \right)^{(\gamma+1)/\gamma} \right]}} \right]$$

$$\frac{\partial \dot{m}_i}{\partial P_i} = \frac{1}{2} \cdot \frac{P_i \cdot A_i}{\sqrt{\gamma \cdot R \cdot T_i}} \cdot \left[\frac{\dfrac{4 \cdot \gamma \cdot P_{i+1}}{(\gamma - 1) \cdot P_i^2} \cdot \left(\dfrac{P_{i+1}}{P_i} \right)^{(2-\gamma)/\gamma} + \dfrac{2 \cdot \gamma \cdot (\gamma + 1) \cdot P_{i+1}}{(\gamma - 1) \cdot P_i^2} \cdot \left(\dfrac{P_{i+1}}{P_i} \right)^{1/\gamma}}{\sqrt{\dfrac{2 \cdot \gamma^2}{\gamma - 1} \cdot \left[\left(\dfrac{P_{i+1}}{P_i} \right)^{2/\gamma} + \left(\dfrac{P_{i+1}}{P_i} \right)^{(\gamma+1)/\gamma} \right]}} \right]$$

The journal orbit can be represented by the superposition of two displacements, $x(t)$ and $y(t)$, along orthogonal axes. In Shultz's [9] model, the orthogonal axes were drawn so that they bisected each of the four pockets, as shown in Figure 3. Displacing the journal a distance x along one axis results in a reduction in the clearance between the journal and the seal blades over the arc length of the pocket towards which the journal was displaced. Due to the curvatures of the blades and the journal, the reduction in clearance will be greatest at the midpoint of the arc. Shultz [9], however, made the assumption that the reduction in clearance is equal to the journal displacement x over the entire arc length. The initial axial flow area and the change in flow area at the ith cavity are given by the following equations in which d is the journal diameter, d_{si} is the inner diameter of the seal, N is the number of pockets, and $\pi d/N$ is the length of the arc between the partition walls.

$$A_i = \frac{\pi \cdot \left(d_{si}^2 - d^2\right)}{4 \cdot N} \qquad\qquad \Delta A_i = \frac{\pi \cdot d \cdot x}{N}$$

Shultz's [9] predictions using this approximated model accurately matched his experimental results. In the case of a seal with more than four pockets, the shorter arc length of each pocket means that the above equation for ΔA_i matches the actual change in area more accurately.

If cross-coupled force coefficients exist, they would be caused by pressure differences between the pockets on the side (pockets B and D along the y axis of Figure 3). However, the x motion of the journal produces only a small change in the clearance areas on the sides. Furthermore, these changes are equal and simultaneous (that is, in phase), so the dynamic pressures are in phase.

The derivatives of the mass flow-rates with respect to the journal displacement can therefore be expanded as follows:

$$\frac{\partial \dot{m}_i}{\partial x} = \frac{\pi \cdot d \cdot P_i}{N \cdot \sqrt{\gamma \cdot R \cdot T_i}} \cdot \sqrt{\frac{2 \cdot \gamma^2}{\gamma - 1} \cdot \left[\left(\frac{P_{i+1}}{P_i}\right)^{2/\gamma} - \left(\frac{P_{i+1}}{P_i}\right)^{\gamma+1/\gamma}\right]}$$

$$\frac{\partial \dot{m}_{i+1}}{\partial x} = \frac{\pi \cdot d \cdot P_{i+1}}{N \cdot \sqrt{\gamma \cdot R \cdot T_{i+1}}} \cdot \sqrt{\frac{2 \cdot \gamma^2}{\gamma - 1} \cdot \left[\left(\frac{P_{i+2}}{P_{i+1}}\right)^{2/\gamma} - \left(\frac{P_{i+2}}{P_{i+1}}\right)^{\gamma+1/\gamma}\right]}$$

$$\frac{\partial \dot{m}_i}{\partial x} = \frac{\pi \cdot d}{N \cdot A_i} \cdot \dot{m}_i \qquad\qquad \frac{\partial \dot{m}_{i+1}}{\partial x} = \frac{\pi \cdot d}{N \cdot A_{i+1}} \cdot \dot{m}_{i+1}$$

To obtain a more compact form of the equations for seal stiffness and damping, the following variables will be used:

$$a_i = \frac{V_i}{\gamma \cdot R \cdot T_{i+1}} \qquad\qquad b_i = \left(\frac{\partial \dot{m}_i}{\partial P_{i+1}} - \frac{\partial \dot{m}_{i+1}}{\partial P_{i+1}} \right)$$

$$(10)$$

$$d_i = \left(\frac{\partial \dot{m}_i}{\partial x} - \frac{\partial \dot{m}_{i+1}}{\partial x} \right) \qquad\qquad e_i = \frac{-P_{i+1} \cdot W_i \cdot d}{N \cdot R \cdot T_{i+1}}$$

These four variables simplify Equation (9) into the following form:

$$a_i \cdot \frac{P_{i+1}(t)}{\partial t} + b_i \cdot P_{i+1}(t) + d_i \cdot x(t) + e_i \cdot \frac{\partial x(t)}{\partial t} = 0 \qquad\qquad (11)$$

Differentiating the assumed sinusoidal displacement of the rotor results in an expression for the time-varying journal velocity.

$$\dot{x}(t) = \frac{dx(t)}{dt} = \omega \cdot X \cdot \cos(\omega \cdot t)$$

The force developed in the seal is proportional to the time dependent displacement and velocity of the journal and the seal can be modeled using the spring-mass-damper system shown in Figure 4.
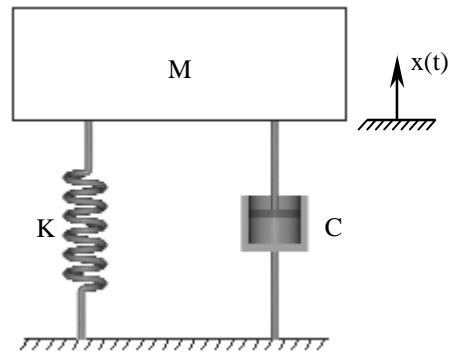
Figure 4 Single Degree of Freedom Model

As a result of the assumed motion of the journal, the seal force will be of a similar form and can be represented by:

$$F(t) = K \cdot x(t) + C \cdot \dot{x}(t) = F_c \cdot \cos(\omega \cdot t) + F_s \cdot \sin(\omega \cdot t) \tag{12}$$

Since this force is developed due to the pressures in the cavities, it can be assumed that the dynamic pressure is given by:

$$P_d(t) = P_c \cdot \cos(\omega \cdot t) + P_s \cdot \sin(\omega \cdot t)$$

The pressure in a given cavity at any instant in time is the summation of this dynamic pressure and the static pressure. The expressions for the cavity pressure and its time derivative are given in Equation (13).

$$P_i(t) = \underbrace{\overline{P_i}}_{\text{Static Pressure}} + \underbrace{P_{ci}(t) \cdot \cos(\omega \cdot t) + P_{si}(t) \cdot \sin(\omega \cdot t)}_{\text{Dynamic Pressure}}$$

(13)

$$\therefore \frac{\partial P_i}{\partial t} = \omega \cdot P_{si}(t) \cdot \cos(\omega \cdot t) - \omega \cdot P_{ci}(t) \cdot \sin(\omega \cdot t)$$

Substituting the sinusoidal pressure expression of Equation (13) and the journal displacement and velocity expressions into Equation (11) and separating sine and cosine terms yields two expressions in the two pressure coefficients P_{si} and P_{ci} unknowns.

$$a_i \cdot \omega \cdot P_{si} + b_i \cdot P_{ci} + e_i \cdot \omega \cdot X = 0$$

$$-a_i \cdot \omega \cdot P_{ci} + b_i \cdot P_{si} + d_i \cdot X = 0$$

These equations can be solved for the pressure coefficients to give:

$$P_{si} = \frac{-\left(b_i \cdot d_i + a_i \cdot e_i \cdot \omega^2\right)}{b_i^2 + a_i^2 \cdot \omega^2} \cdot X$$

(14)

$$P_{ci} = \frac{\left(a_i \cdot d_i - b_i \cdot e_i\right) \cdot \omega}{b_i^2 + a_i^2 \cdot \omega^2} \cdot X$$

Assuming that the pressure in cavity i acts on an area A_{Pi}, the direct rotordynamic coefficients of the seal can be obtained from Equations (12) and (14).

$$K_i = \frac{-\left(b_i \cdot d_i + a_i \cdot e_i \cdot \omega^2\right)}{b_i^2 + a_i^2 \cdot \omega^2} \cdot A_{Pi}$$

(15)

$$C_i = \frac{\left(a_i \cdot d_i - b_i \cdot e_i\right)}{b_i^2 + a_i^2 \cdot \omega^2} \cdot A_{Pi}$$

These coefficients are highly dependent on the frequency of vibration of the journal. They are, however, independent of the amplitude of that vibration, due to the first-order expansion (linearization) of Equation (7). The results of this derivation are the mass flow-rate through the seal and the direct stiffness and direct damping generated in each seal cavity.

SEAL FORCES

The preceding section provided a method of calculating the direct rotordynamic coefficients of a pocket damper seal given the seal geometry, the pressure conditions, and the properties of the fluid. This section describes the equations relating the rotordynamic coefficients to experimentally measured parameters in the test rig of Chapter IV.

If an external excitation force is applied to the seal, a portion of this force goes into overcoming the seal's inertia forces while the remaining portion is reacted by the pressure forces generated in the seal. This was expressed mathematically by Childs and Hale [16] for hydrostatic bearings.

$$\begin{Bmatrix} \ddot{x}_S \\ \ddot{y}_S \end{Bmatrix} \cdot m_S = \begin{Bmatrix} f_x \\ f_y \end{Bmatrix} + \begin{Bmatrix} f_{Sx} \\ f_{Sy} \end{Bmatrix} \tag{16}$$

Expanding the seal forces leads to the following form of the equations of motion:

$$\begin{Bmatrix} f_x - m_S \cdot \ddot{x}_S \\ f_y - m_S \cdot \ddot{y}_S \end{Bmatrix} = \begin{bmatrix} K_{xx} & K_{xy} \\ K_{yx} & K_{yy} \end{bmatrix} \cdot \begin{Bmatrix} \Delta x \\ \Delta y \end{Bmatrix} + \begin{bmatrix} C_{xx} & C_{xy} \\ C_{yx} & C_{yy} \end{bmatrix} \cdot \begin{Bmatrix} \Delta \dot{x} \\ \Delta \dot{y} \end{Bmatrix} + \begin{bmatrix} M_{xx} & M_{xy} \\ M_{yx} & M_{yy} \end{bmatrix} \cdot \begin{Bmatrix} \Delta \ddot{x} \\ \Delta \ddot{y} \end{Bmatrix}$$

Childs and Hale [16] transform Equation (16) into the frequency domain expression given by Equation (17) using a Fast Fourier Transform.

$$\begin{Bmatrix} F_x - m_S \cdot A_x \\ F_y - m_S \cdot A_y \end{Bmatrix} = \begin{bmatrix} H_{xx} & H_{xy} \\ H_{yx} & H_{yy} \end{bmatrix} \cdot \begin{Bmatrix} D_x \\ D_y \end{Bmatrix} \tag{17}$$

F_i, A_i, and D_i are the Fast Fourier Transforms of the time dependent measured forces, accelerations, and relative displacements. The impedances in Equation (17) are given by:

$$H_{ij} = K_{ij} + i\left(\omega \cdot C_{ij}\right) - \omega^2 \cdot M_{ij} \tag{18}$$

Equation (17) represents a system of two equations in four unknowns. In order to obtain a total of four equations required to solve for the impedances, two sets of data are needed; one for an excitation in each orthogonal direction.

$$\begin{bmatrix} F_{xx} - m_S \cdot A_{xx} & F_{yx} - m_S \cdot A_{yx} \\ F_{xy} - m_S \cdot A_{xy} & F_{yy} - m_S \cdot A_{yy} \end{bmatrix} = \begin{bmatrix} H_{xx} & H_{xy} \\ H_{yx} & H_{yy} \end{bmatrix} \cdot \begin{bmatrix} D_{xx} & D_{yx} \\ D_{xy} & D_{yy} \end{bmatrix} \tag{19}$$

The added mass terms of Equation (18) are negligible for labyrinth seals (Childs [17]) and the impedance expression can be simplified to the sum of the stiffness and damping terms.

The force, acceleration, and displacement data obtained experimentally is used to calculate the impedances from Equation (19). The rotordynamic coefficients are then obtained by separating Equation (18) into real and imaginary parts and solving for K_{ij} and C_{ij}.

The direct coefficients obtained using this method can be compared with those resulting from the pocket damper seal analysis of the previous section.

DAMPER SEAL CODE

The basic assumption on which the damper seal code's leakage calculation is based is that the steady-state mass flow-rate through each constriction created by the seal's blades and the journal is the same. Based on this, a logical starting point is to assume a constant value for the mass flow-rate and to then employ a corrective iterative algorithm to obtain the actual value of the flow-rate. The required input parameters to the code are the inlet and exit pressures, the seal geometry, and the properties of the fluid. These variables are related to each other and to the flow-rate by Equation (2).

The three main variables involved in the algorithm are the pressure in a given cavity, the pressure directly upstream of that cavity, and the mass flow-rate through the constriction at the inlet to that cavity.

Since the mass flow-rate is initially assumed, its value and the value of the inlet pressure are known quantities. The only unkown is thus the pressure downstream of the first constriction. This pressure can be calculated from Equation (2) and is used as the upstream pressure to calculate the pressure downstream of the second constriction. In this way, all the pressures can be calculated until a value of the pressure downstream of the last constriction (the back pressure) is obtained. This method is analagous to Holzer's method, which Vance [18] employs for torsional vibration calculations.

This final obtained pressure will match the prescribed exit pressure when the guess for the mass flow-rate is correct. A calculated final pressure that is higher than the specified exit pressure indicates that not enough fluid is leaking through the seal and that the guess for the flow-rate needs to be raised. If the final pressure is lower than the exit pressure, then the guess for the flow-rate is too high and needs to be lowered.

The code can be divided into sections responsible for input, initial estimation of the flow-rate, calculation of the pressures, correction of the flow-rate, final checks on obtained values, and output.

Calculation of Pressures

Input parameters such as fluid properties, seal geometry, and inlet and exit pressures are read and modified as needed. The input values are converted to the appropriate unit system. These data are used to calculate other needed parameters such as constriction areas and pressure drops as well as constants for use in later equations.

The iterative algorithm used to sequentially calculate each cavity pressure is based on solving the St. Venant equation in the slightly modified form of Equation (20).

$$f\left(\dot{m}, P_n, P_{n+1}\right) = \dot{m}_n^2 - \left[\frac{P_n^2 \cdot A_n^2}{\gamma \cdot R \cdot T_n} \cdot \frac{2 \cdot \gamma^2}{\gamma - 1} \cdot \left[\left(\frac{P_{n+1}}{P_n} \right)^{2/\gamma} - \left(\frac{P_{n+1}}{P_n} \right)^{\gamma+1/\gamma} \right] \right] = 0 \qquad (20)$$

The terms of the equation are squared so as to avoid problems with negative numbers under the square root during iteration. In this form, the solution of the equation is the point of intersection of the curve representing the function *f* with the pressure axis. Figure 5 is a sample plot of this function with inlet and exit pressures of 900 Psi (6.90 MPa) and 500 Psi (3.45 MPa) respectively (represented by the two vertical lines).
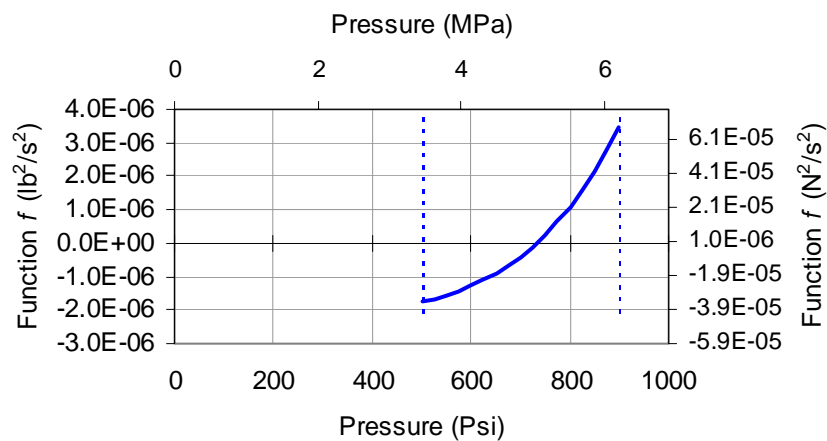
Figure 5 Sample Cavity Pressure Calculation Plot

If $f < 0$, the pressure estimate for a given cavity is too low and needs to be increased. If $f > 0$, then the estimate is too high. A change in the sign of f indicates that the correct value of the pressure is between the current and the last values of the pressure. The incremental change in pressure is then halved and the process continues until the difference between the results of two consequtive iterations is less than an acceptably small predetermined percentage of the newly obtained pressure.

Calculation of Mass Flow-Rate

Before the pressures can be calculated as described above, an initial estimate of the flow-rate must be provided. An estimate that is too high will lead to the function f not intersecting the pressure axis and no solution will be found.

The code first assumes a linear pressure distribution in the seal cavities and calculates the flow-rate across each constriction. The minimum flow-rate value is used as an initial estimate. This value is then checked to see whether or not the function f has a negative value for pressures close to the exit pressure. If this is not the case, then the estimate is too high and is lowered by 25%. The two pressures used in the equation to calculate f are taken as P_{exit} and 110% of P_{exit}.

As mentioned above, if the final pressure is lower than the exit pressure, the flow-rate must be reduced, and if the final pressure is higher than the exit pressure, the flow-rate is too low. As was the case with the incremental change in pressure, the incremental change in flow-rate with each iteration is halved every time the status of the flow-rate changes from being too high to too low and vice versa. Several constants are incorporated into the algorithm to speed up convergence.

Two main checks are carried out as part of the solution. These checks allow the code to run in two special cases: if the flow through any of the constrictions is choked or if the inlet and exit pressure values are close to each other. The algorithm, in a sense,

automatically takes care of the first check. When the flow through a given cavity is choked, the code will not be able to find a cavity pressure that satisfies Equation (20). If this is the case, the code exits the mass flow-rate correction loop and calculates the pressures in the downstream cavities of the constriction through which the flow-rate has been identified as being choked using the modified equation for choked flow.

When the inlet and exit pressure values are close to each other (for example 1000 Psi (6.90 MPa) and 998 Psi (6.88 MPa)), the stopping criteria for the iterative process may be too large. If this is the case, the cavity pressures returned by the code may be lower than the exit pressure or higher than the inlet pressure. The ratio of the pressure drop to the inlet pressure is checked and the stopping criteria is modified accordingly so as to avoid this.

Finally, the code presents the output of the algorithm. This output is in the form of the cavity pressures, the pressure ratios across each constriction, the mass flow-rate, and an indication of which cavities, if any, are downstream of constrictions through which flow is choked. This output is then used to calculate the stiffness and damping of the seal based on the equations presented in this chapter.

CHAPTER IV

TEST-RIG AND METHODOLOGY

The facility used to test the seals was initially built to test hydrostatic bearings at the Turbomachinery Laboratory. It has since then been modified to test annular gas seals. A high pressure pipeline from the nearby wind-tunnel provides air at pressures of up to 2500 Psi. A schematic of the test facility is shown in Figure 6 (from Picardo [19]). The rig consists of a rotor connected by a coupling to a gearbox with the test seals mounted in a stator assembly around the rotor.
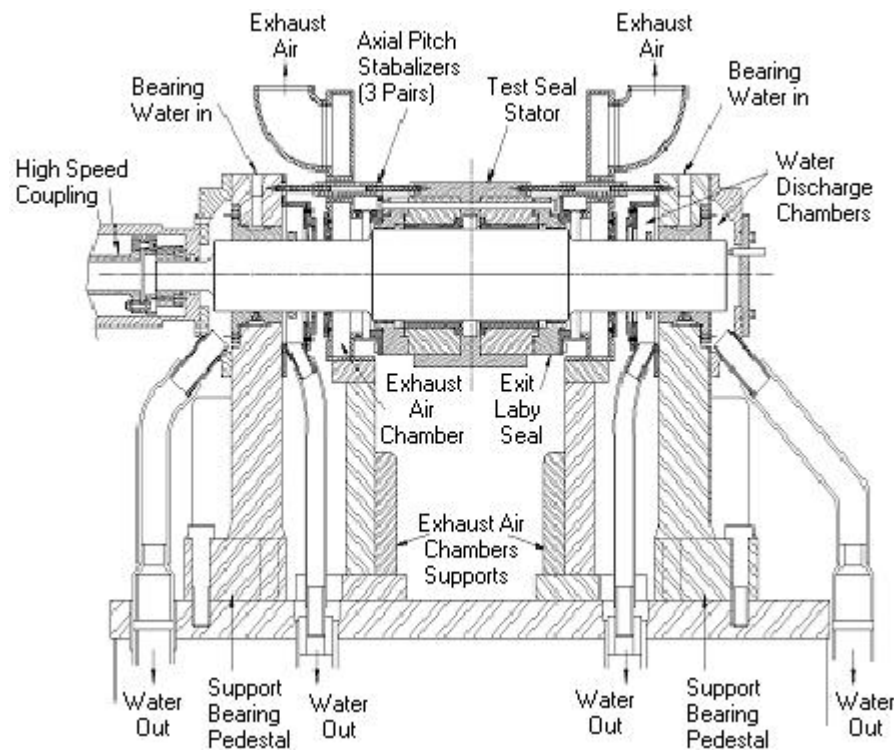
Figure 6 Annular Gas Seal Test-Rig Schematic

The stator is connected to two Zonic® shakers. The rotor is mounted on hydrostatic bearings with a separate water supply system. The rotor is stiff and well balanced and the bearings on which it is mounted have high stiffness. Two air-buffer seals utilizing shop air at 110 Psi (0.76 MPa) prevent leakage of the bearing water.

Figure 7 Assembled Test-Rig

Air enters the assembly through the center of the stator and moves axially outwards through two sets of identical seals. The pressure drop across the seals can be controlled by varying the inlet pressure and by opening or closing the back-pressure valve, thus modifying the seal's exit pressure. A photograph of the test rig (with the stator assembly installed) is shown in Figure 7. A more detailed description of the test facility was given by Childs and Hale [16]. This test rig is concurrently being used to test hole-pattern seals and labyrinth seals.

The stator assembly, shown in Figure 8, consists of five components; a brass stator, two steel pocket damper seals, and two aluminum labyrinth seals. The stator holds the seals in place and provides a method of connection to the shakers and the pressure, temperature, and vibration sensors.

Figure 8 Stator Assembly

The labyrinth seals at either end of the stator control the pressure drop across the test seals by regulating the back-pressure. With the back-pressure valve fully open, there should be almost no flow across the labyrinth seals, and the PDS exit pressure will be on the order of 150 Psi (1.03 MPa). With the valve fully closed, the back-pressure is maintained by the labyrinth seals.

Two seals were tested, a twelve-bladed seal and an eight-bladed seal (Figure 9). Both seals were first tested with a one-to-one clearance ratio and then had their exit blades notched to provide a 1:2 clearance ratio for the twelve-bladed seal and a 1:1.5 clearance ratio for the eight-bladed seal. These notches serve to provide the desired overall positive direct damping in the seal. The actual inside diameters of all the blades are identical. The seals are placed back-to-back in the stator so as to minimize the resulting axial thrust.

In the case of the twelve-bladed seal, the inlet blades for each cavity are beveled on the upstream side, and the exit blades for each cavity are beveled on the downstream side. This could be a major factor in the higher leakage characteristics of the twelve-bladed seal that are to be discussed later.

Figure 9 12-Bladed (left) and 8-Bladed (right) Pocket Damper Seals
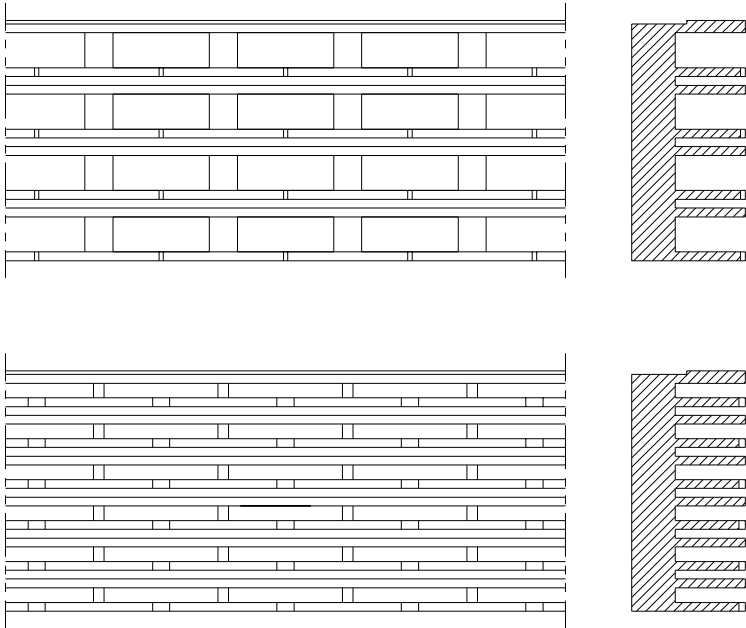
Figure 10 Unwrapped Views of Diverging 8-Bladed (upper) and 12-Bladed (lower) Seals

Table 1 lists the major dimensions of the diverging configurations of the two seals.

The actual seals are 0.05 inches (1.27 mm) longer than the lengths listed in this table. Four O-rings are located at each interface between the stator and either damper seal as well as between each damper seal and its corresponding exit labyrinth seal. The first (upstream) blade of each seal is slightly thicker than the remaining blades. This feature (shown in Figure 10) extends for about half the radial thickness of the seal, thus creating a recess between the stator and the seal, which serves as a safety mechanism in case of an O-ring rupture.

Table 1 Major Dimensions of Test Seals

	8-Bladed Seal		12-Bladed Seal	
	(inches)	(mm)	(inches)	(mm)
Length	3.375	85.73	3.375	85.73
Inner Diameter	4.51	114.55	4.51	114.55
Radial Inlet Clearance	0.005	0.13	0.005	0.13
Radial Exit Clearance	0.0075	0.19	0.010	0.25
Pocket Depth	1.0	25.40	1.4	35.56
Number of Pockets	8	8.00	8	8
Wall Thickness	0.4	10.16	0.3	7.62
Blade Thickness	0.125	3.18	0.125	3.18
Active Pitch	0.5	12.70	0.2083	5.29
Dead Pitch	0.125	3.18	0.125	3.18

There are several differences between the designs of Figure 10 and the actual seals. These differences prove to have significant effects on seal leakage and are discussed in Chapter IX. Four proximity probes are used to measure the displacement of the stator with respect to the rotor in orthogonal directions in two different planes (one through each exit labyrinth seal) perpendicular to the axis of the rotor. Accelerometers are installed in orthogonal directions in the central plane of the stator. Pressure probes pass through the stator and into the seal to monitor pocket pressures, while pressure probes in the central plane and just upstream of the labyrinth seal teeth monitor the inlet pressure

and exit pressures respectively.

     The experiments that were carried out took place on the test-rig described above. The test seals were installed in the stator assembly and assembled onto the test-rig. Rather than the more usual form of excitation of a stationary housing and a vibrating rotor, the test rig has a rigid rotor (Figure 11) mounted on bearings with high stiffness. The shakers vibrate the housing and the proximity probes monitor the resultant relative stator-to-rotor displacement.

Figure 11 Test Rotor

     The accelerometers are used to calculate the inertia forces required to accelerate the stator. These forces are then removed from the relevant equations, thereby leaving only the forces that are applied to the fluid in the seals. The seals were tested at three different speeds (10,200 RPM, 15,200 RPM, and 20,200 RPM) and with several different pressure drops across the seals. The real and imaginary parts of the transfer function that is obtained result, respectively, in the stiffness and damping parameters (the damping is given by the value of the imaginary part of the impedance function divided by the test frequency). These values are for the entire assembly, and so, any effects not caused by the test seals must be removed. For this purpose, a baseline test is conducted using smooth inserts or "blanks" (Figure 12) in place of the seals.

Figure 12 Basline Insert

The inserts are installed to maintain the required O-rings in place and to provide a comparable mass to the actual seal tests. Since the pressure drop across the inserts will be far lower than that across the test seals, the inlet pressure during the baseline test is also lower than that for the seal test. This provides the same pressure drop across the labyrinth seals in both cases. It is assumed that the difference in pressure in the inlet plenum of the stator in both tests has no significant effect. Another factor that should be considered is the possible creation of circumferential flow within the inserts, which lack the pocket walls needed to eliminate the destabilizing cross-coupling.

The procedure followed during testing and the method employed for data acquisition are identical to those used by Marquette, Childs, and San Andrés [20]. The calculation of the leakage through the seals is described by Picardo [19] and is the topic of Chapter V.

CHAPTER V

LEAKAGE AND PRESSURE RESULTS

While the rotordynamic characteristics of pocket damper seals can affect the performance of a turbomachine, and are therefore worthy of study, reducing leakage remains the essential purpose of the seals.

The direct stiffness and damping of a pocket damper seal depend on the mass flow-rate through the seal (Chapter III). It is thus essential to ensure that the mass flow model offers an accurate prediction of the leakage through the seal before attempting to use the damper seal code to predict seal coefficients.

DISCHARGE COEFFICIENTS

The St. Venant equation that was used to calculate the flow across the seal blades (Equation 2, Chapter III) was derived for flow through an orifice of round cross-section. It is to be expected that the flow-rate predicted by this equation would not match the flow through the annular section formed by the blades and the journal.

Shultz [9] used discharge coefficients to compensate for the discrepancy between the actual configuration and configuration for which the St. Venant equation was intended.

$$\dot{m}_i = Cd \cdot \frac{P_i \cdot A_i}{\sqrt{\gamma \cdot R \cdot T_i}} \cdot \sqrt{\frac{2 \cdot \gamma^2}{\gamma - 1} \cdot \left[\left(\frac{P_{i+1}}{P_i} \right)^{2/\gamma} - \left(\frac{P_{i+1}}{P_i} \right)^{\gamma+1/\gamma} \right]} \tag{21}$$

In the modified expression for the flow-rate, Equation (21), the numerical value of the discharge coefficient *Cd* differs based on whether the equation is being written for the inlet blade or the exit blade of an active cavity. Shultz [9] determined that the

discharge coefficients that best matched his experimental data were 1.1 for an inlet blade and 0.95 for an exit blade. However, for the tests reported in this thesis, these coefficients significantly over predicted the leakage through the eight-bladed seal, under-predicted the leakage through the twelve-bladed seal, and over-predicted the static cavity pressures for both seals.

Trial runs of the damper seal code revealed that the static cavity pressures are affected by the ratio of the discharge coefficients and not by their absolute magnitude. Figure 13 represents static pressures in the second and third active cavities of the diverging eight-bladed pocket damper seal with inlet and exit pressures of 1007 Psi and 539 Psi (6.92 MPa and 3.72 MPa) respectively.

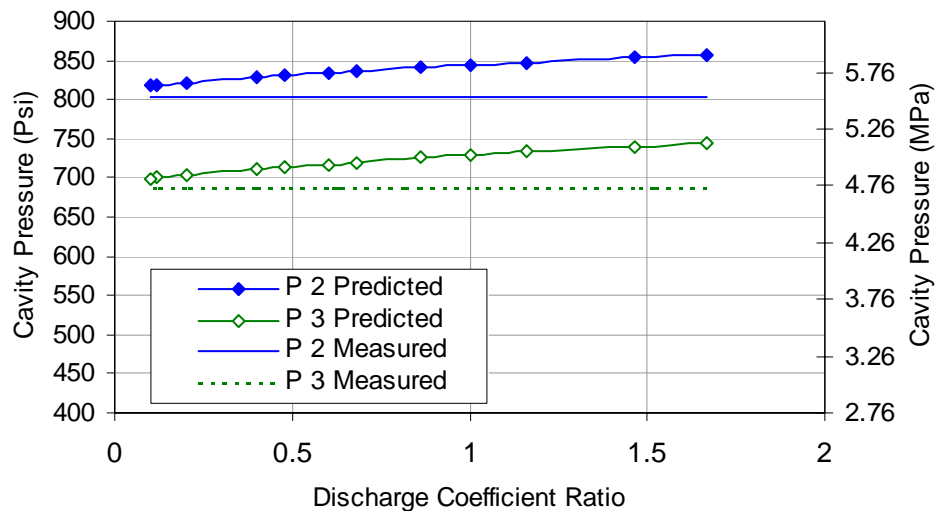
Figure 13 Effect of Discharge Coefficient Ratio on Cavity Pressures

This figure shows that the predicted static pressures match experimental results more closely as the ratio of inlet to exit discharge coefficient decreases.

The predicted leakage through a seal depends on the absolute magnitude of the discharge coefficients, and while using a discharge coefficient ratio close to zero may

closely match pressure readings, the mass flow-rate would be severely under-predicted. There are two possible combinations of discharge coefficients that will result in the same mass flow-rate prediction. The data presented in this chapter are used to obtain new discharge coefficients that more accurately match leakage measurements and that have a ratio that results in acceptably accurate static cavity pressure predictions.

SHAFT GROWTH

Initial analysis of the leakage data showed that there is a significant reduction in leakage as the speed of the rotor increases. At high rotational speeds, the centrifugal forces generated in the material of the rotor increase and cause the rotor to expand. The increase in rotor radius is given by the following equation in which δ is the weight per unit volume of the rotor material (Young [21]).

$$\Delta R = \frac{\delta \cdot \omega^2}{4 \cdot g \cdot E} \cdot (3 + \nu) \cdot R_S^{\,3} \tag{22}$$

Since the clearances between rotor and stator in turbomachines are often a few thousands of an inch wide, any radial expansion in the rotor could be significant.

Figure 14 shows the increase in diameter of the 4.5-inch (114.3-mm) test rotor as the rotational speed is increased. This means that at the highest test speed, the inlet blade radial clearances of the test seals are reduced by about 5%. The importance of taking shaft growth into consideration is made more evident by the results presented in the following sections.
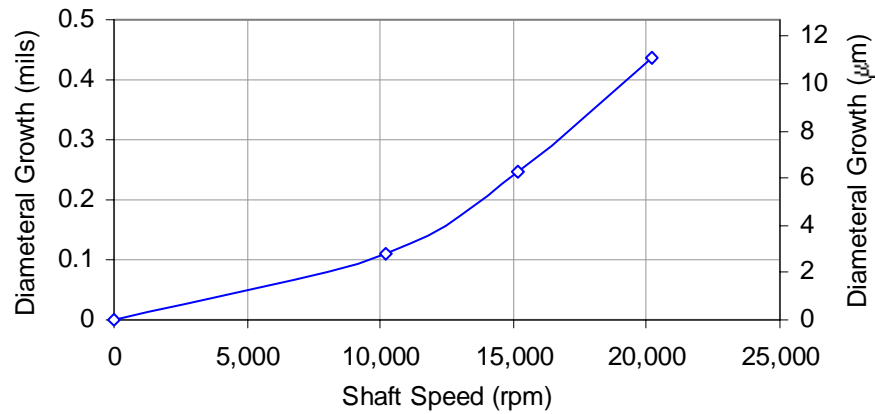
Figure 14 Shaft Growth at High Speeds

LEAKAGE RESULTS

Leakage measurements were taken on the diverging twelve-bladed seal, the straight-through eight-bladed seal, and the diverging eight-bladed seal. The former two seal configurations were tested with three different pressure drops while the latter configuration, due to its high negative stiffness, was only tested with two pressure drops.

Table 2 Average Pressure Conditions for Leakage Tests

Seal	Test ΔP	P_{in}		P_{exit}		ΔP	
		(Psi)	(MPa)	(Psi)	(MPa)	(Psi)	(MPa)
Diverging 12-Bladed	Low	992	6.84	713	4.92	279	1.92
	Intermediate	1009	6.96	458	3.16	551	3.8
	High	1017	7.01	226	1.56	791	5.46
Diverging 8-Bladed	Low	723	4.99	441	3.04	282	1.94
	High	941	6.49	572	3.94	369	2.54
Straight Through 8-Bladed	Low	1027	7.08	525	3.62	502	3.46
	Intermediate	1024	7.06	336	2.32	688	4.74
	High	1024	7.06	129	0.89	895	6.17

For each pressure drop, the seals were tested with rotor speeds of 10,200 RPM, 15,200 RPM, and 20,200 RPM (the diverging eight-bladed seal was also tested at zero rotor speed). For a given seal, the inlet pressure and pressure drop are slightly different for each of these speeds, with a maximum deviation of about 30 Psi (0.67 MPa). Therefore, the results would more accurately be presented in the form of separate plots for each speed and each pressure drop. This is the way in which the leakage data for the straight-through eight-bladed seal is presented. A complete summary of the exact leakage test conditions and the mass flow-rate results for all three seal configurations is given in tabular form in the Appendix. The average test pressures are summarized in Table 2. For the diverging eight and twelve-bladed seals, these average pressures are used and the results are presented on a single plot for each seal.

A comparison of code predictions to experimental data (Figure 15) shows that using the original discharge coefficients that Shultz [9] used for lower pressure seals would lead to significant prediction errors.
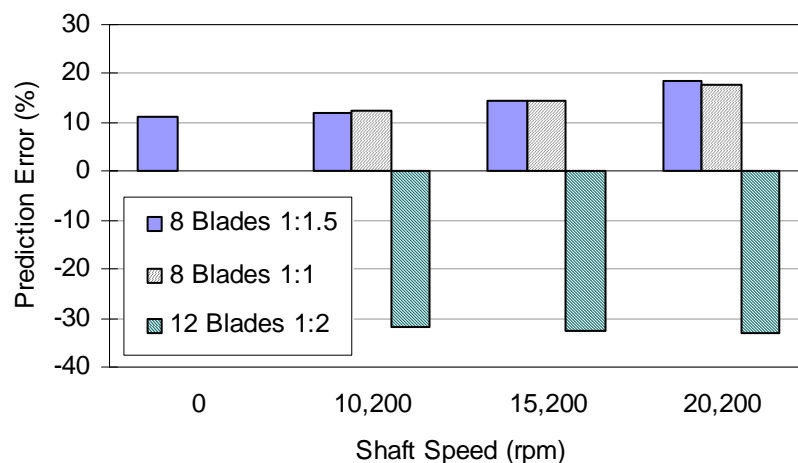
Figure 15 Average Leakage Error (Discharge Coefficients 1.1 Inlet and 0.95 Exit)

The prediction error in Figure 15 is the average of the errors for the different

pressure differences across the seal for each rotor speed. This data takes into consideration shaft growth with speed. Since the original coefficients over-predict the leakage through the eight-bladed seal and under-predict the leakage through the twelve-bladed seal, it is clear that the discharge coefficients that best match the leakage data will be different for each seal. It should be noted that there are significant differences between the blade geometries of the twelve-bladed and eight-bladed seals.

Straight-Through Eight-Bladed Seal

The leakage and static pressure data for the straight-through eight-bladed seal are best matched with an inlet discharge coefficient of 0.75 and an exit coefficient of 0.85. Figure 16, Figure 17, and Figure 18 compare the measured leakage for this seal with predicted values using the damper seal code with these coefficients.
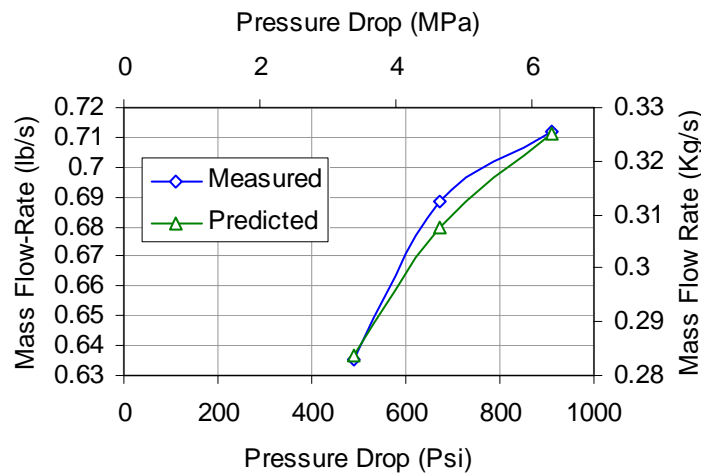
Figure 16 10,200 RPM Leakage (8-Blades, CR = 1:1, Cd_{in} = 0.75 and Cd_{exit} = 0.85)
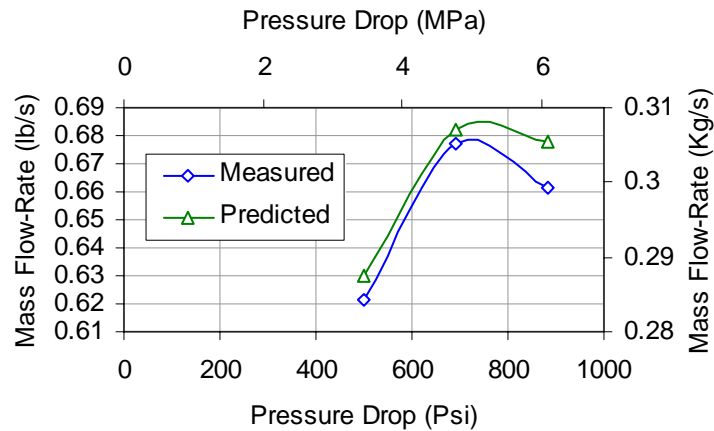
Figure 17 15,200 RPM Leakage (8-Blades, CR = 1:1, Cd_{in} = 0.75 and Cd_{exit} = 0.85)
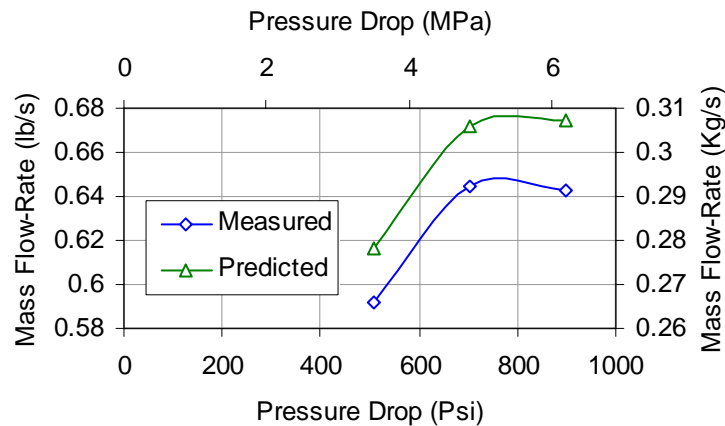
Figure 18 20,200 RPM Leakage (8-Blades, CR = 1:1, Cd_{in} = 0.75 and Cd_{exit} = 0.85)

Even though rotor growth was taken into consideration in this comparison, the damper seal code over-predicts the leakage by a larger amount as the rotor speed increases. The slight drop in flow-rate in the *predicted* curve of Figure 17 is due to the inlet pressure for the third data point being lower than that for the second data point. The code predicts that for the same inlet pressure, the flow-rate will increase with increasing pressure drop. This does not, however, explain why the third *measured* data

points on the plots for both 15,200 rpm and 20,200 rpm show a lower flow-rate than the previous points. For these two pressure drops, the damper seal code predicts choked flow through the last blade of the seal. Theoretically, the flow-rate would increase with increasing pressure drop and would asymptotically approach a maximum value corresponding to the choked flow condition. This does not, however, match the experimental data, which shows a drop in flow-rate after the flow theoretically becomes choked.

Diverging Eight-Bladed Seal

The inlet and exit blade discharge coefficients that best match the leakage data for the 1:1.5 clearance ratio eight-bladed seal are 0.75 and 1.25 respectively. Since the only difference between this seal and the straight-through eight-bladed seal is the inclusion of notches in the exit blades, the same inlet blade coefficient is used for both seals. The exit blade coefficient was increased to match the data. It is important to note that the increased flow area due to the notches is already accounted for in the damper seal code in the form of the exit clearance. The exit blade discharge coefficient merely, as mentioned above, accounts for the difference between the actual flow area and the flow area for which the code equations were intended.

The mass flow-rates through the diverging eight-bladed seal are shown in Figure 19 for two average pressure drops and three rotor speeds.
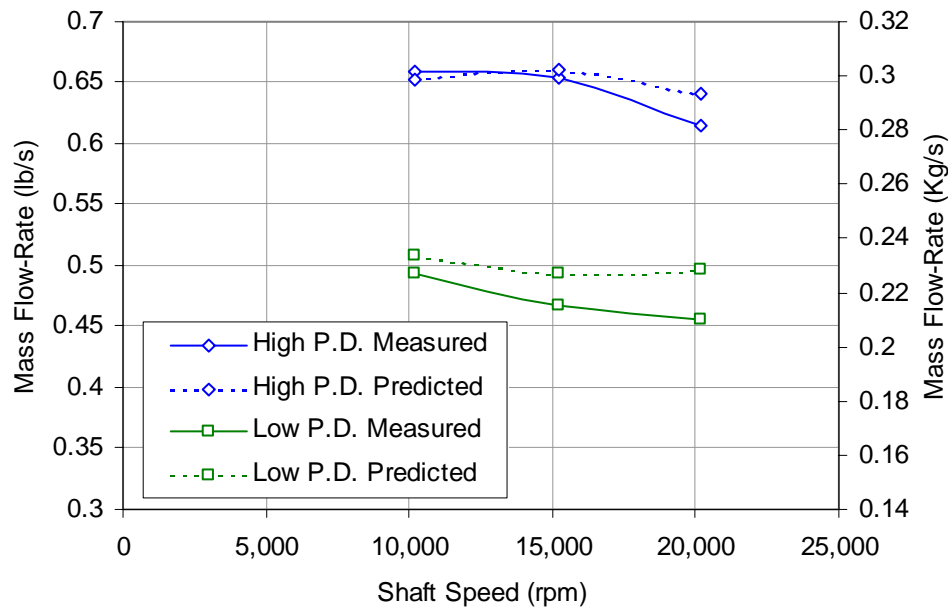
Figure 19 Measured vs. Predicted Leakage - 8-Blades (CR = 1:1.5, Cd_{in} = 0.75 and Cd_{exit} = 1.25)

As can be expected, the measured leakage through the seal decreases with increasing rotor speed for both pressure drops. The high ΔP predicted curve shows a slight increase in leakage at 15,200 rpm over 10,200 rpm. Likewise, the low ΔP curve shows a slight increase in leakage at 20,200 rpm over 15,200 rpm. The increases can be explained by the fact that the inlet pressures for both these cases were slightly higher than the inlet pressures for the previous points (Figure 20).
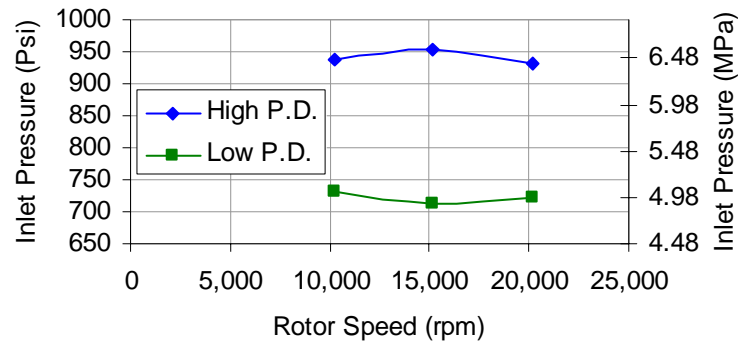
Figure 20 Leakage Test Inlet Pressures (8-Blades, CR = 1:1.5)

These minor inconsistencies in the inlet pressure are apparently large enough to slightly offset the downward trend in leakage with increasing rotor speed.

Diverging Twelve-Bladed Seal

The discharge coefficients that best match experimental results for the diverging twelve-bladed seal are 2.3 for the inlet blades and 2.75 for the exit blades. These values (which are considerably higher than those obtained for the eight-bladed seals) and the corresponding higher leakage rates can, at least in part, be attributed to the blade geometry of the twelve-bladed seal as was mentioned earlier. Leakage data is presented for only one configuration of the twelve-bladed seal, but two different sets of data were taken for the seal during two separate rig assemblies. The results of both sets of tests are almost identical.

The predicted and measured results for this seal with three different rotor speeds and three pressure drops are presented in Figure 21.
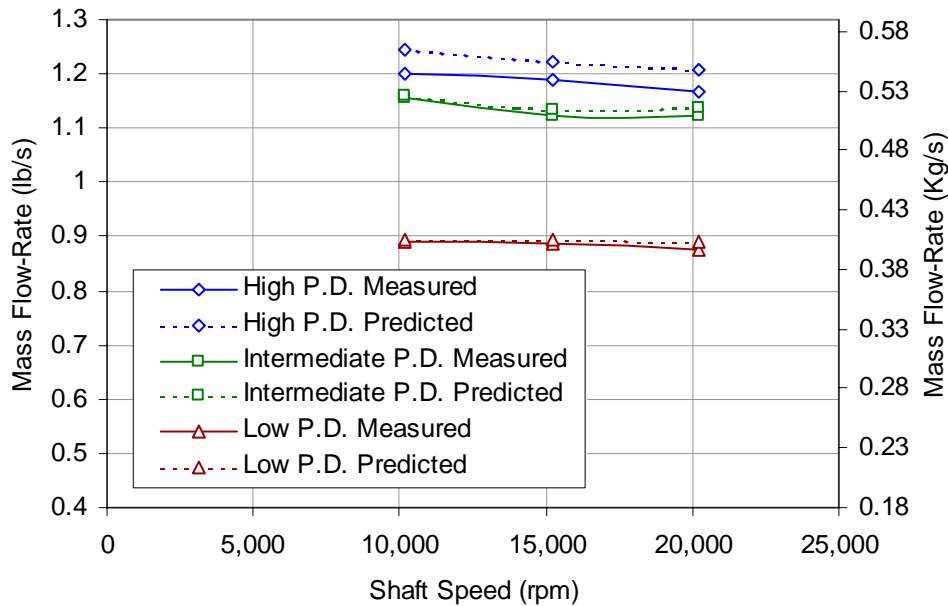
Figure 21 Measured vs. Predicted Leakage - 12-Blades (CR = 1:2, Cd_{in} = 2.3 and Cd_{exit} = 2.75)

Once again, the expected drop in leakage with increasing rotor speed can be seen. The damper seal code predicts that for the high ΔP case, the flow through the last two constrictions of this seal is choked. The marked increase in the over-prediction of the seal's leakage for the high ΔP condition could be due to choked flow in that case.

Prediction Errors

As was mentioned above, the amount by which the damper seal code over-predicts the leakage through a seal increases as the rotor speed increases, even when rotor growth is taken into account. The average percentage over-predictions of flow-rate with and without shaft growth included are shown for the 1:1 CR eight-bladed seal (Figure 22), the 1:1.5 CR eight-bladed seal (Figure 23), and the 1:2 CR twelve-bladed seal (Figure 24). These figures show that while rotor growth accounts for a portion of the over-prediction of flow-rate, there is some other phenomenon, perhaps related to increased

circumferential velocity in the flow, which becomes more pronounced at higher speeds.
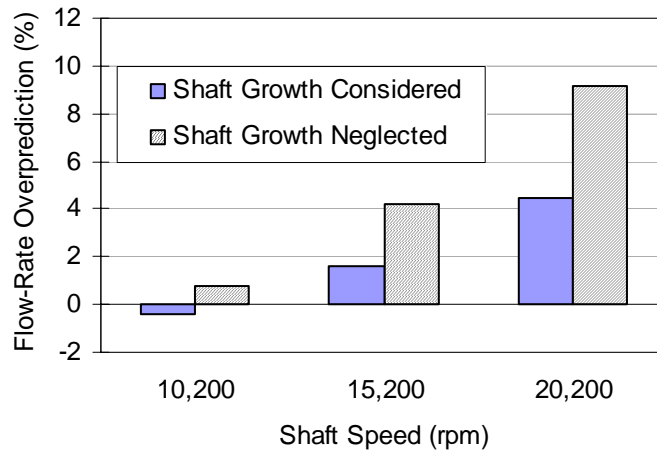
Figure 22 Leakage Over-Prediction (8-Blades, CR = 1:1, Cd_{in} = 0.75 and Cd_{exit} = 0.85)
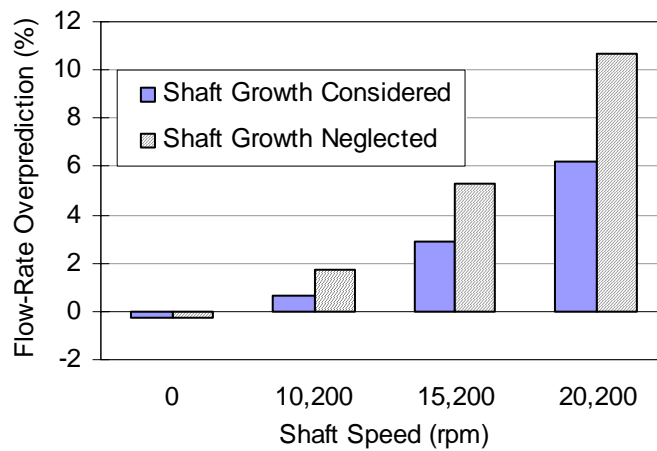
Figure 23 Leakage Over-Prediction (8-Blades, CR = 1:1.5, Cd_{in} = 0.75 and Cd_{exit} = 1.25)
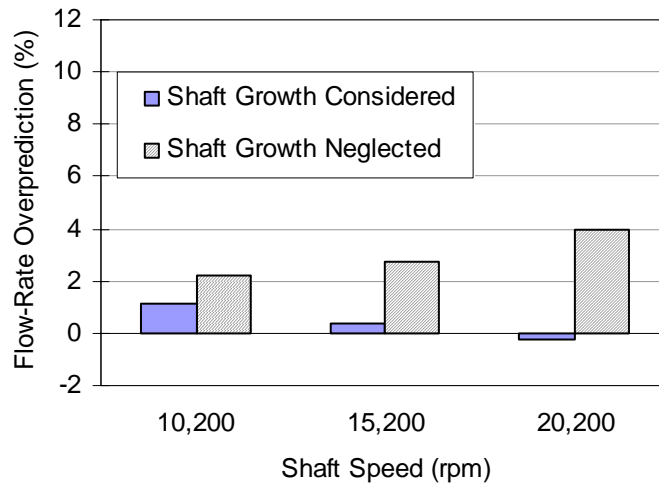
Figure 24 Leakage Over-Prediction (12-Blades, CR = 1:2, Cd_{in} = 2.3 and Cd_{exit} = 2.75)

The error in predicting the leakage through the two configurations of the eight-bladed seal followed a general trend: the over-prediction became more pronounced as either the rotor speed or the pressure drop across the seal increased. The over-prediction of leakage through the diverging twelve-bladed seal also increases with increasing rotor speed, but decreases as the pressure drop across the seal rises. Since the discharge coefficients where altered so that the predicted leakage matched the measured leakage more closely, it could be argued that coefficients could be chosen so that the high pressure drop data is matched closely and the flow-rates for lower pressure drops are under-predicted.

STATIC PRESSURE RESULTS

The discharge coefficients for all three test configurations were chosen so that the inlet to exit coefficient ratio is less than one. This improves the prediction of the static pocket pressures for the eight-bladed seal configurations. Figure 25 shows the static pressures in the second and third active cavities of the straight-through eight-bladed seal and Figure 26 shows the same data for the diverging eight-bladed seal.
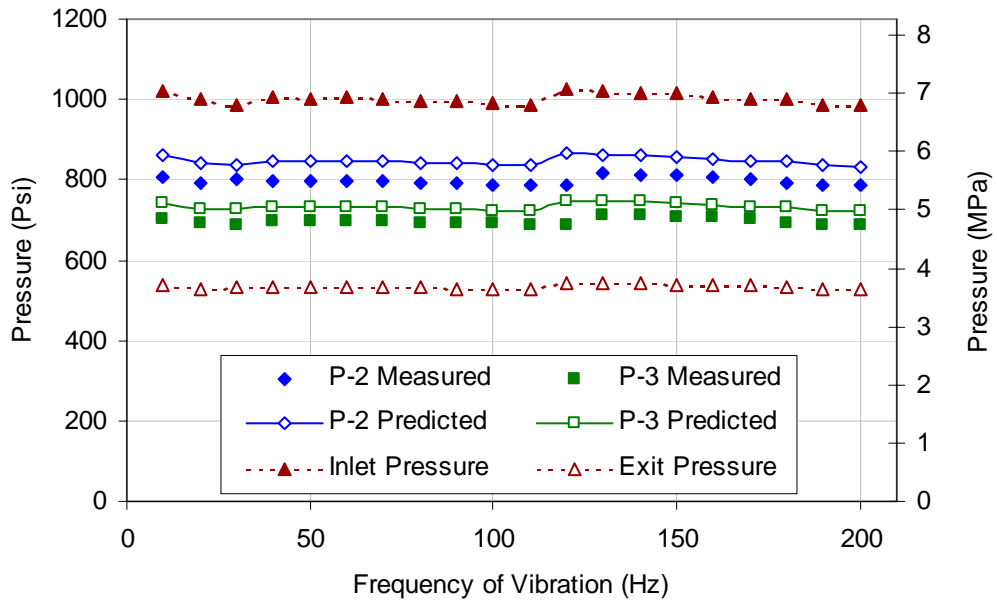
Figure 25 Static Cavity Pressures (8-Blades, CR = 1:1)
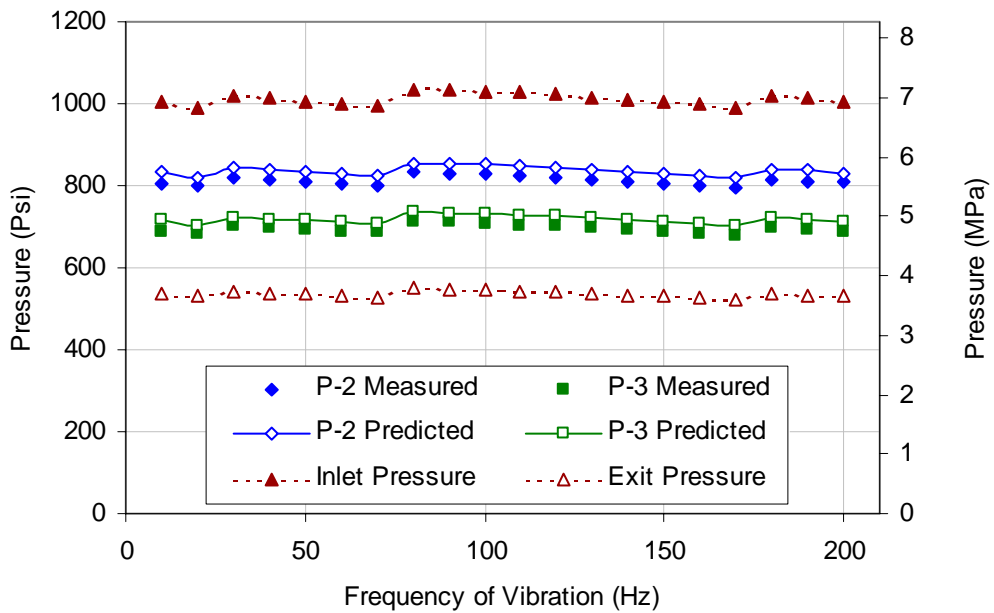
Figure 26 Static Cavity Pressures (8-Blades, CR = 1:1.5)

The static pressure data was taken in conjunction with dynamic pressure measurements (Ertas [22]) taken every 10 Hz from 10 Hz to 200 Hz. The frequency of vibration was not expected to impact the static cavity pressures (an assumption that is supported by the results) and the twenty test frequencies can be thought of as twenty independent test cases.

During the static pressure tests, the inlet pressure was kept as close to 1000 Psi (6.9 MPa) as possible and was raised whenever it dropped below this value. The inlet pressure was raised immediately before the 40 Hz, 60 Hz, and 120 Hz readings for the straight-through seal and immediately before the 30 Hz, 80 Hz, and 180 Hz readings for the diverging seal. The slight deviations in cavity pressures from a constant value are due to these changes in the inlet pressure and not due to any dependency on frequency.

In the case of the straight-through seal, the code over-predicts the second active cavity pressure by an average of 49.9 Psi (0.344 MPa) or 6.3 % and over-predicts the third active cavity pressure by an average of 36.7 Psi (0.253 MPa) or 5.3 %. Since the discharge coefficient ratio ($Cd_{in} : Cd_{exit}$) is smaller for the diverging seal, it was expected that the static pressure data for this seal would be better matched than that for the straight-through seal. This is indeed the case and the average over-predictions of the second and third active cavity pressures in the diverging seal are only 23.3 Psi (0.161 MPa) or 2.9 % and 23.1 Psi (0.159 MPa) or 3.3 % respectively. Table 3 summarizes the discharge coefficients found to best match the experimental leakage and static pressure results for the three seal configurations.

Table 3 Discharge Coefficient Summary

Seal	Inlet Cd	Exit Cd
Straight-Through 8-Bladed	0.75	0.85
Diverging 8-Bladed	0.75	1.25
Diverging 12-Bladed	2.30	2.75

CHAPTER VI

ANALYSIS AND NUMERICAL PREDICTIONS

The phase angle between the pressure vector in a given seal cavity and the vibratory displacement vector can be regarded as a measure of the relative magnitudes and the signs of the stiffness and damping generated in that cavity. Since the seal forces in a pocket damper seal are assumed to be generated solely by the dynamic pressure buildup in the pockets, the force vector resulting from the pressure can be resolved into two components which are in-line with and perpendicular to the direction of vibratory displacement. The seal's stiffness can be derived from the in-line force component while its damping can be derived from the perpendicular component (vector plot shown in Figure 2 of Chapter I). The phase angle is given by the Equation (23).

$$\phi = \tan^{-1}\left(\frac{C_{xx} \cdot \omega}{K_{xx}}\right) \qquad\qquad (23)$$

In designing a pocket damper seal, one of the main objectives is to maximize the damping, which means that it is desirable to get the phase angle as close to 90° as possible. Generally, a pocket damper seal cavity with a diverging clearance produces negative stiffness and positive damping, meaning that the phase angle is greater than 90°.

In attempting to use the phase angle to gauge the effect of various parameters on seal stiffness, it would seem that for a seal with $\phi > 90^{o}$, a change that would make K_{xx} more negative would be seen as an increase in the phase angle (closer to 180°).

Figure 27 is a plot of the predicted variation of K_{xx} with the number of blades in a pocket damper seal. Each of the two curves on the plot represents a different clearance ratio. The seal parameters used to generate this plot are identical to those of the eight-bladed test seal, and the only parameter that was varied was the number of blades.

Figure 27 Effect of Number of Blades on K_{xx}

There is a clear change in the trend-line as the number of blades increases. Figure 28 is a plot of the variation of the phase angle (average of first and last cavity values) with number of blades for the diverging eight-bladed seal for two pressure drops.
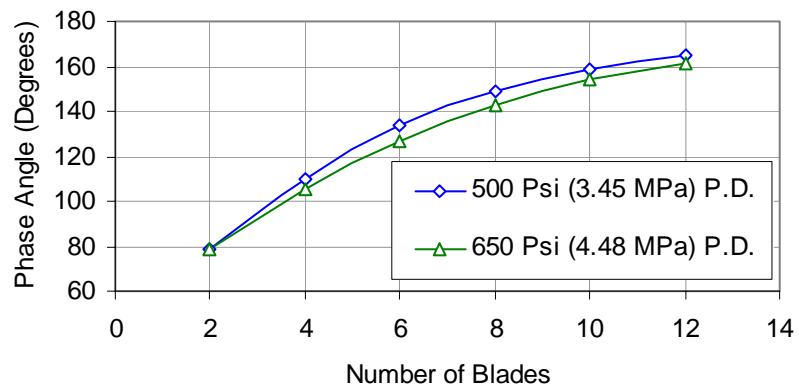
Figure 28 Effect of Number of Blades on Phase Angle

If the phase angle were to be used as the sole measure of the direct stiffness of the

seal, Figure 28 would imply that a pocket damper seal's stiffness becomes more negative as the number of blades increases. This conclusion is contradicted by Figure 27, which shows that K_{xx} reaches a minimum (maximum negative) value and then begins to increase in the case of the diverging seal.

The reason for the contradiction is that the phase angle is only a measure of the relative magnitudes of the stiffness and the damping and because most, if not all, of the seal parameters that have an effect on the seal's stiffness will also have an effect on the damping. In the case of this example seal's parameters, increasing the number of blades reduced the damping at a faster rate than it increased the stiffness, which resulted in a phase angle that steadily increased.

Within a given seal, the phase angle of the pressure generated in each cavity is different. This is due to the differing pressure ratios and pressure drops across the cavities. This can be seen in Table 4, which shows the variation of the phase angle in each active cavity of the diverging eight-bladed and twelve-bladed test seals with an inlet pressure of 1000 Psi (6.90 MPa).

Table 4 Variation of Phase Angle Along Length of Seal

Seal	Active Cavity	500 Psi (3.45 MPa) PD	800 Psi (5.52 MPa) PD
		Degrees	Degrees
12-Blades	1	174.50	173.74
	2	173.82	173.38
	3	173.50	172.85
	4	173.03	171.96
	5	172.28	170.12
	6	170.85	124.61
8-Blades	1	154.42	153.47
	2	153.11	151.37
	3	150.67	146.80
	4	144.96	113.85

The pressure drop across each cavity increases progressively along the length of the seal and this is responsible for the decreasing phase angles along the length of the seal. The increased pressure drop leads to an increase in both the negative stiffness of the seal and in the positive damping. For both test seals, the rate of increase of the latter was more dominant, leading to a phase that approached 90°. The phase angle provides especially useful feedback when examining the data for the diverging twelve-bladed test seal. The phase angles in the first five active cavities for the higher pressure drop case are close to 180° whereas the final phase angle is just over 124°. This is an indication that most of the damping and stiffness in the seal are being generated in the final cavity. In fact, about 46% of the seal's stiffness and 90% of the seal's damping comes from this final active cavity.

The phase angle can also be used as an indicator when examining changes in a seal's direct stiffness. In addition to indicating the relative magnitudes of C_{xx} and K_{xx}, ϕ can indicate the sign of K_{xx}. For a diverging seal, in which C_{xx} is known to be positive, a drop in the value of the phase angle below 90° indicates that K_{xx} has become positive. To examine changes in K_{xx} alone, it is necessary to directly examine the mathematical expression for the stiffness.

STIFFNESS VARIABLES

In order to assist in the attempt to determine the effects of certain parameters on the direct stiffness of a damper seal, the expression for the stiffness as it is used in the damper seal code can be examined. Looking at the components of the expression and at how each of them independently affects the stiffness may provide certain guidelines for the numerical analysis when using the code to determine the sensitivity of the seal's stiffness to such parameters as the number of blades, the clearances and clearance ratio, and the pocket depth.

The formula presented by Shultz [9] for the direct stiffness of a two-bladed seal is as follows:

$$K_{xx} = A_e \cdot \frac{(b \cdot d + a \cdot e \cdot \omega^2)}{b^2 + a^2 \cdot \omega^2} \tag{24}$$

Defining Equations

Each of the four factors *a*, *b*, *d*, and *e* are terms that arise as part of the derivation of the expression for the direct stiffness. The variable *a* can be thought of as a pocket volume factor for a given cavity and is given by Equation (25). The variable *b* (Equation (26)) depends on the mass flow-rate into the cavity, the pressure in the cavity, and the pressure ratio and can be thought of as a pressure ratio factor. The variable *d*, the clearance factor (Equation (27)), is dependent on both the mass flow-rate and the inlet and exit clearances. The pressure factor (Equation (28)) depends mainly on the cavity pressure and the normal area on which it acts.

$$a = \frac{V}{\gamma \cdot R \cdot T} \tag{25}$$

$$b = \frac{\dot{m}}{2 \cdot \gamma \cdot P} \cdot \left[\frac{2 \cdot Z^{\frac{2-\gamma}{\gamma}} - (\gamma-1) \cdot Z^{\frac{1}{\gamma}}}{Z^{\frac{2}{\gamma}} - Z^{\frac{\gamma+1}{\gamma}}} - \frac{2 \cdot (\gamma-1) \cdot Z^{\frac{2-\gamma}{\gamma}} + (1-\gamma) \cdot Z^{\frac{1}{\gamma}}}{Z^{\frac{2-2\cdot\gamma}{\gamma}} - Z^{\frac{1-\gamma}{\gamma}}} \right] \tag{26}$$

$$d = \dot{m} \cdot \left(\frac{1}{Cl_{in}} - \frac{1}{Cl_{exit}} \right) \tag{27}$$

$$e = \frac{P \cdot A_{normal}}{R \cdot T} \tag{28}$$

These four factors determine the sign and magnitude of the direct stiffness generated

in any given cavity and thus determine the sign and magnitude of the direct stiffness of an overall seal. It is clear from the expression for K_{xx} that the denominator of this expression is always positive and that the sign of K_{xx} is determined by the sign of the term $bd + ae\omega^2$. In order to examine the sign of this term, each of the four factors may be considered separately.

FREQUENCY DEPENDENCY

While K_{xx} is frequency dependent, the four factors defined by Equations (25) to (28) are not. Examination of Equation (24) shows that for a given seal, as the frequency increases the right hand terms of both the numerator and denominator become dominant. In other words, at sufficiently high vibration frequencies, the direct stiffness can be approximated by Equation (29):

$$K_{xx} \approx A_e \cdot \frac{e}{a} \qquad (29)$$

This frequency-independent expression for the stiffness matches the predicted variation of stiffness with frequency in which the slope of the stiffness curve tapers off at high frequencies. Figure 29 shows this prediction for the diverging eight-bladed and twelve-bladed test seals.
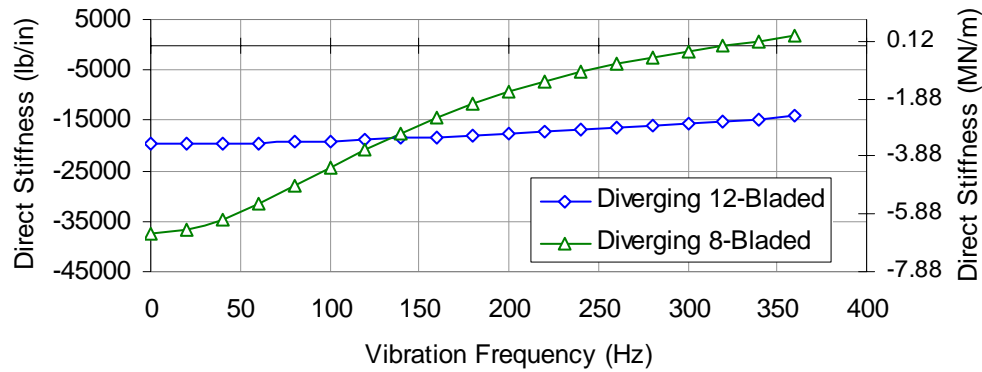
Figure 29 Frequency Dependency of Direct Stiffness

The direct stiffness is zero at approximately 320 Hz and begins to slowly approach a constant value shortly beyond this point. The inlet and exit pressures used to generate Figure 29 were 1000 Psi (6.90 MPa) and 500 Psi (3.45 MPa) respectivley.

The diverging tewlve-bladed seal behaves in the same way, but the stiffness has only begun to increase by the 360 Hz mark. The seal's stiffness eventually reaches zero at about 1500 Hz and only tapers off to a constant value at 5000 Hz. Thus Equation (29) can be expected to hold true for all pocket damper seals provided that the frequency of vibration is sufficiently high. For some seals, this frequency will be far beyond any reasonable operating frequency, but for all diverging seals, there is a frequency beyond which the direct stiffness will be positive. For increased pressure drops across the seal, the frequency at which the stiffness becomes positive is lowered. Equation (24) leads to an expression for the frequency at which the direct stiffness is zero.

$$\omega_0 = \sqrt{\frac{-b \cdot d}{a \cdot e}} \tag{30}$$

On the other hand, the frequency at which the magnitude of the direct stiffness is maximum (most negative in the case of a diverging seal) is $\omega_{max} = 0$, which is the only value that satisfies the local maximum equation (Equation (31)).

$$\frac{\partial K_{xx}}{\partial \omega} = 0 \qquad (31)$$

It is worth mentioning that the direct damping of a PDS behaves in a somewhat similar fashion. For a diverging seal, the maximum value of positive damping occurs at $\omega = 0$. Furthermore, again for a diverging seal, the constant value that the damping asymptotically approaches at high frequencies is always zero.

SIGNS OF STIFFNESS VARIABLES

From Equation (25) and Equation (28) respectively, it can be seen that the factors a and e will be positive. By definition, the pressure ratio Z used in the Equation (26) is between the values of 0 and 1. If Z is less than a certain value (0.528 for air) the flow is choked. The multiplier outside the brackets in the expression for b is always positive. Numerical examination of the two terms within the brackets shows that for gases with $\gamma > 1$, the numerator and denominator of the second term are always positive. The first term also has a denominator that is always positive, but has a numerator that is negative for all cases of unchoked flow. In the case of choked flow, the first term is equal to zero. As a result, for all values of interest, the factor b will be negative.

Equation (27) shows that the factor d will have a positive value in the case of a diverging clearance and a negative value in the case of a converging clearance. Since a diverging clearance is required to generate positive damping in a cavity, it can be assumed that this factor will be positive for most values of interest. This means that for the direct stiffness to be positive, the following condition must apply:

$$|b| < \frac{a \cdot e \cdot \omega^2}{d} \qquad (32)$$

Equation (32) can serve as a guideline in determining a combination of design parameters that will lead to a PDS with positive direct stiffness. The following five points can be deduced from this inequality:

- The frequency term indicates that seal stiffness is more likely to be positive at higher frequencies.

- The mass flow-rate terms in both the factors *b* and *d* indicate that K_{xx} is more likely to be negative for higher leakage rates.

- The smaller the ratio of exit to inlet clearance, the more likely it is that K_{xx} will be positive.

- The deeper the depth of the pockets (and therefore the pocket volume), the more likely it is that K_{xx} will be positive.

- The longer the active cavities (and therefore the pocket volume), the more likely it is that K_{xx} will be positive.

Since several of the design parameters affect more than one factor at a time, it is difficult to say what effect each will have. For instance, the last two points are somewhat contradictory. Making the active cavities longer in an attempt to make K_{xx} positive can be achieved by decreasing the number of blades in the seal. However, as will be discussed later, the lower number of blades will result in the need for shallower pockets to maximize direct damping, which will in turn make K_{xx} more negative. The next section examines the effects of design parameters on the sign and magnitude of the direct stiffness in more detail.

EFFECTS OF SEAL DESIGN PARAMETERS

Using Equation (24) along with the definitions of each of the four factors provides a method for examining the effect of certain parameters on the sign of the direct stiffness. Given a damper seal with specified geometric constraints, pressure data, and leakage and rotordynamic performance requirements, three of the parameters of interest in attempting

to control the negative stiffness of the seal are the number of blades, the depth of the pockets, and the blade clearances. These three factors are not unrelated; in order to maximize the damping generated by a seal, the pocket depth and the clearances have to be optimized, and both these factors are affected by the number of blades.

Effect of Pocket Depth

The only one of the four factors that is affected by a change in the pocket depth is the factor a. If no changes are made to the seal apart from a change in the depth of the pocket, the other three factors will remain constant. An increase in the depth of the pocket would increase the pocket volume and result in a proportional increase in the value of the factor a. For the range of values of interest, an increase in the value of a will make the value of direct stiffness less negative. This can be seen in Figure 30, which is a plot of the direct stiffness of the example eight-bladed seal with varying pocket depth for different clearance ratios.
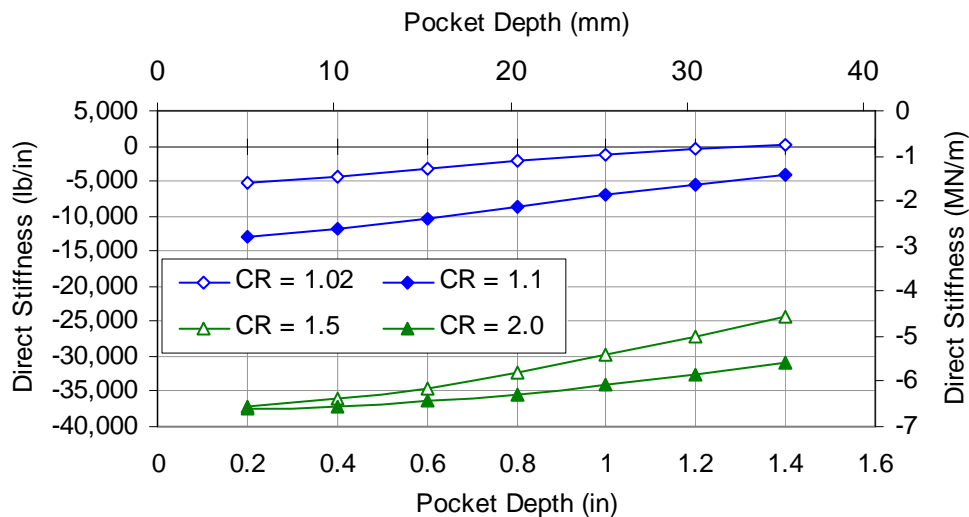

Figure 30 Effect of Pocket Depth on K_{xx}

The inlet and exit pressures used to generate this plot were 1000 Psi (6.90 MPa) and 500 Psi (3.45 MPa) respectively. The pocket depth has a clear effect on the direct stiffness with an increase in pocket depth making the stiffness less negative.

Effect of Number of Blades

As mentioned above, changing the number of blades in a seal design should correspond with a change in the clearance ratio and the pocket depth so as to optimize, if possible, the seal's damping characteristics. If, however, the number of blades is changed without any other modifications to the seal, the seal's stiffness will still be affected. In this case, all four factors will change for different reasons (the following analysis is based on the signs of the four factors in the case of a diverging seal). The factor a will change because changing the number of blades for a prescribed seal length will change the pocket volume. The factor b will change because both the mass flow-rate and the pressure ratios will be affected. The factor d also depends on the mass flow-rate and will change accordingly. The final factor e is affected by changes in both the cavity pressure and in the normal area on which this pressure acts, both of which will change with a change in the number of blades. How each of the four factors will be affected can be examined separately.

Increasing the number of blades will reduce the pocket volume and therefore reduce the value of the factor a. This will in turn cause K_{xx} to become more negative.

The mass flow-rate will be reduced if the number of blades increases, but at the same time, the pressure ratios across the blades will increase. The former has the effect of making b less negative while the latter has the effect of making b more negative. From a numerical analysis it appears that the pressure ratio effect is considerably more dominant and that as a result, increasing the number of blades will make b more negative. From the numerator of the expression for K_{xx}, an increase in the magnitude of b implies an increase in the negative magnitude of the stiffness. However, the b^2 term in

the denominator will cause a decrease in the negative magnitude of the stiffness. This means that as b increases in magnitude, there will be a point at which it will cease causing K_{xx} to become more negative and begin causing it to become less negative.

Since it is also dependent on the mass flow-rate, the factor d will decrease as the number of blades increases. From the expression for K_{xx}, it can be seen that this will result in the stiffness becoming less negative.

The fourth factor, e, is also dependent on two counter-balancing parameters with regard to increasing the number of blades. The cavity pressures will increase with more blades, but the normal area upon which these pressures act will decrease. Once more, from a numerical analysis it appears that the area dependency is more dominant, meaning that increasing the number of blades will reduce the value of e and make K_{xx} more negative.

There are therefore two factors that make K_{xx} more negative as the number of blades increases, one factor that changes its effect as its magnitude increases, and one factor that makes K_{xx} less negative. In addition, two of the factors contain components that work against each other. Keeping this in mind, Figure 27, which shows the variation of direct stiffness with number of blades while maintaining clearances and pocket depth constant, agrees with the idea that K_{xx} depends on factors that counter-balance each other and change in relative magnitude as the number of blades increases.

Effect of Number of Blades (Pocket Depth Optimized)

Each of the factors b, d, and e will not be affected by optimizing the depth of the pocket for maximum damping as the number of blades is changed and they should behave exactly as if there were no changes being made to the pocket depth. The factor a, however, will change. As the number of blades is increased, the pocket volume decreases, but at the same time, the optimum depth increases as show in Figure 31. In the case of the seal described above, the increased pocket depth causes the factor a to increase with increasing number of blades.
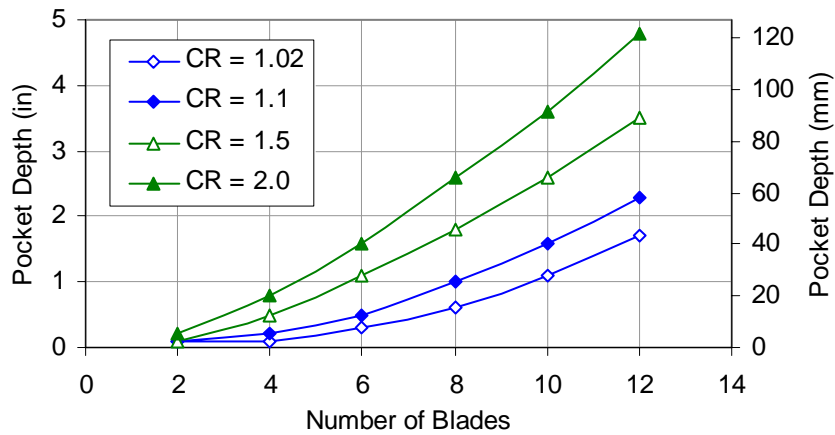
Figure 31 Optimum Pocket Depth for Maximum Damping
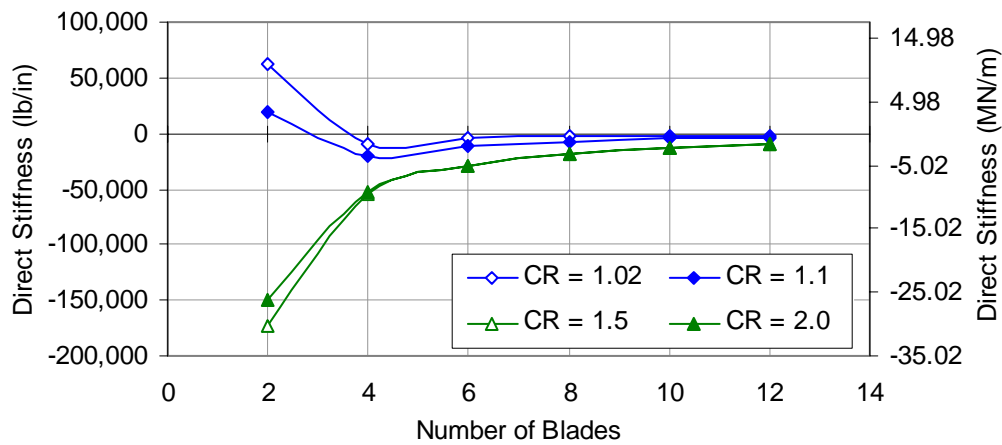
Figure 32 Effect of Number of Blades on K_{xx} (Pocket Depth Optimized)

Figure 32 shows the effect the number of blades has on the seal's stiffness when the pocket depth is optimized for maximum damping (the inlet and exit pressures used were 1000 Psi (6.90 MPa) and 500 Psi (3.45 MPa) respectively). The first points on each of the four curves on this plot have large stiffness magnitudes because of the small optimum pocket depth for low number of blades. Comparing Figure 32 with Figure 27, reveals that for 6, 8, 10, and 12 blades, the seals with the optimized pocket depths have

direct stiffnesses that are less negative than the seals with non-optimized depths.

Increasing the number of blades alters all four factors, and there is an additional change to the factor *a* when the pockets are made deeper as the number of blades increases. It should, therefore, be possible to increase the number of blades until the overall stiffness of the seal becomes positive, provided that the pocket depth corresponding to the increased number of blades is physically realistic.

Effect of Number of Blades (Limited Pocket Depth)

The damper seal code's prediction of the pocket depth that will yield the maximum amount of positive damping does not take into account the physical limitations on this parameter. Figure 31 shows that the value of the optimum pocket depth can be larger than the outer diameter of the seal permits. It is therefore necessary to set an upper limit to the values of pocket depth returned by the damper seal code. Figure 33 shows the predicted results using the major dimensions of the test seals and limiting the pocket depth to a maximum of 0.5 inches (12.7 mm).
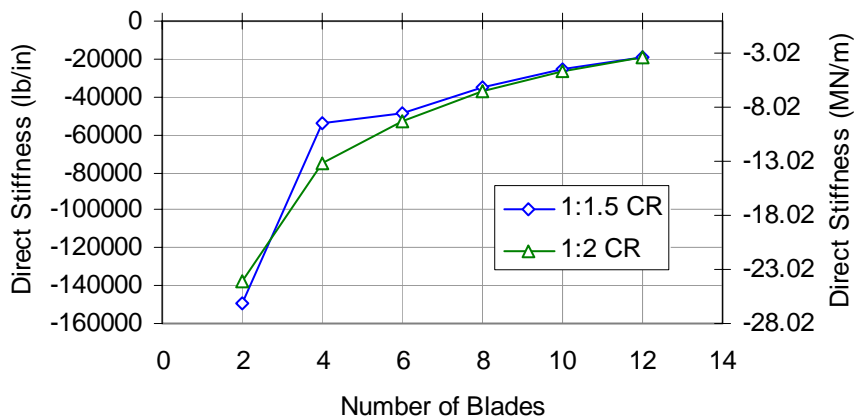

Figure 33 Effect of Number of Blades on K_{xx} (Limited Pocket Depth)

For both clearance ratios, the optimum pocket depth predicted by the damper seal code is higher than the limiting value for all numbers of blades higher than 2. The result is a combination of the behaviors discussed in the previous two cases. Before the limit is reached, the effect on the seal's direct stiffness will be identical to the case in which pocket depth is optimized. Beyond the limit, the effect on stiffness will be as if the pocket depth was held constant as the number of blades increases. This limits the designer's ability to increase the number of blades and make the pockets progressively deeper so as to reduce the negative stiffness. For the case of twelve blades with a 1:1.5 clearance ratio, using the optimum pocket depth of 3.53 inches (89.66 mm) provides a value of negative stiffness that is just over 50% of the value obtained when limiting the pocket depth to 0.5 inches (12.7 mm).

Effect of Clearances (Constant Clearance Ratio)

Due to their dependence on the mass flow-rate, the cavity pressures, and the seal clearances, the factors b and e can be expected to be sensitive to changes in the seal's clearances with the rotor. The factor d, as can be seen from its definition, is dependent on the clearances while the factor a is not. If the clearances are changed so as to maintain a diverging clearance and a constant clearance ratio, it is observed that the only factor that changes is b.

An increase in the inlet and exit clearances (for example from 5 mils (127 μm) and 10 mils (254 μm) to 7 mils (178 μm) and 14 mils (356 μm)) leads to a linearly proportional increase in the mass flow-rate. With regard to the factor d, the two increases cancel each other out.

The factor e is likewise unaffected since it is dependent on the cavity pressures, which are in turn affected by changes in the clearance ratio and not by the absolute values of the clearances.

As the clearances are increased, the value of b becomes more negative. This is because although the cavity pressures and pressure ratios remain unchanged, the mass

flow-rate increases with increasing clearances, thus making the magnitude of b more negative. Examining the numerator of the expression for K_{xx} shows that such a change should cause the seal's stiffness to become more negative as well. However, the b^2 term in the denominator of the expression, reduces the magnitude of the negative K_{xx}, thus making it less negative. As Figure 34 shows, increasing the clearances (for a fixed clearance ratio) makes K_{xx} more negative up to a certain point after which K_{xx} begins to become less negative with increasing clearances. A radial inlet clearance of 5 mils (127 μm) would be typical for a compressor.
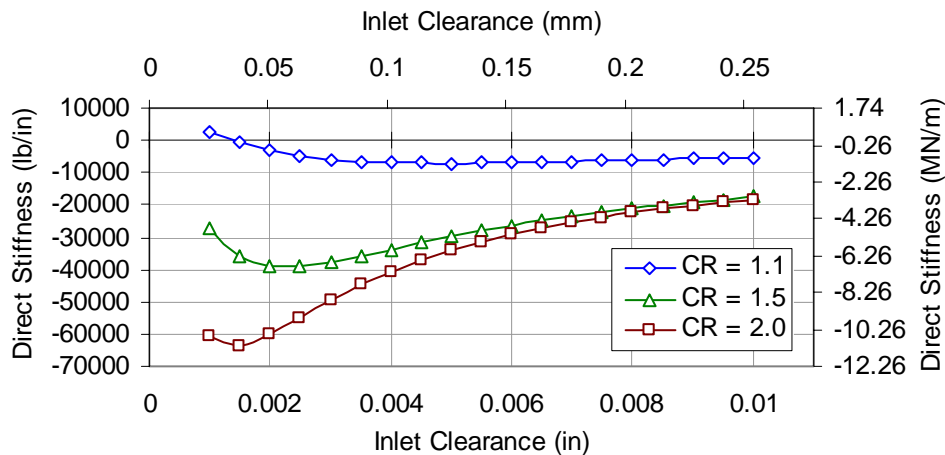
Figure 34 Effect of Clearances on K_{xx} (Eight Blades with Constant Clearance Ratio)

This plot was generated using the same eight-bladed diverging example seal used for previous plots. Clearly, when b grows beyond a certain value, the b^2 term in the denominator becomes the controlling factor. This can be seen in Figure 35, which shows a plot of the same parameters for an example seal identical to the diverging twelve-bladed test seal except for the variable clearances.

In this case, the increased number of blades causes an increase in the magnitude of the factor b and shifts the range of values for which K_{xx} would have become more

negative with increasing clearance beyond the scale of the plot. However, the 1.1 clearance ratio curve begins to slow down its trend as the inlet clearance is lowered even in this case.
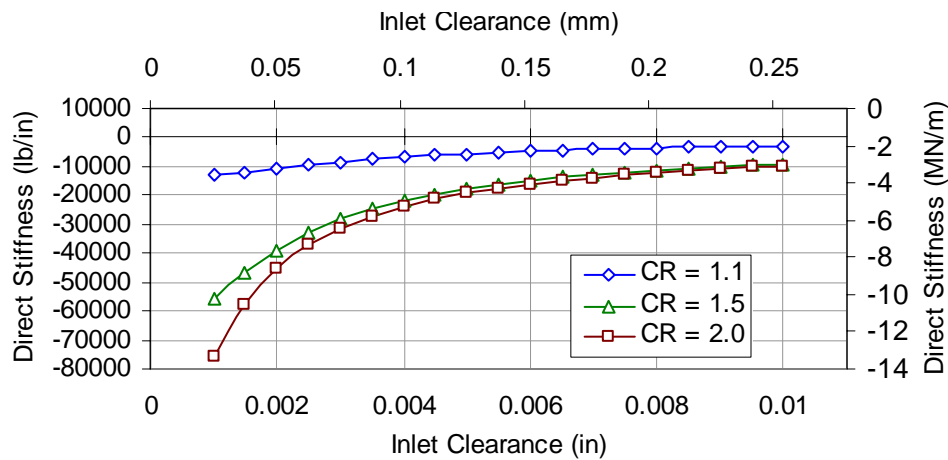
Figure 35 Effect of Clearances on K_{xx} (Twelve Blades with Constant Clearance Ratio)

As a result, it can be said that beyond a minimum inlet clearance, increasing the clearances while holding the clearance ratio fixed can make the direct stiffness of a seal less negative. While, increasing the inlet clearance can reduce the magnitude of the negative stiffness (due to the b^2 term in the denominator of Equation (24)), it will not change the sign of K_{xx}. This is because the sign of K_{xx} is entirely controlled by the sign of $bd + ae\omega^2$, which will become more negative as the factor b becomes more negative with increasing inlet clearance.

Effect of Clearance Ratio

In designing a PDS, the clearance ratio is changed, as is done with the pocket depth, so as to obtain the maximum positive direct damping for a given number of blades.

When the either one or both clearances are changed with no attempt to hold the clearance ratio constant, the resulting change in mass flow-rate is not directly proportional. As a result, the factor d will no longer remain constant as it did in the case of changing clearances with constant clearance ratio. The factors b and e will also change while the factor a will remain constant.
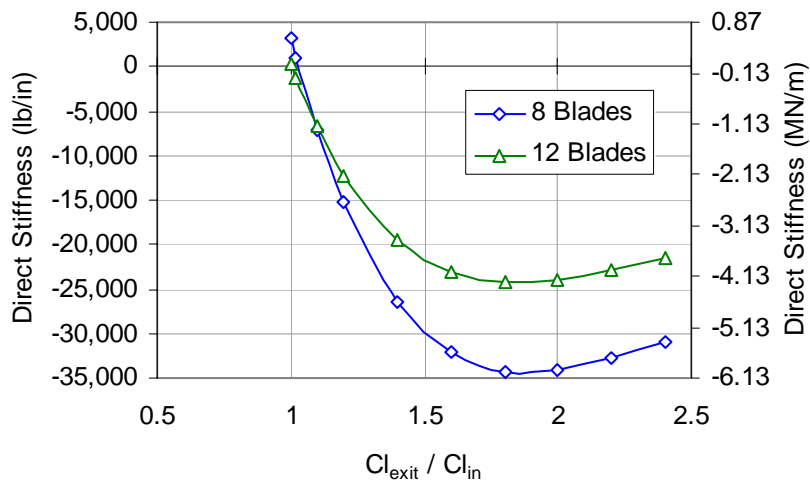
Figure 36 Effect of Clearance Ratio on K_{xx}

Figure 36 was generated using the eight and twelve-bladed test seals with inlet clearances of 5 mils (127 μm) and inlet and exit pressures of 1000 Psi (6.90 MPa) and 500 Psi (3.45 MPa) respectively. Increasing the pressure drop has no effect on the overall trend, but causes the stiffness to become more negative and shifts the clearance ratio at which stiffness is most negative higher. As the number of blades increases, the clearance ratio (Cl_{exit}/Cl_{in}) for optimum damping approaches 1:1 and as the number of blades decreases, the optimum clearance ratio increases.

According to Equation (24), K_{xx} will become more negative as the value of d increases. Likewise, Equation (30) states that K_{xx} will be negative over a wider range of frequencies for higher values of d. This can be seen by comparing the curve for the

eight-bladed seal in Figure 37 with the curve for the 1:1.5 clearance ratio in Figure 34.
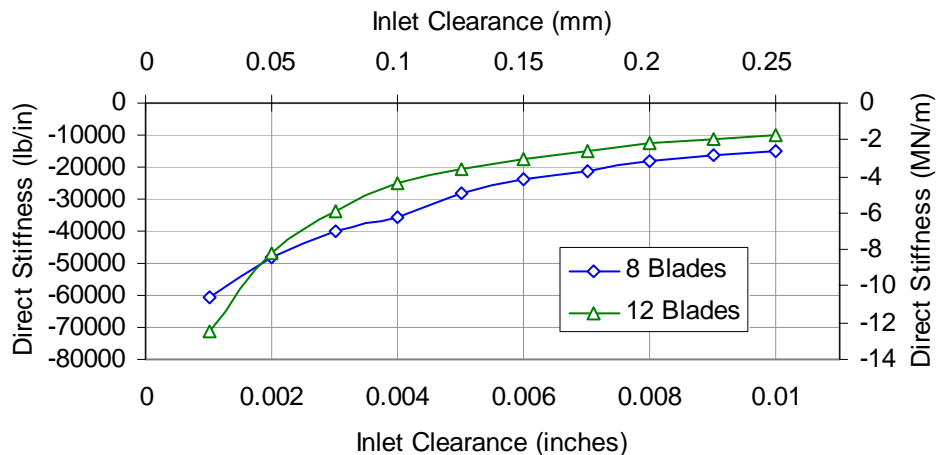
Figure 37 Effect of Clearances (Radial) on K_{xx} (8 Blades with Optimized Clearance Ratio)

Increasing the clearance ratio to obtain an optimum value of damping increases the flow-rate through the seal which in turn increases the magnitude of the direct stiffness (making it more negative for most seals).

NONUNIFORM SEALS

Several of the parameters that can be altered to reduce the negative stiffness of a PDS also lead to a large reduction in the amount of positive damping produced by the seal that may be unacceptable. This section examines the effects of modifying two parameters (the pocket depth and the clearances) for a single cavity in the seal.

Perhaps the simplest parameter to examine is the pocket depth. Whereas there is an optimum value of the pocket depth for which the positive damping is highest, the stiffness becomes less negative with increasing depth for realistic values of pocket depth. In the case of the diverging eight-bladed test seal with inlet and exit pressures of 1000

Psi (6.90 MPa) and 200 Psi (1.38 MPa) respectively, the optimum pocket depth is 0.415 inches (10.54 mm). Examination of the stiffness and damping produced in each cavity reveals that the 75% of the damping comes from the final active cavity compared to only 50% of the negative stiffness. This suggests that if one of the other three active cavities were made deeper, this would have a desirable effect on the seal's stiffness without greatly affecting its damping. For example, increasing the depth of the last cavity to 0.75 inches (19.05 mm) results in a 26% drop in the negative stiffness (less negative) but also a 3.3% drop in the seal's overall damping, which may be deemed an acceptable loss in exchange for improving the seal's stiffness characteristics. On the other hand, the same increase in the third active cavity results in only a 2.2% drop in the negative stiffness but also results in a 5.3% increase in the direct damping. The increase in the latter quantity can be explained by the fact that in calculating the optimum depth for the seal, a uniform pocket depth is used throughout. Increasing the depth of the third active cavity in this case not only provided a higher value of damping, but also reduced the seal's negative stiffness. While the percentage changes in this case were small, they illustrate the usefulness of being able to design non-uniform seals.

For the diverging eight bladed test seal with inlet and exit pressures of 1000 Psi (6.90 MPa) and 500 Psi (3.45 MPa) respectively, changing the seal's exit clearance (for all four active cavities) from 0.006 mils (0.152 mm) to 0.0055 mils (0.140 mm) would cut the negative stiffness by half, but would also reduce the positive damping by about a quarter, which may be unacceptable. Making the same change in clearance, but only for the seal's final blade results in an 11% drop in positive damping and a 16% drop in negative stiffness (less negative), which may prove to be a more valuable change.

The damper seal code as been modified to accommodate changes to any or all of the seal's blade clearances, its cavity lengths, and the its pocket depths. This allows a designer to examine the effect of non-uniformity on the leakage and rotordynamic properties of a seal on a case by case basis.

CHAPTER VII

DYNAMIC TESTS

The results of the impedance shake tests are presented in this chapter. Each of the four seal configurations, except the diverging eight-bladed seal, was tested at three different pressure drops. For each pressure drop, shake tests were conducted with three different rotor speeds. The inlet pressures were kept close to 1000 Psi (6.90 MPa), and the back pressure was varied using the exit valve. Since the seals have different leakage characteristics, the back pressure was not identical in all cases. For instance, fully closing the exit valve provided a back pressure of about 530 Psi (3.66 MPa) for the straight-through twelve-bladed seal but about 660 Psi (4.55 MPa) in the case of the eight-bladed seal.

The diverging eight-bladed seal could not be tested with an inlet pressure of 1000 Psi (6.90 MPa). The seal's negative stiffness made testing at this pressure impossible since any deviation from an approximately centered position of the stator caused it to move further until it came into contact with the rotor. This was the case even with the exit valve fully closed (therefore providing the lowest possible pressure drop).

The criterion used to determine whether or not the seal could be tested at a given pressure and with a given pressure drop was whether or not the stator could be moved until it came into contact with the rotor from one extreme to another in both orthogonal directions without "sticking" to the rotor. Using this criterion, the highest inlet pressure at which this seal could be tested was about 900 Psi (6.21 MPa) with a pressure ratio of approximately 1.7. Limitations on the pressure drop as well as the inlet pressure led to this seal being tested under only two sets of pressure conditions. Table 5 summarizes the test conditions for the two eight-bladed seal configurations while Table 6 lists the same information for the two twelve-bladed seal configurations.

DIRECT STIFFNESS PLOTS

The stiffness results of the shake tests are presented in Figure 38 through Figure 46 for the straight-through eight-bladed seal, Figure 47 through Figure 52 for the diverging eight-bladed seal, Figure 53 through Figure 61 for the straight-through twelve-bladed seal, and Figure 62 through Figure 70 for the diverging twelve-bladed seal. Each figure is a plot of the direct stiffness in the x and y direction for a given pressure drop and rotor speed.

The plots contain a first, second, or third order curve that attempts to best fit the data points. In some cases these trend-lines were omitted to make the scattered nature of the data more apparent. Theoretical predictions generated using the damper seal code are also included on each plot. These predictions take into consideration both the growth of the rotor at higher speeds and the discharge coefficients obtained in Chapter V. In the case of the straight-through twelve-bladed seal (for which no coefficients were determined) the discharge coefficients of the diverging twelve-bladed seal were used to generate the predicted curve.

For each set of tests (using either the baseline inserts or the seals) the test for one of the rotor speeds was repeated 10 times (for a total of 12 shakes in each direction for all three rotor speeds). The standard deviation of the results for each data point provides the uncertainty data for a given test. The error bars for each point on the plots correspond to the square root of the sum of the squares of the test and baseline standard deviations.

The data taken at frequencies associated with electrical noise, namely 30 Hz, 60 Hz, 120 Hz, 180 Hz, and 280 Hz, were deleted due to their high uncertainty values. The 50 Hz data point was also omitted. The 30 Hz data point was not removed from Figure 45 so as to display the relative magnitudes of its error bars to those of the remaining data points.

Table 5 Impedance Test Conditions - Eight-Bladed Seals

Seal	Pressure Drop	Rotor Speed (RPM)	P_{in} (Psi)	(MPa)	P_{exit} (Psi)	(MPa)	Pressure Ratio
1:1 CR	Low	10,200	1030	7.10	539	3.72	1.91
	Low	15,200	1029	7.10	530	3.66	1.94
	Low	20,200	1014	6.99	505	3.48	2.01
	Intermediate	10,200	1014	6.99	343	2.37	2.96
	Intermediate	15,200	1029	7.10	339	2.34	3.04
	Intermediate	20,200	1031	7.11	328	2.26	3.14
	High	10,200	1047	7.22	135	0.93	7.76
	High	15,200	1012	6.98	126	0.87	8.03
	High	20,200	1025	7.07	126	0.87	8.13
1:1.5 CR	Low	10,200	731	5.04	454	3.13	1.61
	Low	15,200	714	4.92	436	3.01	1.64
	Low	20,200	723	4.99	433	2.99	1.67
	Intermediate	10,200	939	6.48	528	3.64	1.78
	Intermediate	15,200	953	6.57	582	4.01	1.64
	Intermediate	20,200	930	6.41	554	3.82	1.68

Table 6 Impedance Test Conditions - Twelve-Bladed Seals

| Seal	Pressure Drop	Rotor Speed (RPM)	P_{in} (Psi)	(MPa)	P_{exit} (Psi)	(MPa)	Pressure Ratio
1:1 CR	Low	10,200	1012	6.98	660	4.55	1.53
	Low	15,200	1021	7.04	660	4.55	1.55
	Low	20,200	1031	7.11	667	4.60	1.55
	Intermediate	10,200	1000	6.90	401	2.77	2.49
	Intermediate	15,200	1000	6.90	396	2.73	2.53
	Intermediate	20,200	1010	6.97	394	2.72	2.56
	High	10,200	1009	6.96	166	1.14	6.08
	High	15,200	1010	6.97	165	1.14	6.12
	High	20,200	1023	7.06	164	1.13	6.24
1:2 CR	Low	10,200	987	6.81	714	4.92	1.38
	Low	15,200	994	6.86	715	4.93	1.39
	Low	20,200	997	6.88	710	4.90	1.40
	Intermediate	10,200	1012	6.98	465	3.21	2.18
	Intermediate	15,200	1000	6.90	455	3.14	2.20
	Intermediate	20,200	1019	7.03	457	3.15	2.23
	High	10,200	1018	7.02	230	1.59	4.43
	High	15,200	1015	7.00	226	1.56	4.49
	High	20,200	1019	7.03	224	1.54	4.55
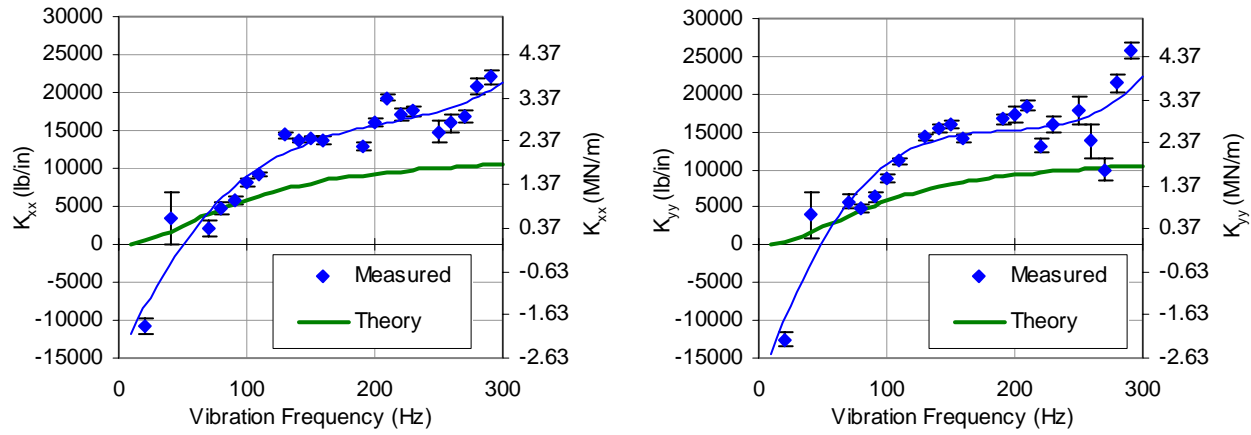
Figure 38 8-Bladed Seal K_{xx} and K_{yy} (1:1 CR – Low P. D. – 10,200 RPM)
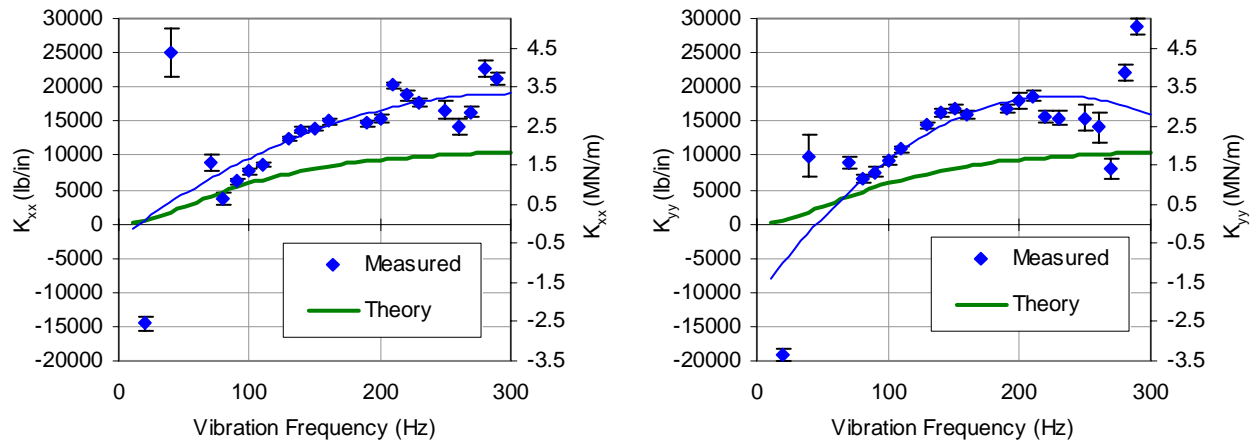

Figure 39 8-Bladed Seal K_{xx} and K_{yy} (1:1 CR – Low P. D. – 15,200 RPM)
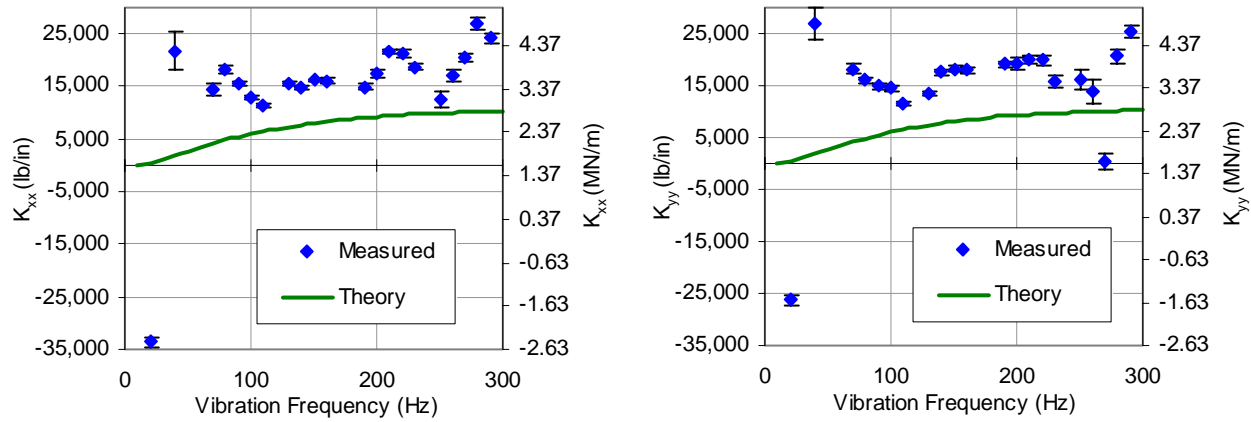
Figure 40 8-Bladed Seal K_{xx} and K_{yy} (1:1 CR – Low P. D. – 20,200 RPM)

Figure 41 8-Bladed Seal K_{xx} and K_{yy} (1:1 CR – Intermediate P. D. – 10,200 RPM)

Figure 42 8-Bladed Seal K_{xx} and K_{yy} (1:1 CR – Intermediate P. D. – 15,200 RPM)

Figure 43 8-Bladed Seal K_{xx} and K_{yy} (1:1 CR – Intermediate P. D. – 20,200 RPM)

Figure 44 8-Bladed Seal K_{xx} and K_{yy} (1:1 CR – High P. D. – 10,200 RPM)

Figure 45 8-Bladed Seal K_{xx} and K_{yy} (1:1 CR – High P. D. – 15,200 RPM)

Figure 46 8-Bladed Seal K_{xx} and K_{yy} (1:1 CR – High P. D. – 20,200 RPM)

Figure 47 8-Bladed Seal K_{xx} and K_{yy} (1:1.5 CR – Low P. D. – 10,200 RPM)

Figure 48 8-Bladed Seal K_{xx} and K_{yy} (1:1.5 CR – Low P. D. – 15,200 RPM)

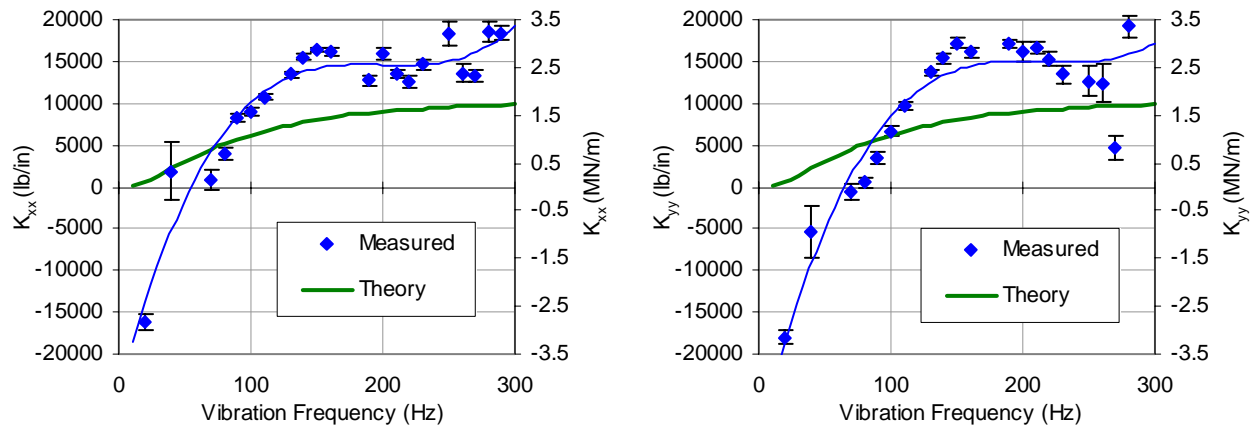**Figure 49** 8-Bladed Seal K_{xx} and K_{yy} (1:1.5 CR – Low P. D. – 20,200 RPM)

Figure 50 8-Bladed Seal K_{xx} and K_{yy} (1:1.5 CR – Intermediate P. D. – 10,200 RPM)
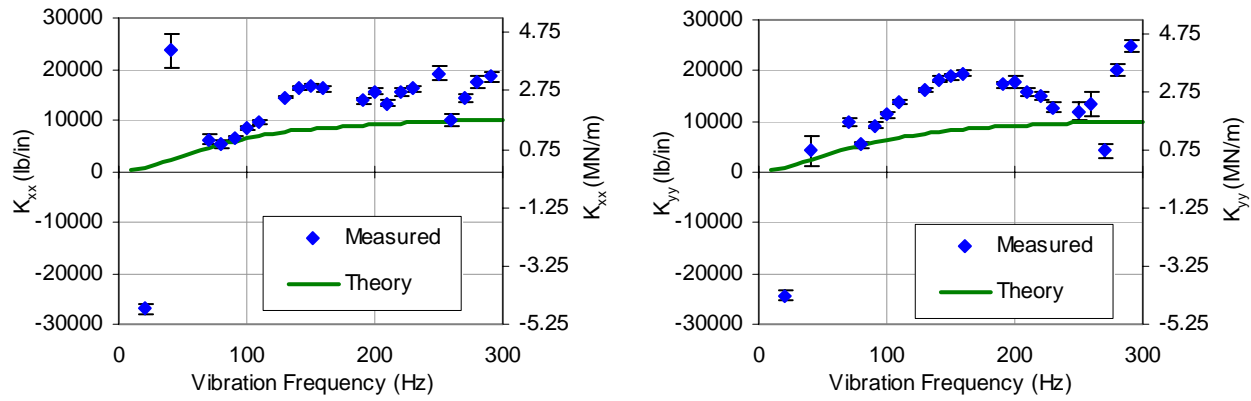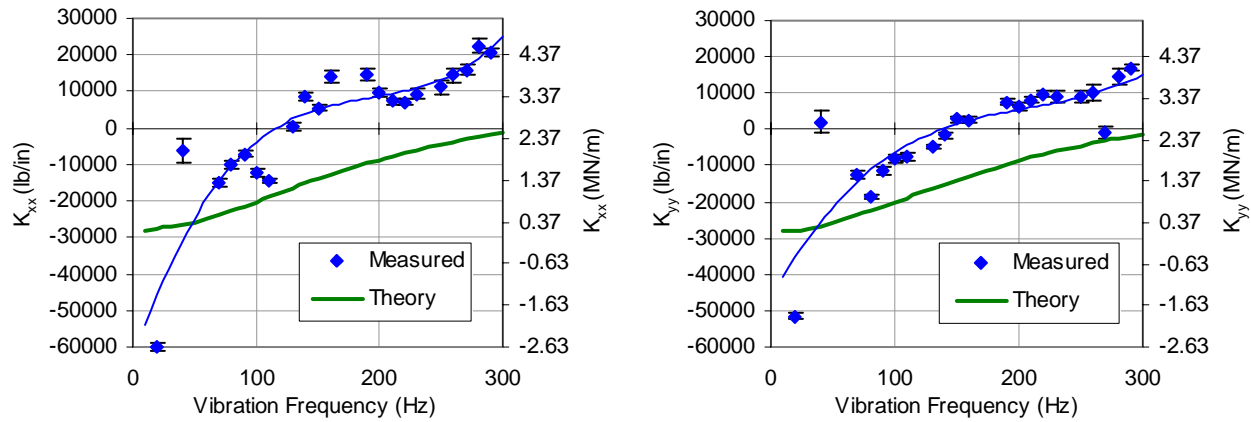

Figure 51 8-Bladed Seal K_{xx} and K_{yy} (1:1.5 CR – Intermediate P. D. – 15,200 RPM)
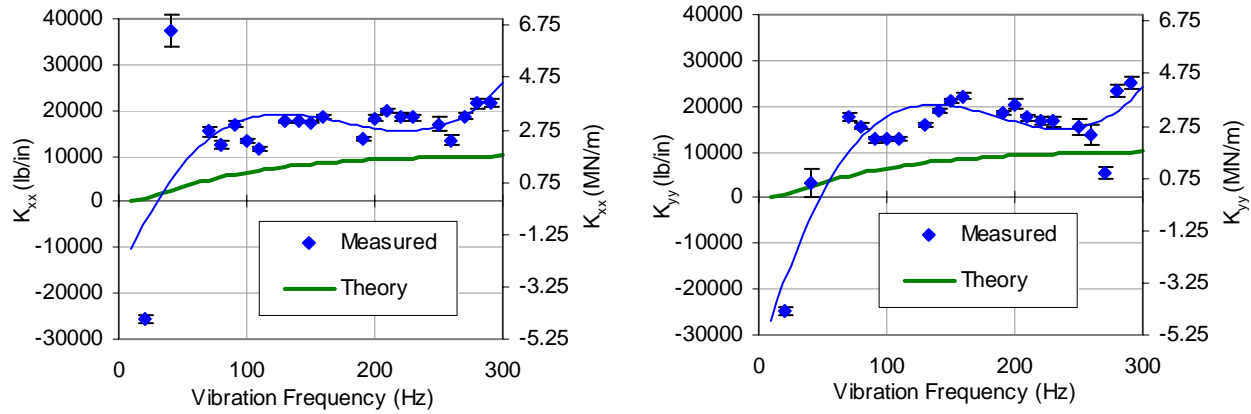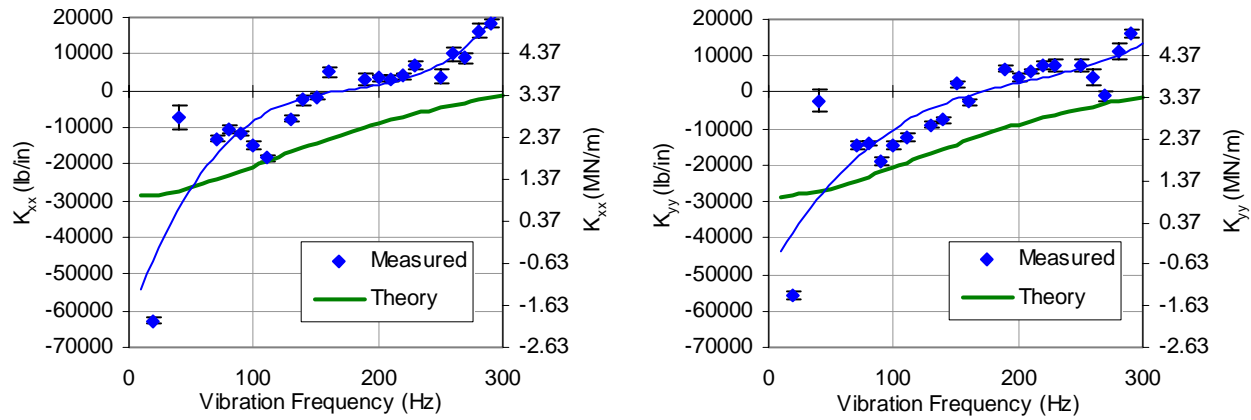
Figure 52 8-Bladed Seal K_{xx} and K_{yy} (1:1.5 CR – Intermediate P. D. – 20,200 RPM)
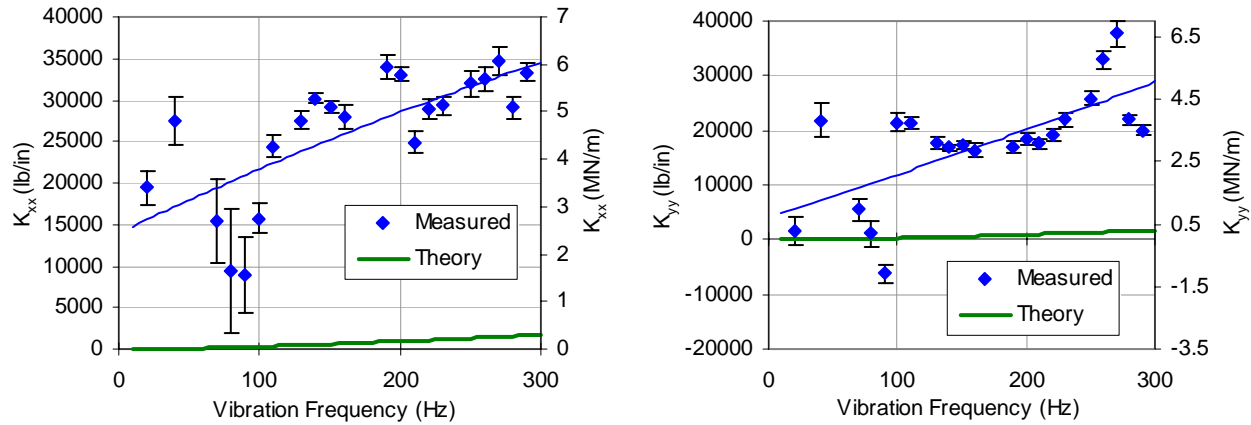
Figure 53 12-Bladed Seal K_{xx} and K_{yy} (1:1 CR – Low P. D. – 10,200 RPM)
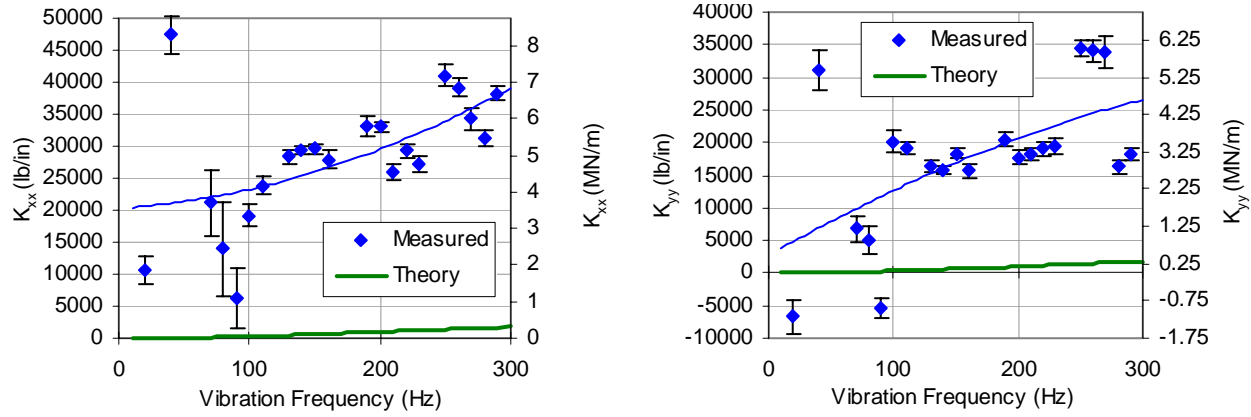
Figure 54 12-Bladed Seal K_{xx} and K_{yy} (1:1 CR – Low P. D. – 15,200 RPM)
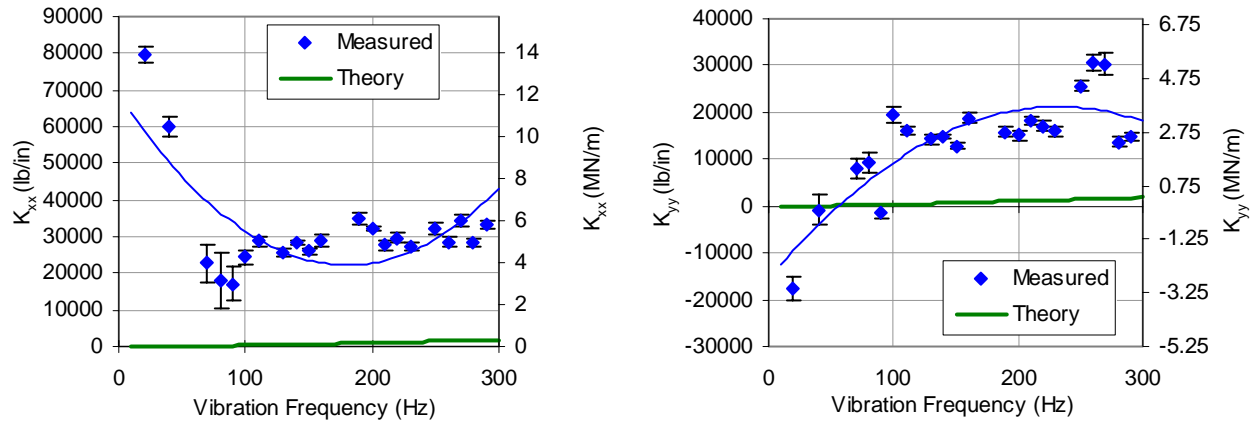
Figure 55 12-Bladed Seal K_{xx} and K_{yy} (1:1 CR – Low P. D. – 20,200 RPM)
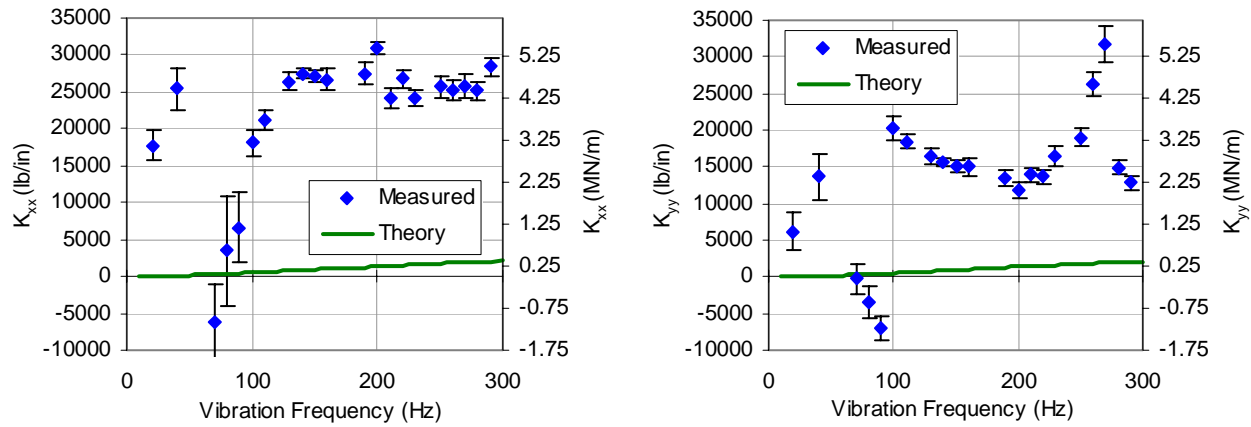
Figure 56 12-Bladed Seal K_{xx} and K_{yy} (1:1 CR – Intermediate P. D. – 10,200 RPM)

Figure 57 12-Bladed Seal K_{xx} and K_{yy} (1:1 CR – Intermediate P. D. – 15,200 RPM)

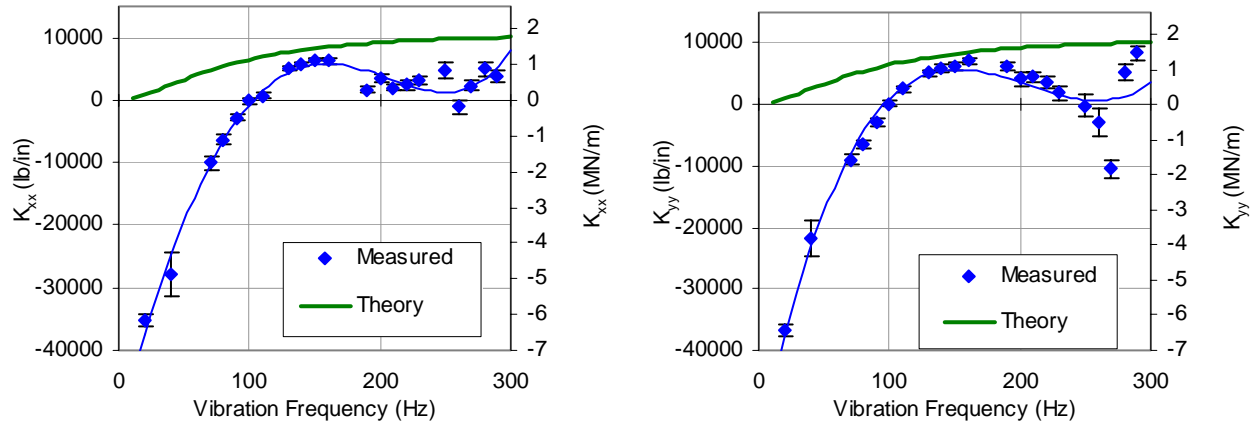**Figure 58** 12-Bladed Seal K_{xx} and K_{yy} (1:1 CR – Intermediate P. D. – 20,200 RPM)

Figure 59 12-Bladed Seal K_{xx} and K_{yy} (1:1 CR – High P. D. – 10,200 RPM)
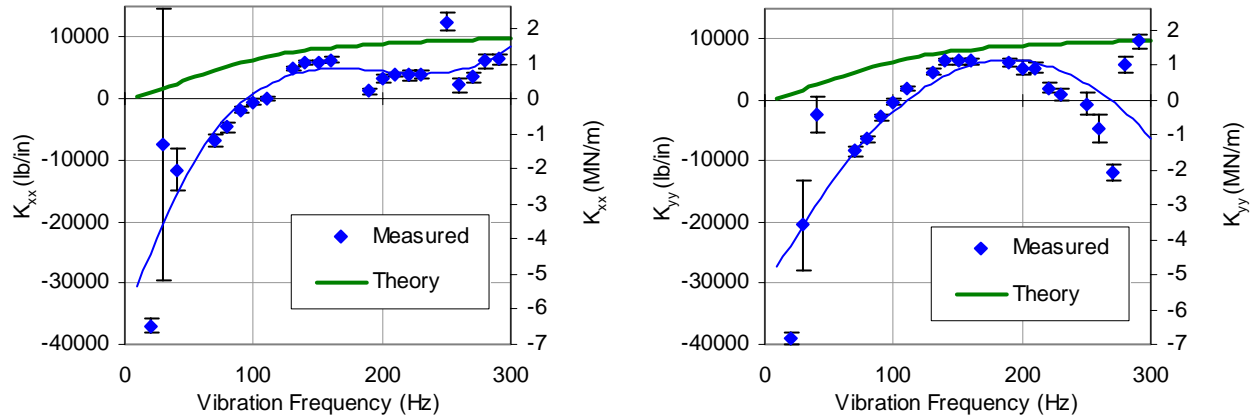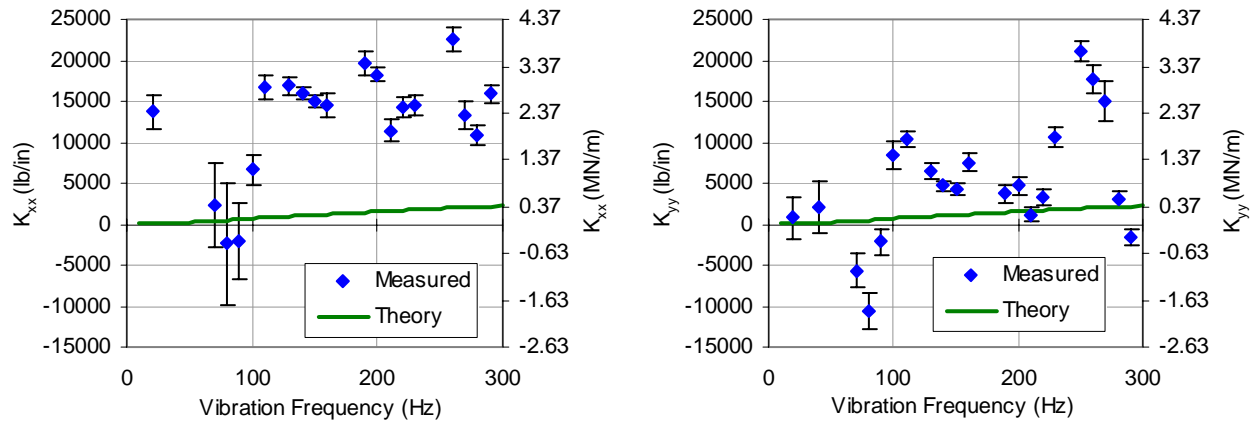
Figure 60 12-Bladed Seal K_{xx} and K_{yy} (1:1 CR – High P. D. – 15,200 RPM)
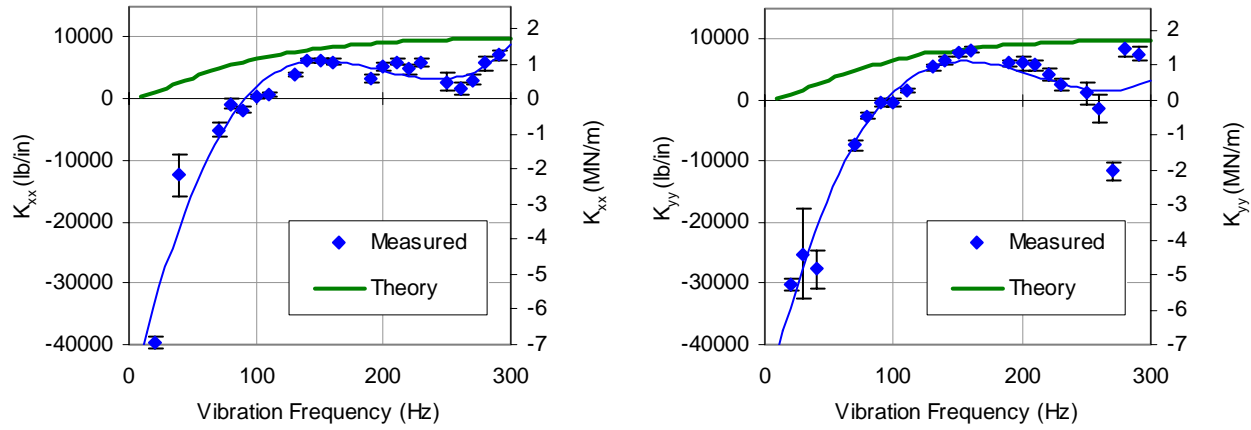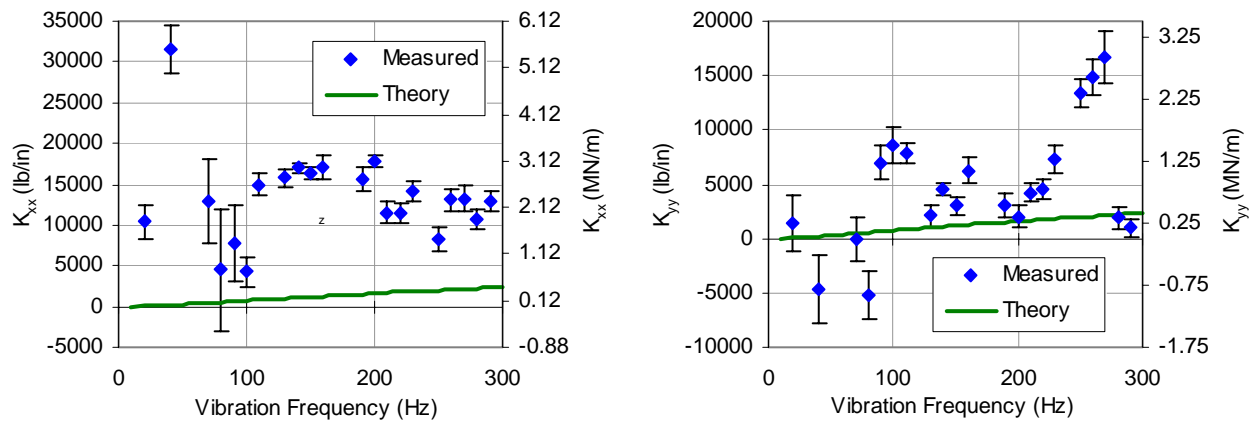

Figure 61 12-Bladed Seal K_{xx} and K_{yy} (1:1 CR – High P. D. – 20,200 RPM)
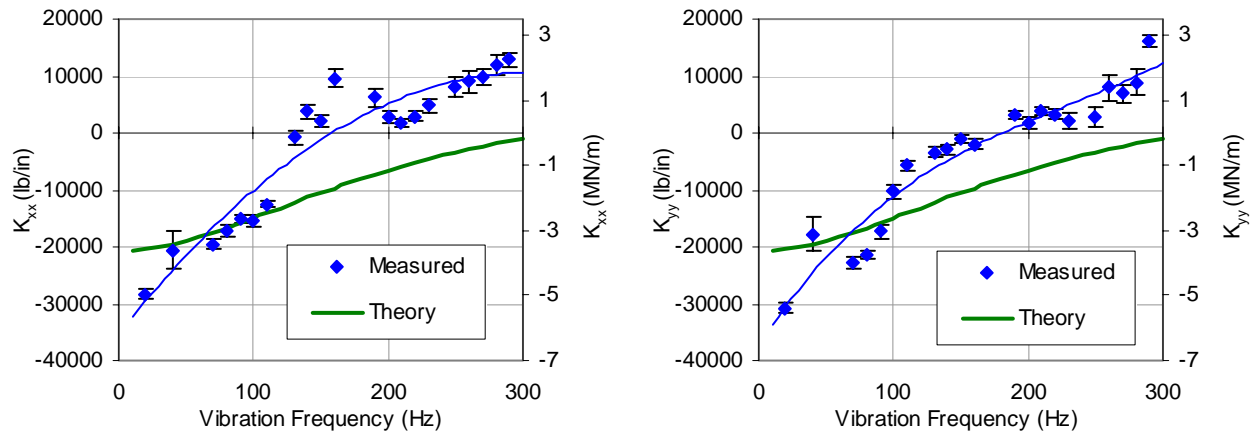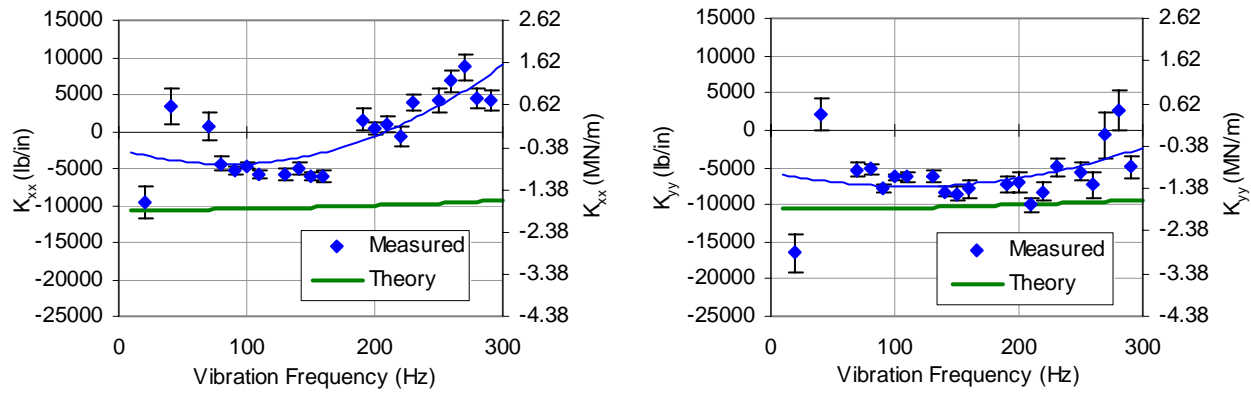
Figure 62 12-Bladed Seal K_{xx} and K_{yy} (1:2 CR – Low P. D. – 10,200 RPM)
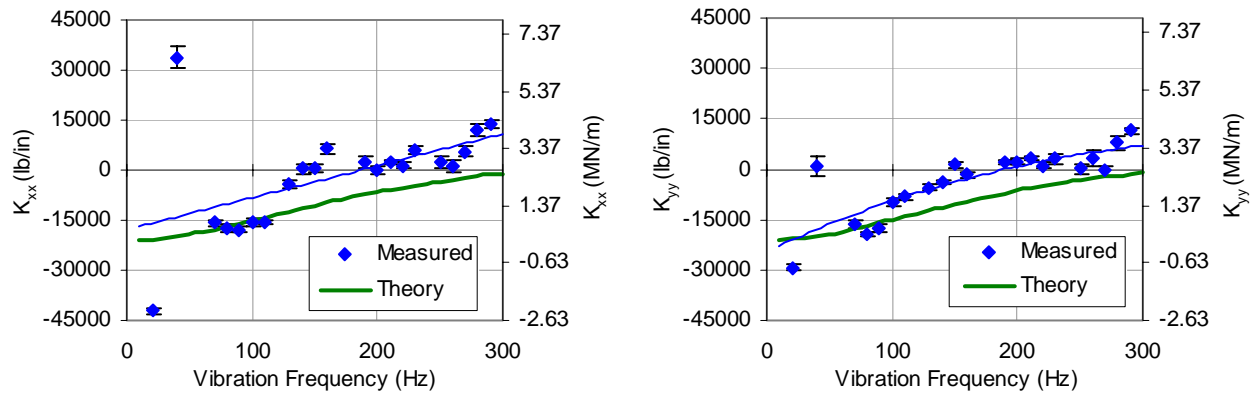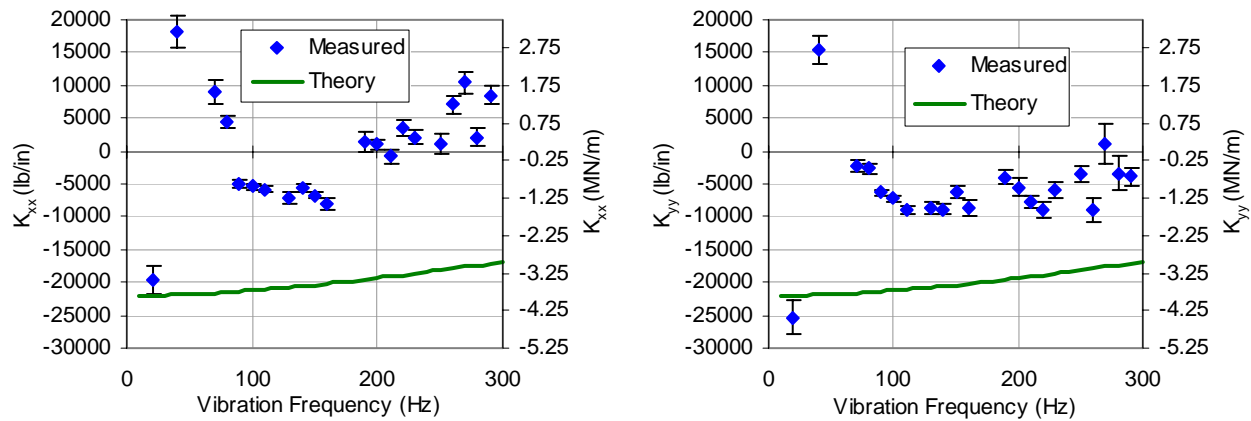

Figure 63 12-Bladed Seal K_{xx} and K_{yy} (1:2 CR – Low P. D. – 15,200 RPM)
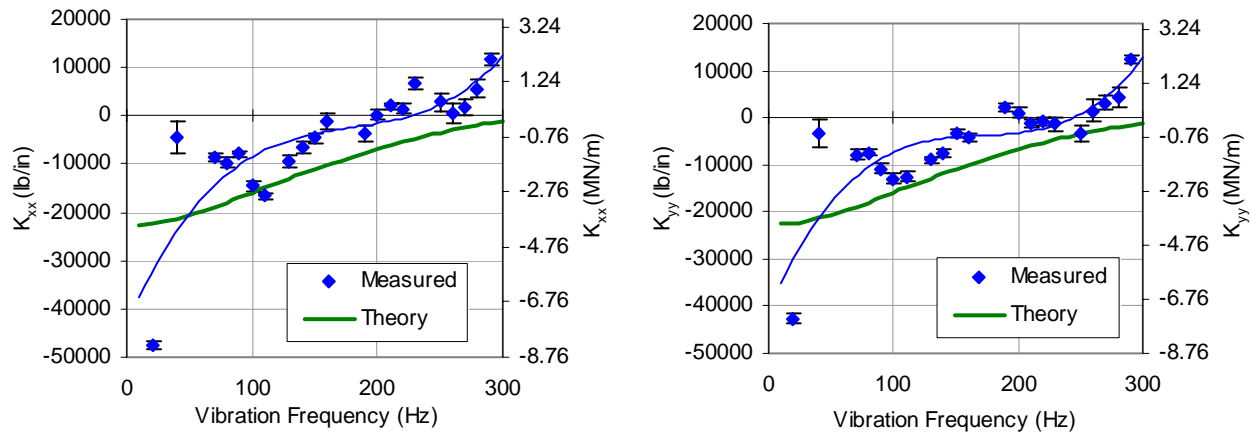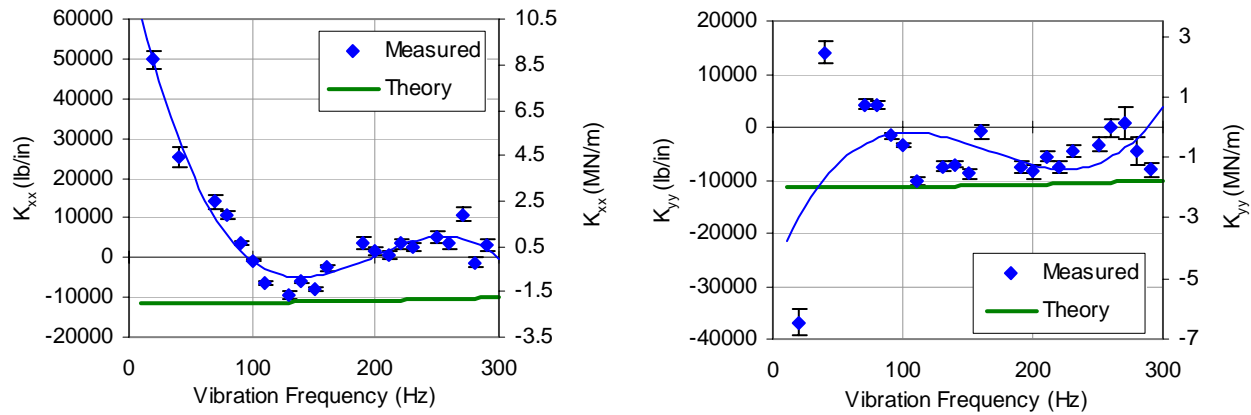
Figure 64 12-Bladed Seal K_{xx} and K_{yy} (1:2 CR – Low P. D. – 20,200 RPM)
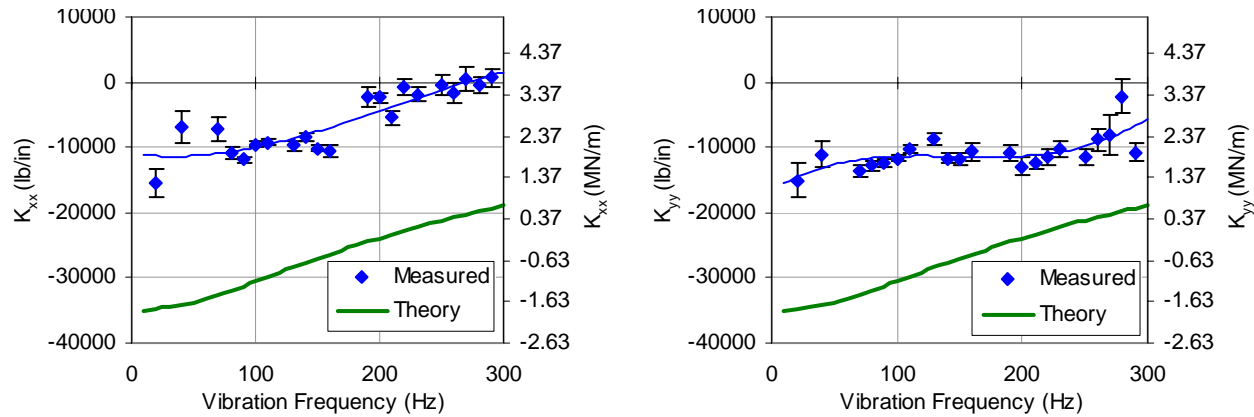
Figure 65 12-Bladed Seal K_{xx} and K_{yy} (1:2 CR – Intermediate P. D. – 10,200 RPM)
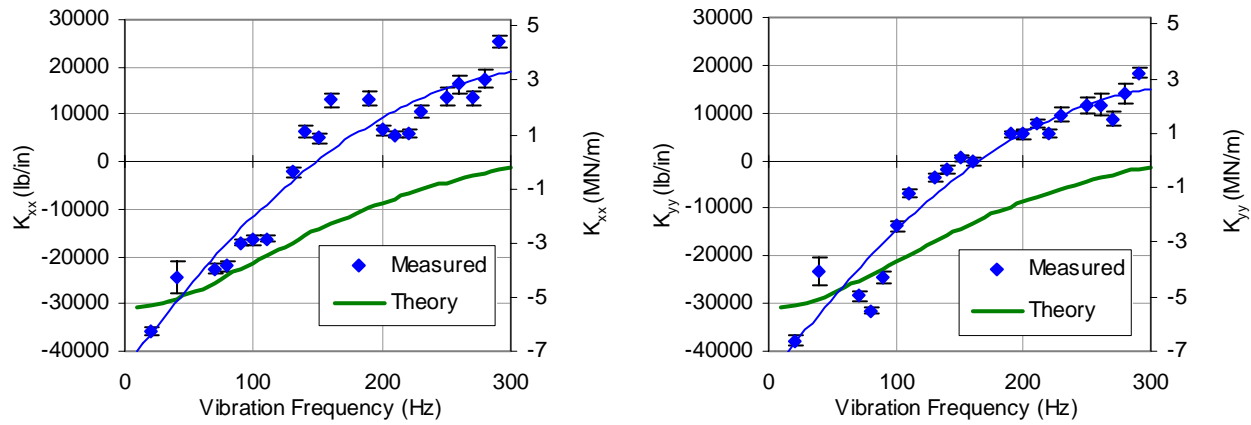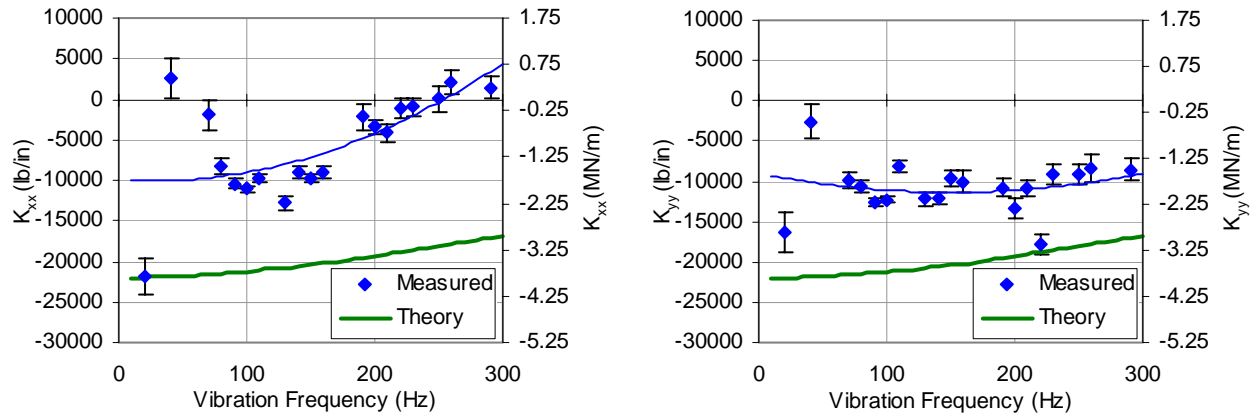
Figure 66 12-Bladed Seal K_{xx} and K_{yy} (1:2 CR – Intermediate P. D. – 15,200 RPM)
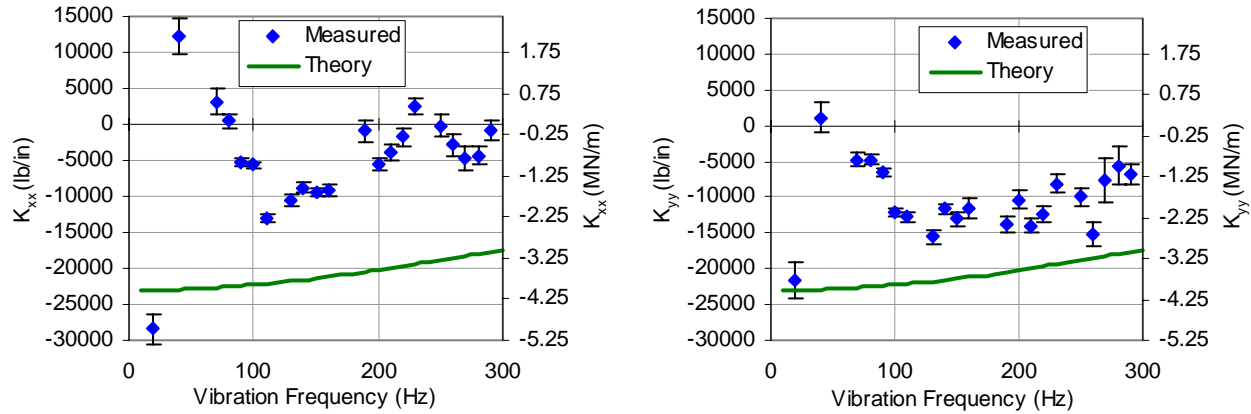
Figure 67 12-Bladed Seal K_{xx} and K_{yy} (1:2 CR – Intermediate P. D. – 20,200 RPM)
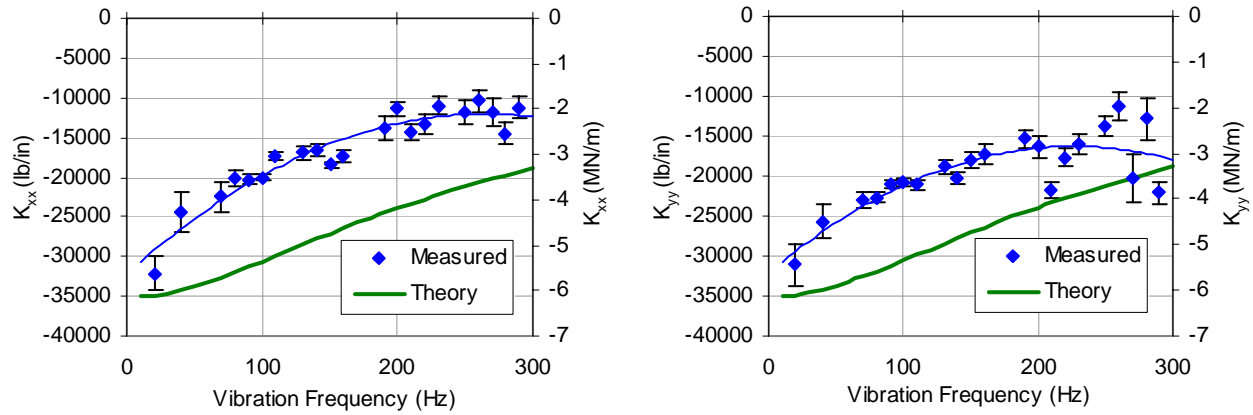
Figure 68 12-Bladed Seal K_{xx} and K_{yy} (1:2 CR – High P. D. – 10,200 RPM)
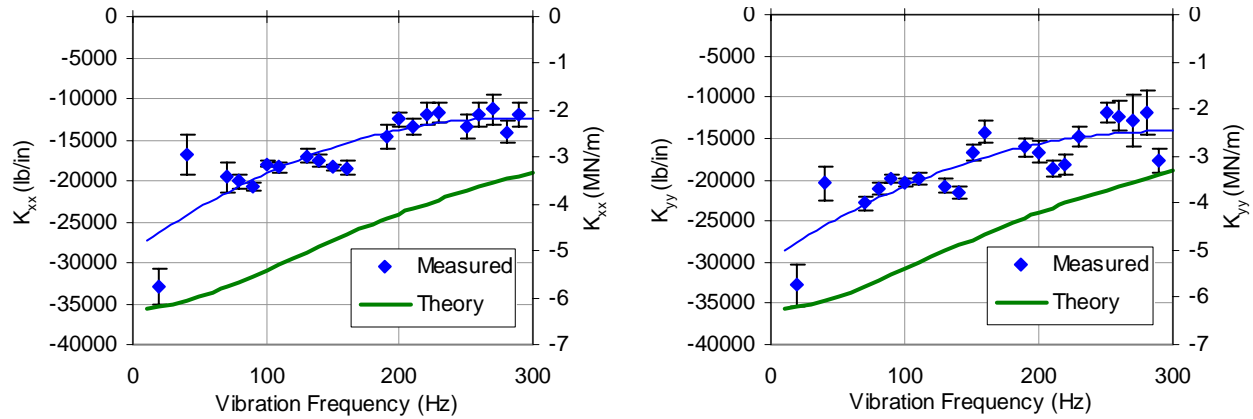
Figure 69 12-Bladed Seal K_{xx} and K_{yy} (1:2 CR – High P. D. – 15,200 RPM)

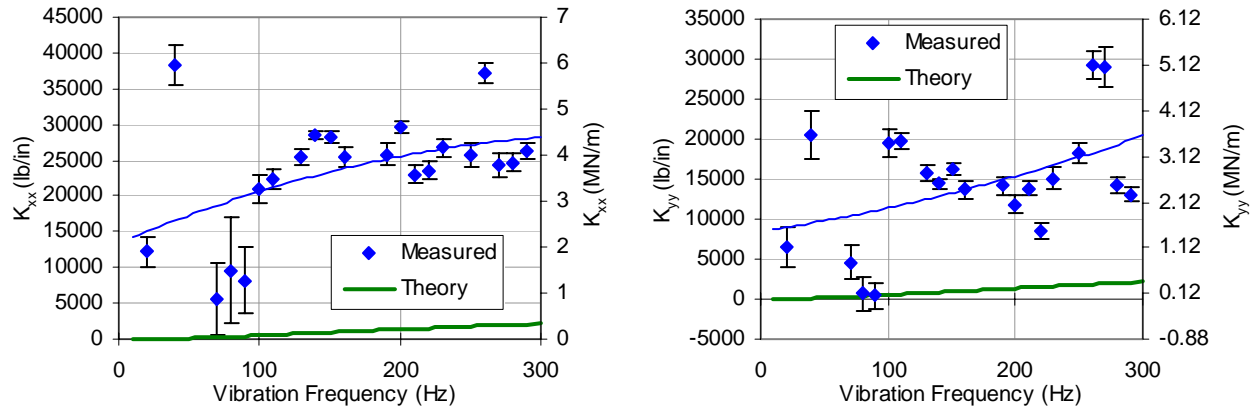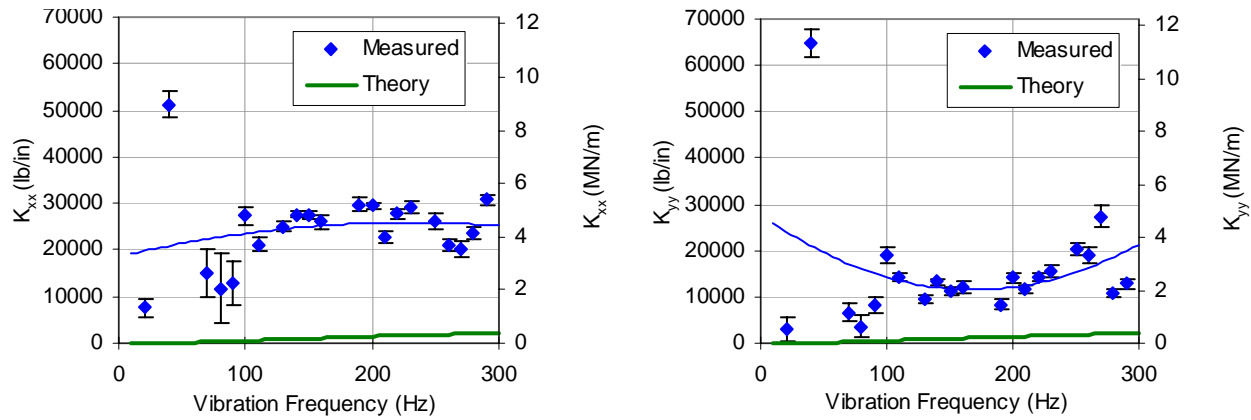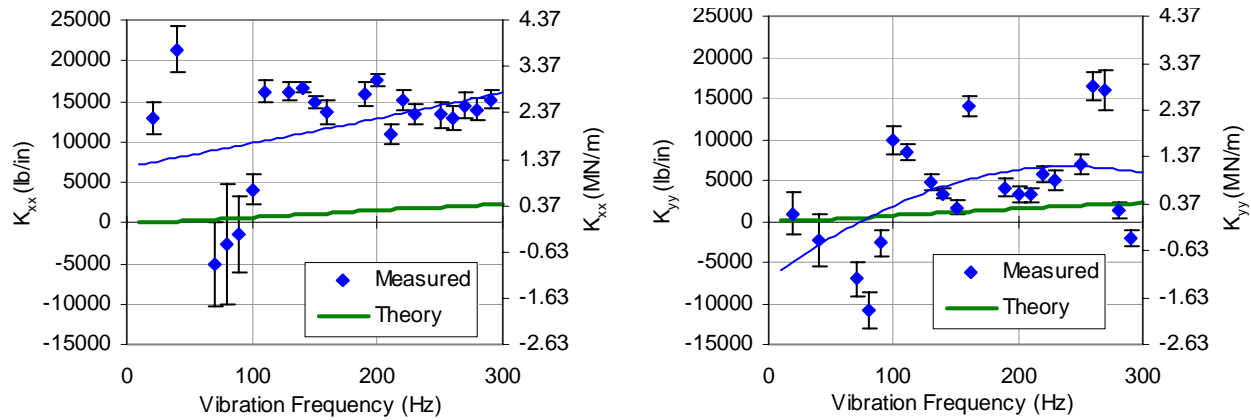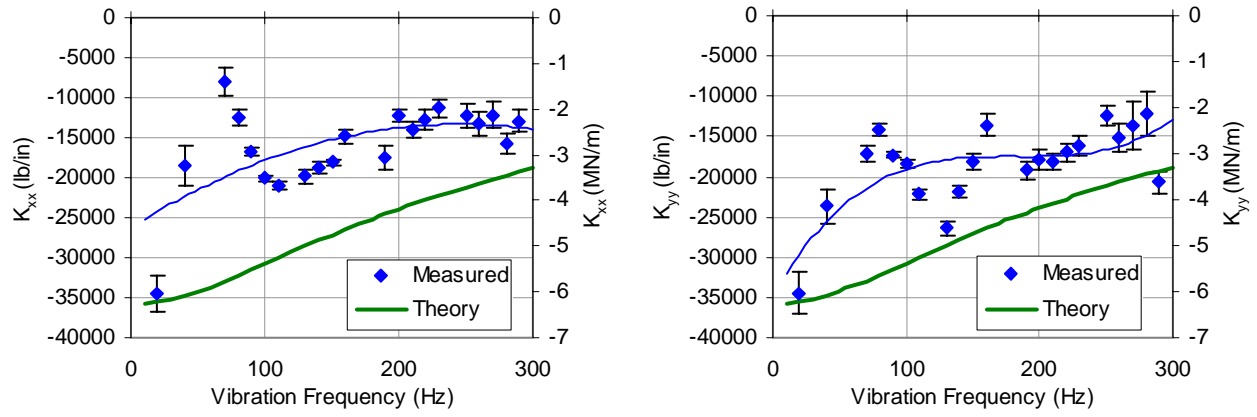**Figure 70** 12-Bladed Seal K_{xx} and K_{yy} (1:2 CR – High P. D. – 20,200 RPM)

STRAIGHT-THROUGH EIGHT-BLADED SEAL

The results presented for this seal agree well with the theoretical predictions insofar as the overall behavior of the seal over a range of frequencies is concerned. Except for the 20 Hz data point, both K_{xx} and K_{yy} are positive and increase with increasing frequency. The 40 Hz data point is a clear deviation from the trend, but it has high uncertainty associated with it and varies widely in value for the x and y directions as can be seen in Figure 43.

For the low pressure drop case, the damper seal code predicts the direct stiffness reasonably well up to a frequency of about 120 Hz. Beyond that point, the stiffness is under-predicted with a theoretical value of approximately 60% of the measured value at 250 Hz for the low pressure drop and intermediate speed case.

For all three speeds, the low pressure drop results diverge from the theory at frequencies beyond 270 Hz more than the results obtained for the higher pressure drops. Almost every plot also shows a slight dip in stiffness in the 230 Hz to 260 Hz range. This is especially evident in the K_{yy} plots. The uncertainty associated with these data points is, however, slightly above average, perhaps due to their proximity to the deleted 240 Hz data point.

The low and intermediate pressure drop data seems to indicate that the highly negative 20 Hz data point should be ignored even though there is no high uncertainty associated with this reading in any of the plots. According to the data for every pressure drop and rotor speed condition and in both the x and y directions, the seal has a negative stiffness at 20 Hz that is on the same order of magnitude as the positive stiffness values obtained at other frequencies. For the low pressure drop condition, removal of this data point allows a reasonable straight line curve fit of the data. This line passes close to zero stiffness at 0 Hz, which is in agreement with the theory.

That this data point should not be ignored becomes more evident, however, when the high pressure drop data is examined. For all three rotor speeds, all values of K_{xx} and K_{yy} for frequencies under 100 Hz are negative. Furthermore, as can be seen in Figure 44,

the reading at 20 Hz now follows the general trend.

Figure 45 is a good example of the importance of using baseline data with a low level of scatter. The K_{yy} data points in the range of 220 Hz to 270 Hz clearly deviate from the trends shown in other tests and from the K_{xx} data for the same test. While the test uncertainty for these points is on the same order as the uncertainties for the other points on the plot, the baseline uncertainty values associated with these points are three to four times as high as those for lower frequencies. This suggests that the seal's behavior is more likely given by the K_{xx} data than the K_{yy} data in this case.

The damper seal code predicts the overall trend of the data well for the low and intermediate pressure drop conditions. The first major deviation from the theoretical predictions is the magnitude of direct stiffness, which can be as high as twice the predicted value at high frequencies. The second deviation, and perhaps more significant one, is the failure to predict negative stiffness at lower frequencies especially for the high pressure drop condition.

DIVERGING EIGHT-BLADED SEAL

For the low pressure drop condition, the theoretical predictions match the direct stiffness results reasonably well. For instance, Figure 48 shows that K_{xx} in the 70 Hz to 100 Hz range is predicted almost exactly by the damper seal code. Many of the frequencies of vibration that are encountered in turbomachinery applications fall within this range.

The slope of the theoretical curve and the data trend match for the 15,200 RPM and 20,200 RPM rotor speeds, but there is an offset between the two, with the code under-predicting the stiffness by about the same amount over the range of test frequencies above 100 Hz. The offset between the data and the theoretical curve for the diverging eight-bladed seal means that the point at which the seal stiffness becomes positive occurs at a significantly lower frequency than is predicted. This occurs at about 200 Hz for all rotor speeds for the low pressure drop condition and more than 50 Hz lower than that for

the intermediate pressure drop condition.

The 20 Hz and 40 Hz data points behave in very similar fashions to the same points for the straight-through eight-bladed seal. The former is highly negative and is somewhat removed from any general trend for the low pressure drop condition, but fits in better for the high pressure drop condition. The latter is inconsistent with the data at other frequencies in all but a few cases.

For this seal configuration, the prediction error is lower for the low pressure drop condition, especially at lower frequencies. A comparison of the x direction direct stiffnesses of the two eight-bladed seal configurations is presented in Figure 71 for frequencies of 70 Hz, 150 Hz, and 220 Hz.

STRAIGHT-THROUGH TWELVE-BLADED SEAL

The results for this seal are not easily interpreted for three reasons. First, the data is highly scattered, especially in the y direction as can be seen in Figure 60. Second, the uncertainties associated with the 70 Hz to 100 Hz frequencies are high, and these points do not follow a particular trend or fit in with the higher frequency data. Third, for several tests, there is little correlation between the stiffnesses in the x and y directions.

The K_{xx} data for frequencies above 120 Hz, seems to be only slightly frequency dependent. For example, Figure 56 shows that K_{xx} varies between approximately 25,000 lb/in (4.38 MN/m) to 30,000 lb/in (5.25 MN/m) in the 120 Hz to 300 Hz frequency range for the intermediate pressure drop condition with a rotor speed of 10,200 RPM.

The theory also predicts only a minor trend of stiffness increasing with frequency, but greatly under-predicts the magnitude of the stiffness by an entire order of magnitude in several cases. The data is, however, consistent when it comes to the sign of the stiffness. With the exception of the data points with high uncertainty values in the 70 Hz to 100 Hz range, all test conditions yielded positive stiffness values over the entire frequency range.

70 Hz - 8 Blades - 1:1.5 CR

70 Hz - 8 Blades - 1:1 CR

150 Hz - 8 Blades - 1:1.5 CR

150 Hz - 8 Blades - 1:1 CR

220 Hz - 8 Blades - 1:1.5 CR

220 Hz - 8 Blades - 1:1 CR
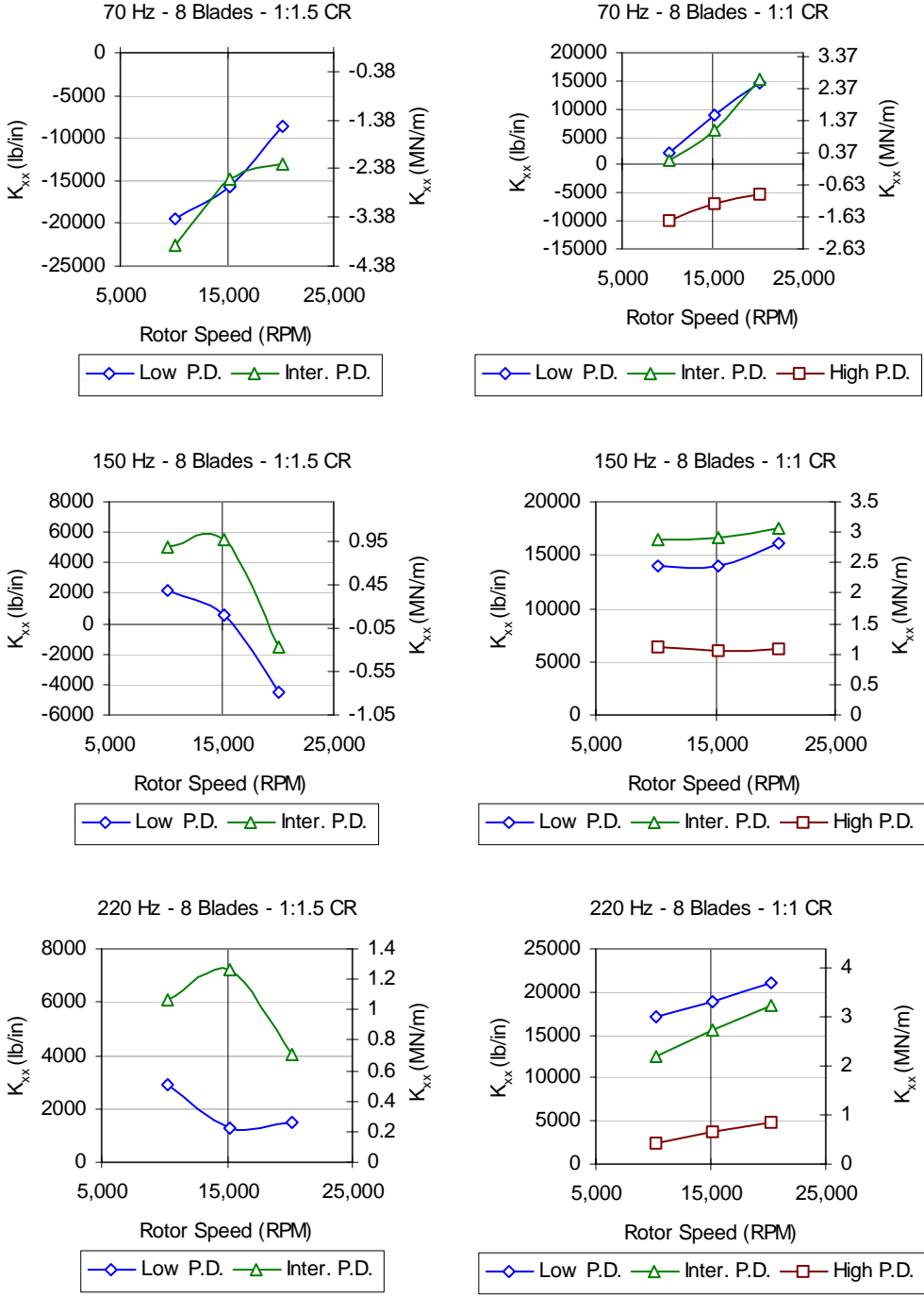
Figure 71 Comparison of K_{xx} for the Diverging and Straight-Through 8-Bladed Seals

DIVERGING TWELVE-BLADED SEAL

Like the diverging eight-bladed seal, this seal has a stiffness that is negative at lower frequencies and eventually becomes positive beyond a certain frequency. This is clearly seen in the 100 Hz to 300 Hz range of the results for the low and intermediate pressure drop conditions. With a higher pressure drop across the seal, the stiffness across the entire frequency range becomes negative, but still follows the predicted trend as shown in Figure 68.

The results obtained for frequencies below 100 Hz for the low pressure drop condition suggest that the stiffness initially starts out positive and decreases rapidly before increasing and becoming positive once more. While this can also be seen in several plots for the other two pressure drop conditions, these points have high uncertainty values.

The stiffness values are highly dependent on the pressure drop. At a frequency of 100 Hz and a rotor speed of 10,200 RPM, the seal's stiffness in the x direction is approximately -20,000 lb/in (-3.50 MN/m) for a high pressure drop, -10,000 lb/in (-1.75 MN/m) for an intermediate pressure drop, and -5,000 lb/in (-0.88 MN/m) for a low pressure drop.

The damper seal code predicts stiffness values that are considerably more negative than the measured values. The over-prediction of negative stiffness increases with increasing pressure drop across the seal.

The diverging twelve-bladed and eight-bladed seal data are reexamined in Chapter VIII in a comparison of the results of the shake tests with static test results.

CHAPTER VIII

STATIC TESTS

To verify the results obtained through the impedance analysis by dynamically testing the seals, the diverging configurations of the eight-bladed and twelve-bladed seals were tested statically to determine their stiffness coefficients.

During these tests, the shakers induced a purely translatory motion in the stator. The term *static* refers to this zero frequency nature of the excitation and not to the fact that the rotor was not spinning during the tests. The latter was simply a precaution that prevented potentially damaging contact between the rotor and the stator at extreme test locations.

THEORETICAL MODEL

The system of equations relating the seal forces to the motion of the stator are greatly simplified for zero frequency excitation since all velocity and acceleration terms are eliminated.

$$\begin{bmatrix} F_{xx} & F_{yx} \\ F_{xy} & F_{yy} \end{bmatrix} = \begin{bmatrix} K_{xx} & K_{xy} \\ K_{yx} & K_{yy} \end{bmatrix} \begin{bmatrix} D_{xx} & D_{yx} \\ D_{xy} & D_{yy} \end{bmatrix}$$

These four equations can be solved for the stiffness coefficients in terms of the direct and cross-coupled forces and displacements.

$$K_{xx} = \frac{F_{xx}D_{yy} - F_{yx}D_{xy}}{D_{xx}D_{yy} - D_{yx}D_{xy}} \qquad K_{xy} = \frac{-F_{xx}D_{yx} + F_{yx}D_{xx}}{D_{xx}D_{yy} - D_{yx}D_{xy}}$$

(33)

$$K_{yx} = \frac{F_{xy}D_{yy} - F_{yy}D_{xy}}{D_{xx}D_{yy} - D_{yx}D_{xy}} \qquad K_{yy} = \frac{-F_{xy}D_{yx} + F_{yy}D_{xx}}{D_{xx}D_{yy} - D_{yx}D_{xy}}$$

If the proximity probes in the direction orthogonal to the direction of excitation read no displacement, the equations would be decoupled the stiffness coefficients would be given by the slopes of the force versus displacement curves.

$$K_{xx} = \frac{F_{xx}}{D_{xx}} \qquad K_{xy} = 0$$

(34)

$$K_{yx} = 0 \qquad K_{yy} = \frac{F_{yy}}{D_{yy}}$$

However, since the seals may exhibit some cross-coupling and since both shakers are connected to the stator regardless of which one is being used to excite the stator, these simplified expressions for the stiffness coefficients may be inaccurate. As a result, Equations (33) were used to obtain the static stiffness coefficients.

PROCEDURE

The assembly, centering, and data acquisition procedures followed for the static and dynamic tests are identical. The shakers were used to center the stator and the force and displacement readings taken at the centered position were taken as zero datum values.

One shaker was used to move the stator along one axis in increments of approximately 0.5 mils (12.7 μm) first moving away from the centered position then, once contact with the rotor was made, back towards the centered position. At each of

these locations, displacement data from the four proximity probes and force data from the two force transducers were recorded. The same procedure was then repeated for the orthogonal direction.

As was the case for the dynamic tests, solving the system of equations governing the motion of the stator requires two tests; one in each orthogonal direction. The centered position readings were subtracted from the data at each incremental location, and x and y direction readings were combined in Equations (33) to calculate the stiffness coefficients.

The data becomes nonlinear when the stator and the rotor come close to making contact. These nonlinear readings were eliminated before calculating the means of the remaining stiffness coefficients.

For each seal two pressurized tests and a zero pressure baseline test were carried out. The inlet and exit pressures were chosen so as to match the pressures at which the seals were tested dynamically as closely as possible. The six sets of test conditions are listed in Table 7.

Table 7 Static Stiffness Test Conditions

Test	P_{in} (Psi)	P_{in} (MPa)	P_{exit} (Psi)	P_{exit} (MPa)
8-Bladed Test 1	700	4.83	370	2.55
8-Bladed Test 2	1000	6.90	500	3.45
12-Bladed Test 1	1000	6.90	700	4.83
12-Bladed Test 2	1000	6.90	180	1.24
8-Bladed Baseline	0	0	0	0
12-Bladed Baseline	0	0	0	0

Theoretically, one baseline test should have sufficed for both seals, but the use of squirrel cages to overcome limits on testing the eight-bladed seal meant that the baselines were not identical for both seals.

BASELINE TESTS

The two baseline tests were carried out under zero pressure conditions and the rotor was not spinning during the tests. Table 8 and Table 9 summarize the test results.

Table 8 Baseline Static Stiffness Coefficicients

Test Case	K_{xx} (lb/in)	K_{xy} (lb/in)	K_{yx} (lb/in)	K_{yy} (lb/in)
Without Squirrel Cages	15,916.77	-359.53	-251.64	14,858.55
With Squirrel Cages	72,096.19	91.61	6,027.74	72,067.43

Table 9 Baseline Static Stiffness Coefficients (SI Units)

Test Case	K_{xx} (MN/m)	K_{xy} (MN/m)	K_{yx} (MN/m)	K_{yy} (MN/m)
Without Squirrel Cages	2.787	-0.063	-0.044	2.602
With Squirrel Cages	12.625	0.016	1.056	12.620

Although these two tests did not have the same seal installed in the stator assembly, the fact that there was no pressure drop across the seals means that any difference in the coefficients from one test to the other is due to the addition of the squirrel cages. Table 8 shows that the two squirrel cages combined resulted in a symmetric increase in baseline direct stiffness of about 57,000 lb/in (9.98 MN/m).

The cross-coupled coefficients are of the same sign and arise due to the mechanical cross-coupling caused by the shakers and the other connections between the stator assembly and the housing. The results of baseline test for the eight-bladed seal show that there is considerable difference between the magnitudes of K_{xy} and K_{yx}. This may be in part due to improper fastening of the two halves of the squirrel cages or to minor angular warping in the ribs of one squirrel cage.

The baseline stiffness coefficients were subtracted from the coefficients calculated

from the pressurized data so as to give the stiffness coefficients for the each seal.

PRESSURIZED TESTS

The results of the four pressurized tests with the baseline values subtracted are presented in Table 10 and Table 11. All coefficients have been divided by two to obtain the results for one seal. As was expected, the magnitude of the negative stiffness for the eight-bladed seal is higher than that for the twelve-bladed seal. In addition, for both seals, the magnitude of negative stiffness increases with increasing pressure drop.

Table 10 Seal Static Stiffness Coefficients (Baseline Subtracted)

Test	K_{xx} (lb/in)	K_{xy} (lb/in)	K_{yx} (lb/in)	K_{yy} (lb/in)
8-Bladed Test 1	-46,373.84	767.51	8,719.28	-41,075.65
8-Bladed Test 2	-64,304.27	912.30	3,074.13	-60,803.19
12-Bladed Test 1	-11,094.20	-10.01	-751.51	-9,932.93
12-Bladed Test 2	-39,212.94	-3,330.31	-1,879.96	-36,302.19

Table 11 Seal Static Stiffness Coefficients (Baseline Subtracted – SI Units)

Test	K_{xx} (MN/m)	K_{xy} (MN/m)	K_{yx} (MN/m)	K_{yy} (MN/m)
8-Bladed Test 1	-8.121	0.134	1.527	-7.193
8-Bladed Test 2	-11.261	0.160	0.538	-10.648
12-Bladed Test 1	-1.943	-0.002	-0.132	-1.739
12-Bladed Test 2	-6.867	-0.583	-0.329	-6.357

This data supports the decision to include the data points at a frequency of 20 Hz even though in some cases, these points did not fall in line with the rest of the data (Chapter VII). For both diverging seals, the K_{xx} and K_{yy} have significantly large negative

values, even at lower pressure drop conditions.

Table 12 presents a comparison of the static results with the results of the shake tests. Extrapolating a curve fit of the dynamic test data provided an estimate of the direct stiffness at 0 Hz. It would be logical to assume that the best correlation would be obtained using the 10,200 RPM data, since that speed is the closest to the zero rotor speed of the static tests. However, the fact that the data is somewhat scattered and that any curve fit might yield highly erroneous results necessitated the use of the data for all three rotor speeds. A positive value in Table 12 indicates that the magnitude of the static stiffness was higher than that of the dynamically calculated stiffness.

While these discrepancies are not negligible, the results of both tests are close, indicating that the methodology used to obtain the direct stiffness from the shake tests is sound.

The curves that were extrapolated for the comparison with the static test results were those that best fit data that was, in some cases, highly scattered. Straight lines were used to fit the data for the twelve-bladed seal under the lower pressure drop conditions, while second order curves were used for the remaining three cases.

Table 12 Deviation of Shake Test Results from Static Test Results

Test	Direction	Percentage Deviation		
		10,200 RPM	15,200 RPM	20,200 RPM
8-Bladed Test 1	x	19.53	0.74	7.91
	y	8.57	13.50	9.73
8-Bladed Test 2	x	27.28	5.83	10.24
	y	16.19	11.60	6.96
12-Bladed Test 1	x	5.90	4.35	222.24
	y	-11.23	-23.97	-14.17
12-Bladed Test 2	x	17.96	16.36	27.36
	y	11.88	10.12	17.88

The 222% deviation in K_{xx} at 20,200 RPM for Test 1 of the twelve-bladed seal

resulted from a curve fit of data that was highly scattered at low frequencies as can be seen from Figure 64 of Chapter VII.

Note that the pressure conditions for the shake and static tests that were compared were not exactly identical. The most severe discrepancy was in the case of the 10,200 RPM data for the eight-bladed seal (for the lower pressure drop condition) in which the inlet and exit pressures were 731 Psi (5.04 MPa) and 454 Psi (3.13 MPa) instead of 700 Psi (4.83 MPa) and 370 Psi (2.55 MPa). Most of the other discrepancies were not as large such as in the case of the 15,200 RPM data for the twelve-bladed seal (for the lower pressure drop condition) in which the inlet and exit pressure were 994 Psi (6.86 MPa) and 715 Psi (4.93 MPa) instead of 1000 Psi (6.90 MPa) and 700 Psi (4.83 MPa). Taking into consideration the scattered nature of the data and the lack of exactly identical pressure conditions, the deviations in the results of static and shake tests fall within reasonable limits.

CHAPTER IX

DISCUSSION

The theory and results presented in this thesis were discussed in their respective chapters. The current chapter attempts to address outstanding issues and provides any necessary additional comments on models and methodology or on the interpretation of analytical or empirical data.

DISCHARGE COEFFICIENTS

Estimates of the discharge coefficients for the inlet and exit blades of three of the four tested seal configurations were presented in Chapter V. These seals were tested at considerably higher pressures than previously tested seals, but there were also significant geometric differences between the test seals used in this analysis and the seals previously tested. Furthermore, there are differences between the eight-bladed and twelve-bladed seals of this thesis that doubtless contribute to the need for different discharge coefficients for each seal configuration.

Figure 72 shows close-up views of the blades and partition walls of the diverging eight and twelve-bladed seals respectively.
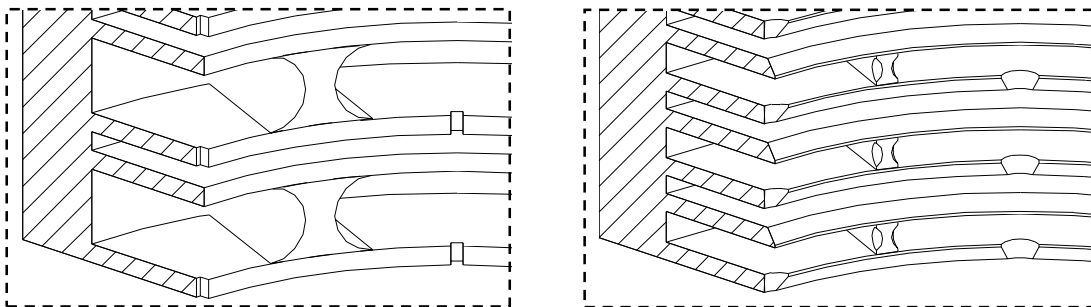
Figure 72 Blade Geometry for Diverging 8-Bladed (left) and 12-Bladed (right) Seals

The first difference between the two seals is the shape of the notch. Notch shape effects were examined by Kannan [23], but were not taken into consideration in the theory used to predict the direct stiffnesses of the test seals presented in Chapter VII. The analysis simply used the difference in area to calculate an enlarged equivalent clearance between seal and rotor and used the St. Venant equation for flow through an orifice to calculate the mass flow-rate and subsequently the stiffness.

Another geometric inconsistency can be seen in the partition walls of the eight-bladed seal. The wall thickness used in the damper seal code was 0.4 inches (10.16 mm), which is the thickness of the actual wall at its narrowest point. In other words, the pocket volume used in the damper seal code was slightly larger than the actual pocket volume.

A geometric factor with more influence on the leakage and the discharge coefficients is the shape of the blade tips of the twelve-bladed seal. The relatively high discharge coefficients for this seal are at least in part due to increased leakage across these forward and backward beveled blades.

The differences between the discharge coefficients obtained for the test seals and those used by Shultz [9] are probably due in part to such geometric differences, but are also increased by the difference in test pressures. Wittig, et al. [24] present numerical predictions for the discharge coefficients of labyrinth seals that show their dependence on the ratio of pressures across the seals.

The importance of taking into consideration shaft growth in labyrinth seal applications is cited by Waschka, Wittig, and Kim [25], who also discuss the speed dependency of discharge coefficients due to rotational effects. While such effects can be expected to have less importance in a PDS with its partition walls, this does go some way in explaining the error in predicting mass flow-rates are higher speeds (Chapter V).

SHAKE TESTS

Attempts to test the diverging eight-bladed seal with higher pressure drops than those presented in Chapter VII were unsuccessful for the same negative stiffness reason associated with attempting to raise the inlet pressure. In one case the stator was able to move from one extreme to another without "sticking" to the rotor before shaking, but began to rub against the rotor in a circular motion around its circumference as soon as a translatory shake was induced.

As was mentioned earlier, the 30 Hz, 50 Hz, 60 Hz, 120 Hz, 180 Hz, and 240 Hz data points were not included in results of Chapter VII. For all four seal configurations, the 40 Hz data point had higher values of variance than those for the higher frequencies. For the twelve-bladed seal configurations this variance is less than that of the data points around 40 Hz, but for the eight-bladed configurations it is clearly the largest variance. Additional justification is offered by the comparison of the static and dynamic stiffnesses of both diverging seals in Chapter VIII. The results agreed reasonably well only when the 40 Hz data point was omitted. In addition, the results of the static tests suggest that the direct stiffness measurements at 20 Hz are accurate regardless of what seems like a deviation from the general trend in several cases.

The curves used to fit the results of the shake tests are only intended to serve as a general indication of any trends in the data. To fit the data perfectly, a curve of order one less than the number of points would be needed, but no curve with an order higher than three was used to fit the data. In some cases, such as the 15,200 RPM test of the straight-through eight-bladed seal with a low pressure drop (Figure 39), a second order curve seemed to best fit the lower frequency data while a higher order curve would better fit the high frequency data. On the other hand, the results of the 10,200 RPM test of the diverging twelve-bladed seal with an intermediate pressure drop (Figure 65), seems to be best fit by a straight line. Neither of these sets of data is highly scattered. The curves selected to fit the data for the comparison of static and dynamic test results were those that best represented the trend followed by the data points, especially those

below 100 Hz.

The negative values of stiffness obtained for the straight-through eight-bladed seal at frequencies below 100 Hz is a significant deviation from the theory of the PDS. It can be argued that imperfections in manufacturing the seal could have led to a diverging seal with a frequency-dependent stiffness that becomes positive beyond a certain frequency, as was discussed in Chapter VI. This assumption does not, however, explain the overwhelmingly positive stiffness values obtained for this seal under the low and intermediate pressure drop conditions.

While it is highly dependent on pressure drop, the direct stiffness of the straight-through eight-bladed seal is more or less independent of rotor speed. This follows from the fact that the mass flow-rate exhibits only minor changes from one speed to another and indicates that rotational effects in a PDS have only minor effects on direct stiffness.

The offset between the predicted and measured curves for the diverging eight-bladed seal means that while the theory under-predicts the stiffness at higher frequencies, it either over-predicts (predicts more negative values) or accurately predicts the stiffness at lower frequencies. This indicates that multiplying by a simple correction factor may result in more accurate prediction of this seal's stiffness at either higher or lower frequencies, but not both simultaneously.

DAMPER SEAL CODE

It is possible to model any pocket damper seal with an even number of blades as a superposition of two-bladed sub-models. Each of these two-bladed seals would have a length equal to the active cavity length of the original seal plus twice the blade thickness. The inlet and exit pressures for each two-bladed seal would be the pressures immediately upstream and downstream of their corresponding active cavities. Since these pressures are taken from modeling the actual seal, and since the corresponding cavity lengths and blade clearances are identical in both models, the mass flow-rates should also be the same.

The original damper seal code contained some errors. It calculated different flow-rates through each blade and used the minimum value as the flow-rate through the seal. A comparison of a model of the entire seal and a series of four two-bladed sub-models for the diverging eight-bladed test seal resulted in an difference of over 17% in predicting the direct stiffness using inlet and exit pressures of 950 Psi (6.55 MPa) and 500 Psi (3.45 MPa) respectively. An identical comparison using the corrected flow-rate calculation presented in this thesis leads to an error of less than one hundredth of a percent.

For cases in which the flow through the last blade (or several blades) is choked, the pressure downstream of the final blade calculated using the maximum allowable pressure ratio (Equation 3, Chapter III) is not the same as the prescribed back pressure. The pressure immediately downstream of a constriction through which flow is choked is given by this calculated value and not by the prescribed back pressure (Fox and McDonald [26]) and, as a result, it is this pressure that is used in calculating the rotordynamic coefficients of the seal.

CHAPTER X

CONCLUDING SUMMARY

The following points summarize the topics covered in this thesis and the results that were presented as well as possible steps that can be taken to follow up on this research.

- The mass flow-rate calculation used in the existing damper seal code was corrected using an iterative technique analogous to Holzer's method.

- The static pressures in the second and third active cavities of both configurations of the eight-bladed seal were measured. Examination of these pressures led to the determination that the correlation between measured and predicted values of the pocket pressures was improved by selecting discharge coefficients such that the ratio of the inlet to the exit coefficient was as low as possible.

- Whereas the ratio of these coefficients was found to affect the static pressure predictions, the actual values of the coefficients determine the amount of leakage through the seal. Therefore, in order to avoid significantly under-predicting the leakage, there is a lower limit to the discharge coefficient ratio mentioned above. The coefficients that were selected were those that offered the best match between theoretical and measured values for both the pressures and the leakage data.

- The comparatively high values of the discharge coefficients selected for the diverging twelve-bladed seal are, at least in part, attributable to increased leakage due to the beveled blades of that seal.

- The effect of reduced clearances due to shaft growth on the leakage characteristics of the seals was examined. Taking shaft growth into account resulted in more accurate leakage predictions, but the error in prediction increased with increasing shaft speeds due to rotational effects.

- The effects of seal design parameters, namely the pocket depth, the clearances, and the number of blades, were examined. In addition, the use of non-uniform seal designs was discussed. The analytical results show that for a given diverging

PDS, making the pockets deeper or increasing the length of the active cavities results in a drop in the value of the seal's negative stiffness (making it less negative). Decreasing a seal's clearance ratio reduces the leakage through the seal, which reduces its negative stiffness. Increasing a seal's inlet clearances while holding the clearance ratio constant results in an initial increase in the seal's negative stiffness, but this effect is reversed as the inlet clearness are enlarged beyond a given value. In addition to resulting in such effect reversals, making changes to some design parameters leads to effects that counterbalance each other. For instance, increasing the number of blades results in shorter active cavities, but in higher optimum pocket depth values; two changes that have opposite effects on the seal's stiffness. Limitations on the use of these design parameters to manipulate seal performance arise due to one of two considerations. The first is that the effect of the change being considered may not be large enough to justify possible undesirable results (a change that makes a seal's stiffness less negative may also reduce its positive damping). Secondly, the required change may not be physically feasible (for example, there is a physical limit to the depth of the pockets). Analysis of seals with non-uniform geometries shows that changing design parameters in selected cavities can decrease a seal's negative stiffness while reducing or eliminating adverse effects on its positive damping.

- The damper seal code, with the corrected mass flow-rate calculation and the appropriate discharge coefficients, was used to predict the direct stiffnesses of the test seals for various rotor speeds and test pressures. The magnitudes of the direct stiffness were significantly under-predicted by the code in the cases of the straight-through twelve-bladed seal and both eight-bladed seal configurations. For the diverging twelve-bladed seal, however, the measured values of the negative stiffness were considerably lower than the predicted magnitudes. The code over-predicted the frequency at which the stiffness of a diverging seal becomes positive and failed to predict the negative stiffness values that were measured at low frequencies for straight-through seals. The code does, however,

accurately predict general trends in the frequency dependency of the direct stiffness as well as the effects of changing rotor speed and pressure drop.

- Static tests were carried out in order to validate the results of the shake tests. The static test data supported the results of the dynamic tests reasonably well and also assisted in the interpretation of those results.

Further examination of the effects of seal geometry on the mass flow-rate would provide better understanding of the factors which led to the need for the discharge coefficient values used for each seal in this thesis. Further detailed examination of the magnitude and phase of the dynamic pocket pressures may help explain the reasons for the poor correlation between the measured and predicted stiffness magnitudes and may aid in improving the models currently used.

REFERENCES

[1]   Alford, J. S., October 1965, "Protecting Turbomachinery from Self-Excited Rotor Whirl," ASME Journal of Engineering for Power, pp. 333-334.

[2]   Benckert, H., and Wachter, J., 1980, "Flow Induced Spring Coefficients of Labyrinth Seals for Applications in Rotordynamics," IMechE Proceedings of the 2nd International Conference on Vibrations in Rotating Machinery, Cambridge, England, pp. 53-63.

[3]   Murphy, B. T., and Vance, J. M., 1980, "Labyrinth Seal Effects on Whirl Instability," IMechE Proceedings, No. C306/80, pp. 369-373.

[4]   Childs, D. W. and Vance, J. M., 1997, "Annular Gas Seals and Rotordynamics of Compressors and Turbines," Proceedings of 26th Turbomachinery Symposium, Texas A&M University, College Station, TX, pp. 201-220.

[5]   Sundararajan, P., and Vance, J. M., 1995, "A Theoretical and Experimental Investigation of a Gas-Operated Bearing Damper for Turbomachinery - Part I & II: Experimental Results and Comparison with Theory," ASME Journal of Engineering for Gas Turbines and Power, **117**, pp. 742-756.

[6]   Armstrong, J. and Perricone, F., 1996, "Turbine Instability Solution - Honeycomb Seals," Proceedings of the 25th Turbomachinery Symposium, Texas A&M University, College Station, TX, pp. 47-56.

[7]   Lund, J. W., 1974, "Stability and Damped Critical Speeds of a Flexible Rotor in Fluid Film Bearings," ASME Journal of Engineering for Industry, **96**, pp. 509-517.

[8]   Vance, J. M., and Shultz, R. R., 1993, "New Damper Seal for Turbomachinery," Proceedings of the 14th Vibration and Noise Conference, ASME, Vibration of Rotating Systems, **60**, pp. 139-148.

[9]   Shultz, R. R., 1996, "Analytical and Experimental Investigation of a Labyrinth Seal Test Rig and Damper Seals for Turbomachinery," M.S. thesis, Mechanical Engineering Department, Texas A&M University, College Station, TX.

[10] Li, J., and Vance, J. M., 1995, "Effects of Clearance and Clearance Ratio on Two and Three Bladed TAMSEALs," Turbomachinery Research Consortium, TRC-Seal-4-95, Turbomachinery Laboratory, College Station, TX.

[11] Vance, J. M. and Li, J., October 1996, "Test Results of a New Damper Seal for Vibration Reduction in Turbomachinery," ASME Transactions, Journal of Engineering for Gas Turbines and Power, **118**, pp. 843-846.

[12] Richards, R.L., Vance, J. M., and Zeidan, F. Y., 1995, "Using a Damper Seal to Eliminate Subsynchronous Vibrations in Three Back to Back Compressors," Proceedings of the 24th Turbomachinery Symposium, Texas A&M University, College Station, TX, pp. 59-71.

[13] Ransom, R. L., Li, J., San Andres, L., and Vance, J. M., 1999, "Experimental Force Coefficients for a Two-Bladed Labyrinth Seal and a Four-Blade Pocket Damper Seal," ASME Journal of Tribology, **121**, pp. 370-376.

[14] Laos, H.E., 1999, "Rotordynamic Effects of Pocket Damper Seals," Ph.D. dissertation, Mechanical Engineering Department, Texas A&M University, College Station, TX.

[15] Li, J., Kushner, F. and De Choudhury, P., 2002, "Experimental Evaluation of Slotted Pocket Gas Damper Seals on a Rotating Test Rig," Proceedings of ASME Turbo Expo, 47th International Gas Turbine & Aeroengine Technical Congress, Exposition & User Symposium, pp. 1125-1138.

[16] Childs, D. W. and Hale, K., 1994, "A Test Apparatus and Facility to Identify the Rotordynamic Coefficients of High-Speed Hydrostatic Bearings," ASME Journal of Tribology, **116**, pp. 337-344.

[17] Childs, D. W., 1993, *Turbomachinery Rotordynamics – Phenomena, Modeling, and Analysis*, John Wiley & Sons, New York.

[18] Vance, J. M., 1988, *Rotordynamics of Turbomachinery*, John Wiley & Sons, New York.

[19] Picardo, A. M., 2003, "High Pressure Testing of See-Through Labyrinth Seals," M.S. thesis, Mechanical Engineering Department, Texas A&M University, College Station, TX.

[20] Marquette, O. R., Childs, D. W., and San Andrés, L., 1997, "Eccentricity Effects on the Rotordynamic Coefficients of Plain Annular Seals: Theory Versus Experiment," Transactions of the ASME, **119**, pp. 443-448.

[21] Young, Warren C., 1989, *Roark's Formulas for Stress and Strain*, 6th edition, McGraw-Hill, New York.

[22] Ertas, B. H., 2003, Lab Notes, Mechanical Engineering Department, Texas A&M University, College Station, TX.

[23] Kannan, B. S., 2003, "Development and Validation of an Analytical Model for the Notched Pocket Damper Seal," M.S. thesis, Mechanical Engineering Department, Texas A&M University, College Station, TX.

[24] Wittig, S., Schelling, U., Kim, S., and Jacobsen, K., 1987, "Numerical Predictions and Measurements of Discharge Coefficients in Labyrinth Seals," ASME Paper 87-GT-188.

[25] Waschka, W., Wittig, S., and Kim, S., 1992, "Influence of High Rotational Speeds on the Heat Transfer and Discharge Coefficients in Labyrinth Seals," ASME Journal of Turbomachinery, **114**, no. 2, pp. 462-468.

[26] Fox, R. W. and McDonald, A. T., 1998, *Introduction to Fluid Mechanics*, 5th edition, John Wiley & Sons, New York.

APPENDIX

This appendix contains additional data referred to in the body of this thesis. This consists of the detailed leakage test data that was used to determine the discharge coefficients of the test seals in Chapter V.

Table A lists all data for the leakage tests carried out on both the straight-through and diverging eight-bladed seals. The modified inlet and exit discharge coefficients for the straight-through seal are 0.75 and 0.85 respectively and 0.75 and 1.25 respectively for the diverging seal. Table B lists all data for the leakage tests carried out on the diverging twelve-bladed seal (two sets of data). The modified inlet and exit discharge coefficients for this seal are 2.30 and 2.75 respectively. The original discharge coefficients are 1.10 for inlet blades and 0.95 for exit blades.

Table A Leakage Data for Eight-Bladed Seal (Pressures in Psi and Mass Flow-Rates in lb/s)

Seal	RPM	P_{in}	P_{exit}	ΔP	Measured Flow	Flow 1	Flow 2	Flow 3
1:1 Clearance Ratio	10,200	1046	135	912	0.7120	0.8004	0.7112	0.7192
	10,200	1013	342	671	0.6882	0.7674	0.6798	0.6874
	10,200	1030	539	491	0.6357	0.7202	0.6370	0.6442
	15,200	1011	126	885	0.6611	0.7630	0.6780	0.6951
	15,200	1029	338	691	0.6768	0.7704	0.6825	0.6998
	15,200	1028	530	498	0.6212	0.7124	0.6301	0.6460
	20,200	1025	126	899	0.6427	0.7586	0.6741	0.7048
	20,200	1031	328	703	0.6443	0.7585	0.6722	0.7028
	20,200	1014	505	509	0.5921	0.6964	0.6160	0.6441
1:1.5 Clearance Ratio	0	1009	599	410	0.7275	0.8069	0.7252	0.7252
	0	1012	601	411	0.7341	0.8092	0.7272	0.7272
	0	1027	615	412	0.7319	0.8177	0.7349	0.7349
	0	1016	604	412	0.7385	0.8119	0.7297	0.7297
	0	1027	613	414	0.7297	0.8190	0.7362	0.7362
	10,200	939	582	357	0.6592	0.7263	0.6527	0.6596
	10,200	731	454	277	0.4938	0.5647	0.5075	0.5129
	15,200	953	581	372	0.6548	0.7350	0.6600	0.6757
	15,200	714	436	278	0.4674	0.5502	0.4941	0.5057
	20,200	930	553	377	0.6151	0.7142	0.6407	0.6679
	20,200	723	432	291	0.4564	0.5539	0.4969	0.5180

Flow 1 - Original discharge coefficients. Shaft growth considered.

Flow 2 - Modified discharge coefficients. Shaft growth considered.

Flow 3 - Modified discharge coefficients. Shaft growth neglected.

Table B Leakage Data for Twelve-Bladed Seal (Pressures in Psi and Mass Flow-Rates in lb/s)

Seal	RPM	P_{in}	P_{exit}	ΔP	Measured Flow	Flow 1	Flow 2	Flow 3
1:2 Clearance Ratio # 1	10,200	1018	229	789	1.1993	0.8392	1.2442	1.2572
	10,200	1011	464	547	1.1552	0.7789	1.1598	1.1718
	10,200	987	713	273	0.8907	0.6005	0.8957	0.9049
	15,200	1014	226	789	1.1883	0.8256	1.2234	1.2524
	15,200	999	454	545	1.1243	0.7619	1.1341	1.1605
	15,200	993	715	279	0.8885	0.5989	0.8928	0.9135
	20,200	1019	224	795	1.1684	0.8153	1.2072	1.2587
	20,200	1018	457	561	1.1221	0.7650	1.1381	1.1858
	20,200	997	710	288	0.8752	0.5976	0.8904	0.9275
1:2 Clearance Ratio # 2	10,200	1018	238	781	1.1995	0.8385	1.2436	1.2566
	10,200	1010	494	516	1.1498	0.7655	1.1402	1.1520
	10,200	1023	744	278	0.9372	0.6180	0.9217	0.9312
	15,200	1011	236	776	1.1924	0.8224	1.2192	1.2480
	15,200	1006	491	515	1.1443	0.7536	1.1220	1.1481
	15,200	1019	742	277	0.9339	0.6072	0.9053	0.9263
	20,200	1016	237	779	1.1988	0.8119	1.2030	1.2542
	20,200	999	488	511	1.1369	0.7352	1.0940	1.1398
	20,200	1014	738	276	0.9302	0.5941	0.8853	0.9222

Flow 1 - Original discharge coefficients. Shaft growth considered.

Flow 2 - Modified discharge coefficients. Shaft growth considered.

Flow 3 - Modified discharge coefficients. Shaft growth neglected.

VITA

Ahmed Mohamed Gamal Eldin

4 Tehran Square, No. 142, Dokki - 12311, Giza, Egypt

EDUCATION

Master of Science in Mechanical Engineering

Texas A&M University, College Station, Texas

August 2000 – December 2003

Bachelor of Science in Mechanical Engineering

The American University in Cairo, Egypt

September 1994 – June 1999

EXPERIENCE

Turbomachinery Laboratory, Texas A&M University, College Station, TX

Graduate Research Assistant

January 2001 – December 2003

Mechanical Engineering Department, Texas A&M University, College Station, TX

Graduate Teaching Assistant

August 2000 – December 2001

Mechanical Engineering Unit, The American University in Cairo, Egypt

Teaching Assistant

September 1999 – June 2000